2015 年度

博士学位申請論文

Photochromism of Biaryl-Bridged Radical Complexes

ビアリール架橋型ラジカル複合体のフォトクロミズム

指導教員　　阿部　二朗　教授

青山学院大学大学院

理工学研究科

理工学専攻化学コース

山口　哲生

Contents

Chapter 1

Introduction

1.1. Photochromism

"Photochromism is a reversible transformation of a chemical species, induced in one or both directions by the absorption of light irradiation between two forms having different absorption spectra."[1] Photochromism is classified in two types: P-type and T-type photochromism. In P-type photochromism, the back reaction from the photogenerated colored form to the colorless form is induced only by light irradiation. Conversely, in T-type photochromism, the back reaction is induced by light irradiation and heat.

Well-known P-type photochromic compounds include diarylethenes and fulgides.[2–5] In the photochromism of diarylethene systems, the colorless open-ring isomer isomerizes to the colored closed-ring isomer upon UV light irradiation (**Scheme 1.1.1a**). The closed-ring isomer reverts to the initial colorless open-ring isomer upon visible light irradiation. However, this back reaction does not occur by heat because of the high thermal stability of the closed-ring isomer.[6,7] The photochromism of diarylethenes can be observed both in solution and in the crystalline form. Notably, some crystals of diarylethenes reversibly change their shapes upon light irradiation because of the collective motions of the molecules in the single crystals as they isomerize, which cause macroscale motions such as bending and twisting of the crystal.[8–10] Photoinduced lotus and petal effects[11–14] and the photocontrol of electrical conductance[15–17] have also been demonstrated.

Azobenzenes, hexaarylbiimidazoles, and chromenes[18–22] are well-known T-type photochromic compounds. The photochromism of azobenzene is attributed to the photoinduced *trans*-*cis* isomerization of the azo group (**Scheme 1.1.1b**). *Trans*-azobenzene isomerizes to the *cis*-isomer upon UV light irradiation. The *cis*-isomer is thermally unstable; therefore, it can revert to the *trans*-isomer by heating or visible light irradiation.[23–26] The half-lives of the *cis*-isomers of azobenzenes depend on their substituents and vary from several ns to months.[27–30] Because of large structural differences between *trans*- and *cis*-isomers of azobenzenes, these compounds are promising materials for the photomechanical materials, holographic memory,[31–35] photoalignment,[36–42] and photoinduced phase transitions of the liquid crystal,[43–45] and so on.[46–48]

These examples show that both P- and T-type photochromic compounds act as switches not only at the molecular level but also at the macroscale and that these materials will be essential for daily life in the future. However, one of the drawbacks of both P- and T-type photochromic compounds is that the photochromism can be initiated only near the surface of the material because of the reabsorption of the excitation light by the photogenerated colored species. Although the origin of the bending and twisting of diarylethene crystals is the gradient of the photochromic reaction from the surface to the interior of the crystal, this point becomes a critical issue when the induction of photochromism throughout thick photochromic films and the crystals is desired.

Scheme 1.1.1. Photochromism of a) diarylethene and b) azobenzene.

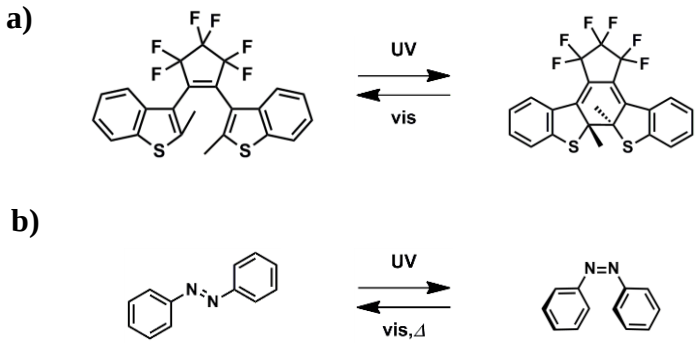

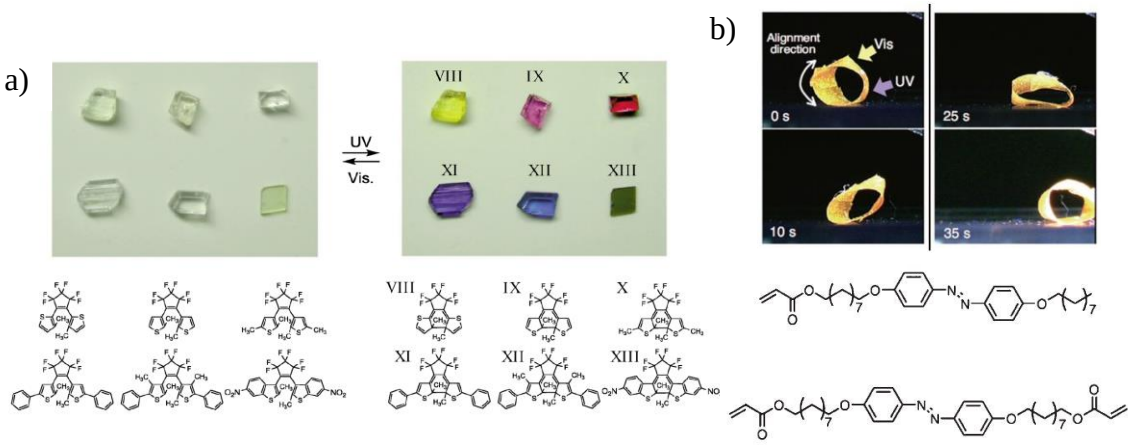

Figure 1.1.1. a) Color change of diarylethene derivatives in the single crystalline phase upon photoirradiation (Reprinted (adapted) with permission from Irie, M.; Fukaminato, T.; Matsuda, K.; Kobatake, S. *Chem. Rev.* **2014**, 12174–12277. Copyright (2014) American Chemical Society. b) Photoinduced rolling motion of a continuous ring of a liquid crystalline elastomer film. Reproduced from Ref. 32 with permission from John Wiley and Sons.

1.2. Negative photochromism

Almost all photochromic molecules change from colorless to colored upon light irradiation. On the other hand, some photochromic molecules exhibit the opposite phenomenon against conventional photochromism, in which the thermally stable colored form converts to the colorless form following visible light irradiation, and the colorless species thermally reverts to the colored form.[49–52] This phenomenon is called "negative photochromism." In the case of conventional T-type photochromic molecules, the colorless form is more stable than the colored form and the thermal back reaction occurs from the photogenerated colored form to the thermally stable colorless form (**Figure 1.2.1 left**). In negative photochromic systems, the colored form is more stable than the colorless form and the colored form changes to the colorless form upon visible light irradiation (**Figure 1.2.1 right**). One of the advantages of negative photochromism compared to conventional photochromism is that the photogenerated species does not absorb the visible light. In conventional photochromic systems, the photogenerated colored form also absorbs the excitation light, thus limiting the conversion efficiency of the photochromic reaction, which occurs only near the surface. In negative photochromic systems, because the photogenerated colorless form does not absorb the excitation visible light, the conversion efficiency is predicted to be higher and the reaction can be initiated deeper inside the sample. Several reported negative photochromic molecules are described in the following section.

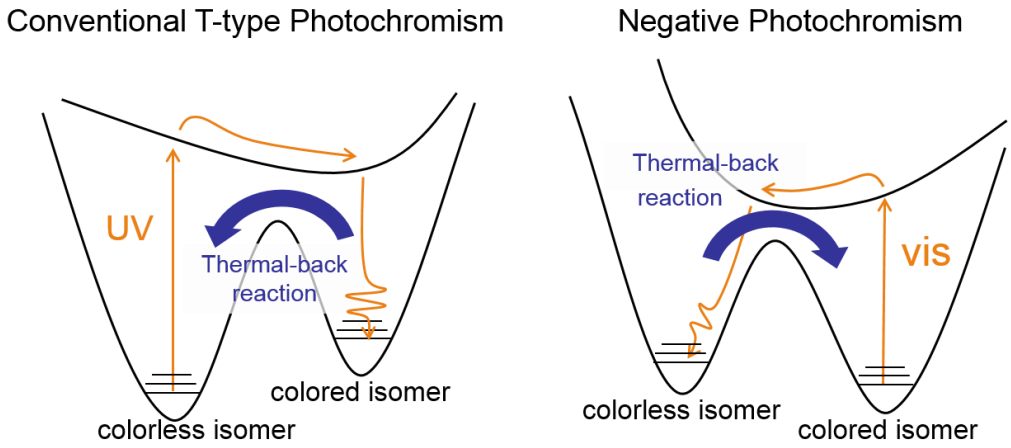

Figure 1.2.1. Energy diagrams for general T-type photochromism (left) and negative photochromism (right).

1.2.1. Spiropyran-type negative photochromic compounds

The photochromism of conventional spiropyran is attributed to the reversible bond cleavage of the C–O bond upon UV light irradiation and to the formation of the zwitterionic conjugated form, which is known as the merocyanine form (**Scheme 1.2.1**).[22] Solutions of merocyanine are red. However, upon heating, merocyanine reverts to the initial colorless spiropyran form. Photogenerated merocyanine has zwitterionic characteristics that were employed for the development of a photoswitching receptor for guanine–guanine dinucleoside derivatives[53] and a photoswitch for the intercalation of merocyanine derivatives to DNA.[54] For certain spiropyran derivatives, the merocyanine form is more stable than the spiropyran form. Moreover, these compounds exhibit negative photochromism, as shown below.

Scheme 1.2.1. Photochromism of spiropyran

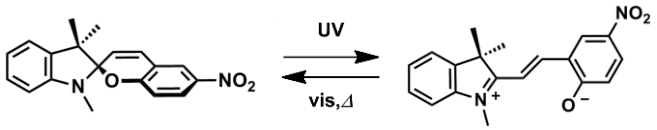

When spiropyran has a polar substituent, such as a carboxyl group, the merocyanine form is stabilized in aqueous solution because of its ionic properties.[55–64] Hirai *et al.* reported a spiropyran derivative with a hydroxyl substituent that exhibits negative photochromism in aqueous media but exhibits conventional photochromism in organic solvents.[65] Minami *et al.* reported that the introduction of two nitro substituents to the phenolate moiety of spiropyran stabilizes the merocyanine form (**Scheme 1.2.2**).[66] Moreover, they modified the indoline ring and investigated the effects of the substituents on the negative photochromic reactions. They found that some of these spiropyrans exhibited negative photochromism even in nonpolar chloroform. Ubukata *et al.* reported the formation of a photoinduced surface relief grating (SRG) on a polymer film doped with a negative photochromic spiropyran.[67] The depth of the SRG was 200 nm, which was the highest value reported for a spiropyran doped film. Although the authors did not mention the conversion efficiency of the negative photochromic spiropyran, the deep depth of the SRG suggests that negative photochromic compounds are promising for SRG materials.

Scheme 1.2.2. Negative photochromism of spiropyran

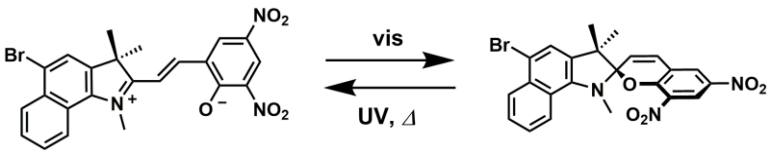

Raymo *et al.* reported the negative photochromism of a spiropyran derivative combined with cadmium sulfide quantum dots.[68] Cadmium sulfide nanoparticles are known to encourage adsorption by charged organic compounds. The same interactions would tend to stabilize zwitterionic merocyanine.

Kitao *et al.* introduced a crown ether to the nitrogen atom of the indoline moiety of spiropyran and revealed that this spiropyran derivative exhibited negative photochromism in solutions containing alkaline-earth metal ions. Kimura *et al.* also reported that spiropyrans substituted with crown ethers exhibited negative photochromism only in solutions containing alkaline-earth metal ions.[69,70] Furthermore, they revealed that the thermal-back reaction from the merocyanine form to the spiropyran form depended on the size of the crown ether and alkaline-earth ion. These results indicated that the crown ether moiety selectively bound the metal ion and a particular metal ion stabilizes the merocyanine form. To explain this phenomenon, the authors suggested the binding model for the merocyanine form shown in **Figure 1.2.2**.

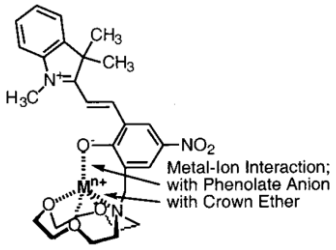

Figure 1.2.2. Model for the binding of a metal ion and merocyanine by a crown ether moiety. Reprinted (adapted) with permission from Tanaka, M.; Ikeda, T.; Xu, Q.; Ando, H.; Shibutani, Y.; Nakamura, M.; Sakamoto, H.; Yajima, S.; Kimura, K. *J. Org. Chem.* **2002**, *67*, 2223–2227. Copyright (2002) American Chemical Society.

1.2.2. Dimethyldihydropyrene-type negative photochromic compounds

Trans-dimethyldihydropyrene (DHP) was first reported by Blattmann *et al.* in 1965.[71] Moreover, recently DHP has been systematically studied by Mitchell and Nishihara.[72–76] DHP has a pyrene-like structure with the 15- and 16-positions substituted by methyl groups and its solution shows green (**Scheme 1.2.3**). Visible light irradiation of DHP in solution induces cleavage of the C–C bond between the 15- and 16-positions, and the solution turns colorless. The colorless form of DHP has a cycrophanediene (CPD) structure. CPD is a metastable isomer, and CPD solutions gradually revert to the initial green color in the dark or upon UV light irradiation. The half-life of CPD is approximately 2 h at 50 °C in the dark. Notably, the half-life of CPD and the quantum yield of the photochemical ring-opening reaction from DHP to CPD can be controlled by substitution of the methyl groups.[77] Mitchel *et al.* reported a long half-life of approximately 36 years at 20 °C for CPD substituted by two cyano groups (**Scheme 1.2.4**).[74,78] The authors suggest that this DHP derivative may be applicable for optical memory. However, a sigmatropic rearrangement occurs in the dicyano DHP above 50 °C, and the dicyano DHP is ultimately converted to compound **5** via compounds **3** and **4**, as shown in **Scheme 1.2.4**. This sigmatropic rearrangement was also observed for bisformyl DHP.[74] Thus, the decomposition reaction is considered to be induced by electron-withdrawing substituents.

Scheme 1.2.3. Photochromism of DHP. The C–C bond between the 15- and 16-positions is cleaved under visible light irradiation, and the photogenerated CPD thermally reverts to the initial DHP.

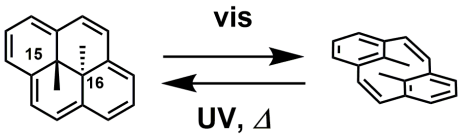

Scheme 1.2.4. Molecular structures of dicyano DHP and its byproducts (Ayub, K.; Mitchell, R. H. *J. Org. Chem.* **2014**, *79*, 664–678.).

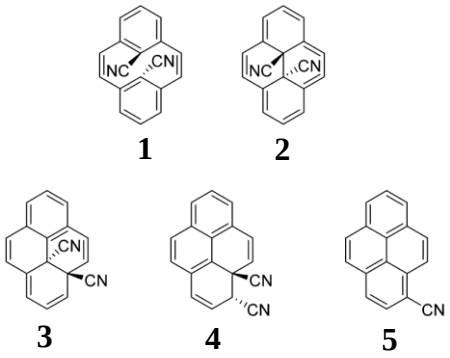

Mitchell *et al.* reported that the use of isobutenyl rather than methyl substituents in DHP suppressed byproduct formation via sigmatropic rearrangement (**Scheme 1.2.5**). Furthermore, isobutenyl DHP substituted with a naphthonyl group exhibited a maximum quantum yield value for the ring-opening reaction (0.66).[73]

Scheme 1.2.5. Negative photochromism of disobutenyl DHP. Reprinted (adapted) with permission from Ayub, K.; Li, R.; Bohne, C.; Williams, R. V.; Mitchell, R. H. *J. Am. Chem. Soc.* **2011**, *133*, 4040–4045. Copyright (2005) American Chemical Society.

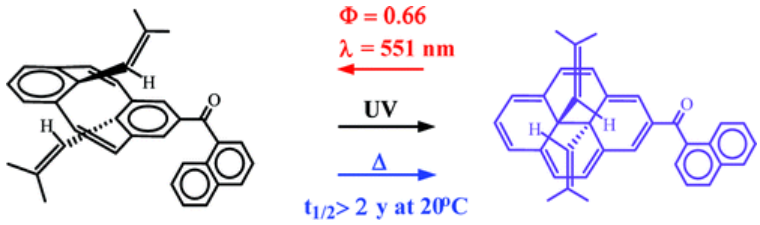

The thermal back reaction of CPD is forbidden by the rule of conversion orbital symmetry. To explain the mechanism of the thermal-back reaction of CPD, Robinson *et al*. calculated the transition state (TS) of the ring-closing reaction using density functional theory (DFT).[79] The optimized structures are shown in **Figure 1.2.3**. The spin contamination $<S^2>$ of the wave function at the TS ($<S^2>$ = 1.03) indicates an approximate 1:1 mixture of the singlet ($<S^2>$ = 0) and triplet ($<S^2>$ = 2) states and a biradical character for the TS. The symmetry breaking of the spin suggests that the potential surface of the singlet state crosses that of the triplet state. This behavior is the most probable explanation for the acceleration of the thermal back reaction of CPD.

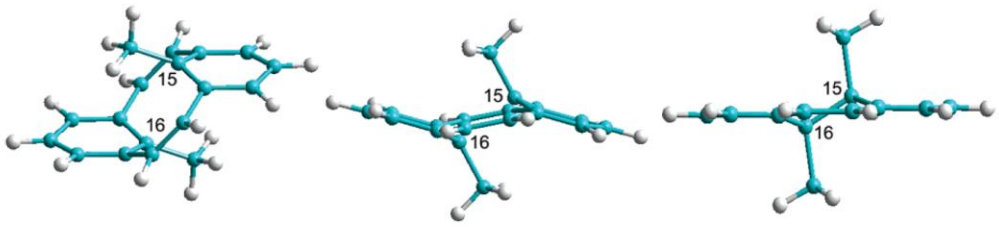

Figure 1.2.3. Optimized structures for CPD, the transition state TS, and DHP calculated using DFT at the UB3LYP/6-31G* level of theory. Reprinted (adapted) with permission from Williams, R. V.; Edwards, W. D.; Mitchell, R. H.; Robinson, S. G. *J. Am. Chem. Soc.* **2005**, *127*, 16207–16214. Copyright (2005) American Chemical Society.

Nishihara *et al.* reported a DHP derivative substituted with ferrocene units that exhibits negative photochromism in THF solution (**Figure 1.2.4**).[75,76,80] In addition, the ring-closing reaction of the CPD form also occurs via oxidation of the ferrocene unit. This result was explained by the strong d–π interactions between the ferrocene units and DHP moiety because of the very close frontier orbital energy levels.

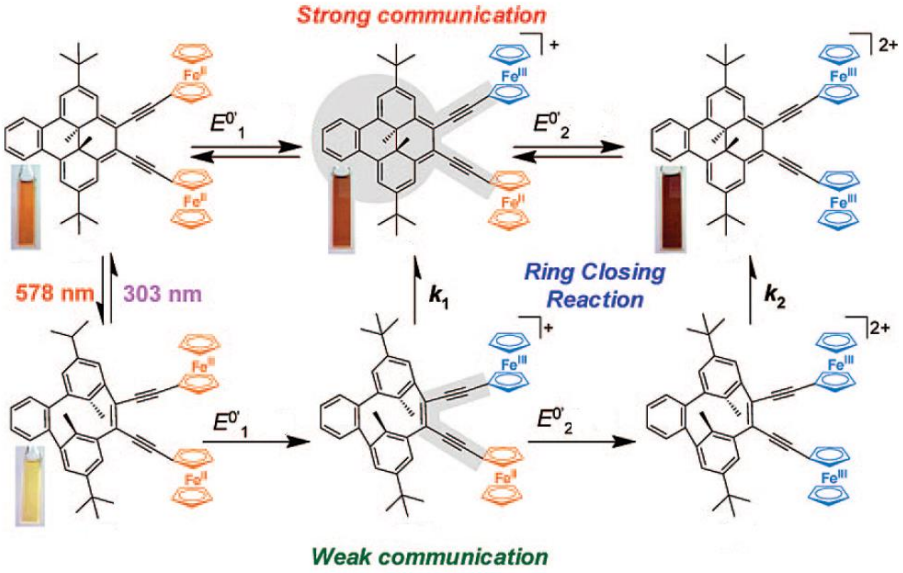

Figure 1.2.4. Photochromic and electrochromic properties of DHP substituted with ferrocene units. Reprinted (adapted) with permission from Muratsugu, S.; Kume, S.; Nishihara, H. *J. Am. Chem. Soc.* **2008**, *130*, 7204–7205. Copyright (2008) American Chemical Society.

1.2.3. Donor-acceptor Stenhouse adduct-type negative photochromic compounds

Scheme 1.2.6. Photochromism of DASAs.

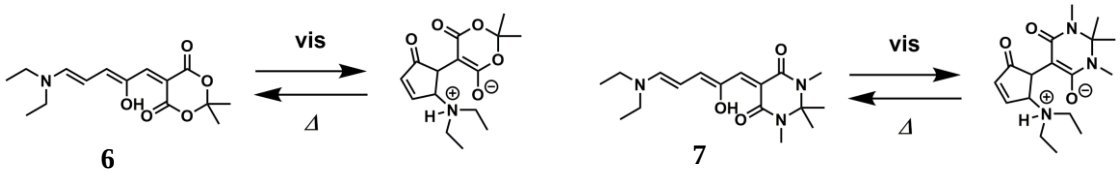

Donor–acceptor Stenhouse adducts (DASAs) were reported in 2014 by Alaniz *et al.*[81,82] DASAs are synthesized from furfural in only two steps. The thermally stable colored form of DASAs has a triene structure with an amine donor and a 1,3-dicalbonyl acceptor, whereas the photogenerated colorless form has a ring-closed zwitterionic structure (**Scheme 1.2.6** and **Figure 1.2.5d**). The ring-closing and opening reactions are proposed to proceed via a Nazalov-type 4π electron cyclization. Notably, the colored and colorless forms are hydrophobic and hydrophilic, respectively. Thus, visible light irradiation leads to the phase transfer of DASAs from the organic phase to the aqueous phase (**Figure 1.2.5c**). With this unique property, DASAs are expected to find use for on-demand light mediated disassembly and cargo release.

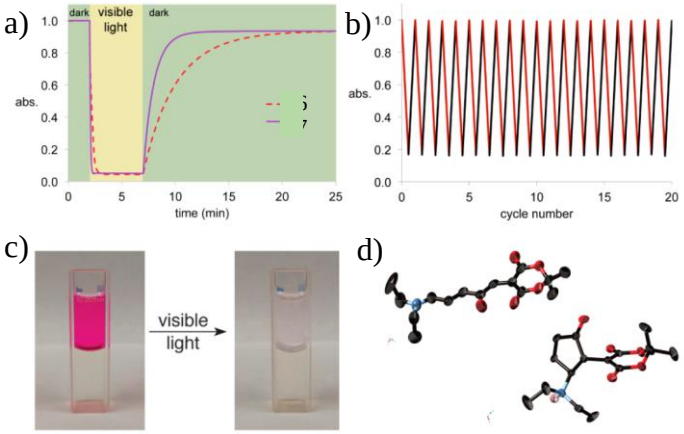

Figure 1.2.5. Photochromic properties of DASAs. a) Time profiles of the absorbance changes (545 nm) with visible light irradiation in toluene, b) multiple photoswitching cycles for **7** in toluene, c) photographs of the phase transition for **6** upon visible light irradiation, and d) ORTEP representation of each isomer of **6** (50% probability ellipsoids, hydrogen atoms were omitted for clarity). Reprinted (adapted) with permission from Helmy, S.; Leibfarth, F. a; Oh, S.; Poelma, J. E.; Hawker, C. J.; Alaniz, J. R. De; Read, J. *J. Am. Chem. Soc.* **2014**, *136*, 8169–8172. Copyright (2014) American Chemical Society.

1.2.4. Diarylethene-type negative photochromic compounds

Upon UV light irradiation, conventional diarylethenes, bis(3-thienyl)ethene, undergo photoisomerization from the colorless open-ring isomer to the colored closed-ring isomer. The closed-ring isomer can then be returned to the initial open-ring isomer under visible light irradiation. Conversely, bis(2-thienyl)ethene derivatives undergo decoloration from the colored open-ring isomer to the colorless closed-ring isomer (**Scheme 1.2.7 and Figure 1.2.6**),[83,84] and the photogenerated closed-ring isomer reverts to the open-ring isomer under UV light irradiation. In the conventional bis(3-thienyl)ethene system, the π-conjugation in the closed-ring isomer is longer than that in the open-ring isomer. However, in the bis(2-thienyl)ethene system, the π-conjugation in the open-ring isomer is longer than that in the closed-ring isomer. Thus, the bis(2-thienyl)ethene system exhibits the opposite photochromic behavior.

Scheme 1.2.7. Molecular structures and photochromism of oxidized bis(2-thienyl)ethene derivatives **8** and **9**. Reproduced from Ref. 83 with permission from The Royal Society of Chemistry.

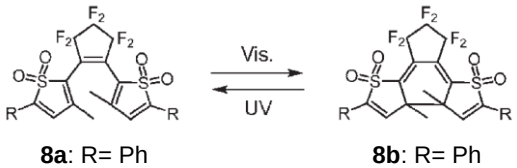

8a: R= Ph
9a: R= CH_3

8b: R= Ph
9b: R= CH_3

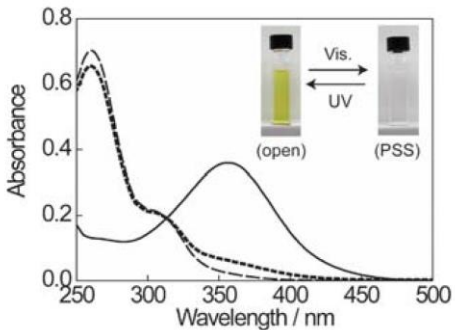

Figure 1.2.6. Absorption spectra for the open-ring isomer (solid line), the photostationary state under irradiation with 430 nm light (dashed line), and the closed-ring isomer (broken line) of **8** in 1,4-dioxane solutions (2.4×10^{-5} M) at room temperature. The conversion from the open- to the closed-ring isomer under irradiation with 430 nm light was estimated to be 92%. Inset: photographs of a solution of 1a and the photostationary state upon irradiation with 430 nm light. Reproduced from Ref. 83 with permission from The Royal Society of Chemistry.

1.2.5. Bridged imidazole dimer-type negative photochromic compounds

Scheme 1.2.8. Photochromism of a 1,1'-binaphthyl-bridged imidazole

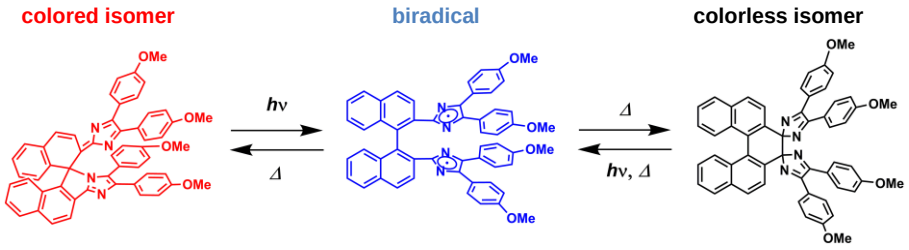

Recently, a new type of negative photochromic molecule, 1,1′-binaphthyl (BN)-bridged imidazole dimer, was reported by Abe *et al*.[85] The BN-bridged imidazole dimer was obtained as a red powder by oxidizing a precursor compound. X-ray crystallographic analysis revealed the molecular structure of the colored isomer, which was found to have a diazafulvene structure and a C–N bond between the 1-position of the binaphthyl unit and the 1-position of the imidazole ring (**Scheme 1.2.8**). The colored isomer of the BN-bridged imidazole dimer in benzene is red (**Figure 1.2.7**), and DFT calculations revealed that the absorption band in the visible region is attributed to the π–π* transition of the diazafulvene moiety. The colored isomer shows decoloration from red to colorless by visible light irradiation, and the colorless solution thermally returns to the initial red state in the dark (**Figure 1.2.8**). The molecular structure of the colorless isomer was predicted to be the 2,2′-isomer with the C–C bond between the two imidazole rings. Both the colored and colorless isomers produce the short-lived biradical under light irradiation (**Figure 1.2.9**). The major and minor products of the thermal back reaction of the biradical are the 2,2′-isomer and the colored isomer, respectively. Thus, three structural isomers (the colored isomer, the metastable 2,2′-isomer, and the short lived biradical) are involved in the photochromism of the BN-bridged imidazole dimer (**Scheme 1.2.8**). A biradical is generated following light irradiation of the thermally stable colored isomer that isomerizes to the colorless isomer as the main product upon heating. Because visible light can excite only the colored isomer, a solution of the BN-bridged imidazole dimer undergoes decoloration. The biradical is then generated following heating of the photogenerated colorless isomer; therefore, the colorless isomer thermally returns to the colored isomer via the biradical.

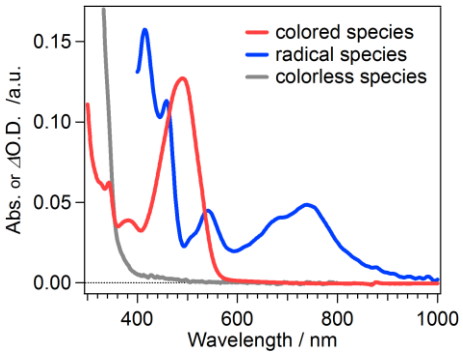

Figure 1.2.7. UV-vis absorption spectra of the three different isomers of the BN-bridged imidazole dimer.

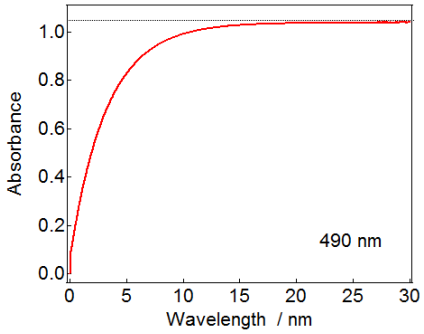

Figure 1.2.8. Time profile for the colorless isomer of the BN-bridged imidazole dimer in benzene at 25 °C.

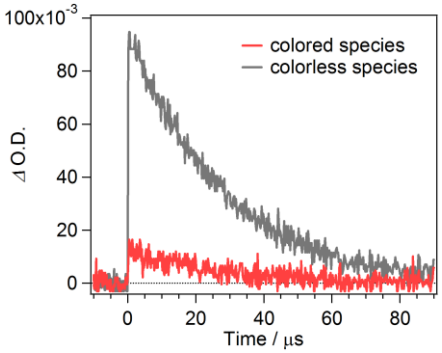

Figure 1.2.9. Decay profiles for the biradical species generated from the colored and colorless species of the BN-bridged imidazole dimer in benzene at 25 °C.

As described above, very few compounds show negative photochromism. Moreover, negative photochromic molecules that exhibit fast photoswitching have not yet been reported. The discovery of a new material that shows instantaneous decoloration and rapid coloration in the dark would lead to the development of a new industry. The purpose

of the present study is the development of fast negative photochromic molecules based on BN-bridged imidazole dimers and the functionalization of BN-bridged imidazole dimers. The photochromism of BN-bridged imidazole dimers is based on the photochromism of hexaarylbiimidazole (HABI). In the next section, the photochromism of HABI and bridged imidazole dimers is explained.

1.3. Hexaarylbiimidazole (HABI)

In 1960, Hayashi and Maeda reported that the oxidation of 2,4,5-triphenylimidazole (lophine) at room temperature gives hexaarylbiimidazole (HABI), which is an imidazole dimer with a C–N bond between the 1- and 2′-positions of the two imidazole rings (**Scheme 1.3.1**).[86] The 1,2′-isomer of HABI exhibits T-type photochromism from pale yellow to purple. The absorption spectra of HABI and triphenylimidazolyl radical (TPIR) are shown in **Figure 1.3.1**. TPIR has two absorption bands at 327 and 543 nm. This photochromic behavior is attributed to cleavage of the C–N bond between the two imidazole rings.[87–90] Although the photogenerated TPIR thermally returns to the initial dimer, the thermal back reaction of the TPIR solution takes several minutes in the dark because of the diffusion of TPIR in the medium. Thus, although the initial phase of the back reaction obeys second-order kinetics,[91,92] the longer reaction time reveals a deviation from this rate law. Wilks and Sathe reported that the reaction kinetics are well-fitted as a 3/2 order. Moreover, after several half-lives, the reaction order changes to first-order kinetics as the radical species disappears.[93–95] HABI has also been studied by numerous companies. For example, E. I. DuPont de Nemours and Company has been investigating HABI since the 1960s.[96–100] HABI has been used as a photopolymerization initiator due to the high quantum yield of the bond cleavage reaction and its high sensitivity to light.[101]

Scheme 1.3.1. Photochromism of HABI.

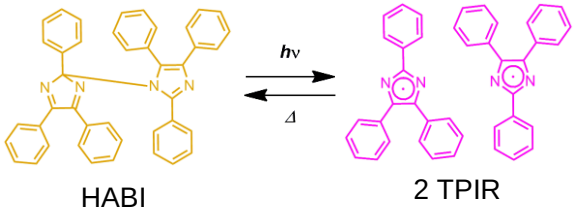

The initial process for photoinduced bond cleavage of HABI derivatives was reported by Miyasaka and coworkers.[102,103] The formation of TPIR after excitation proceeds in two steps. First, TPIR forms via bond fission and then undergoes vibrational cooling (**Figure 1.3.2**). The time constants for the steps are hundreds of femtoseconds and picoseconds. Because the C–N bond between the two imidazole rings of the lowest unoccupied molecular orbital (LUMO) of HABI has antibonding character, the S_1 state of HABI has been considered as the potential curve for dissociation. Therefore, bond cleavage in HABI has no activation energy and proceeds with a high quantum yield.

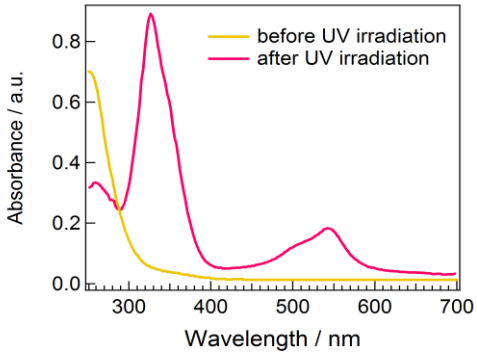

Figure 1.3.1. UV-vis absorption spectra for HABI before (yellow, HABI) and after (red, TPIR) UV irradiation.

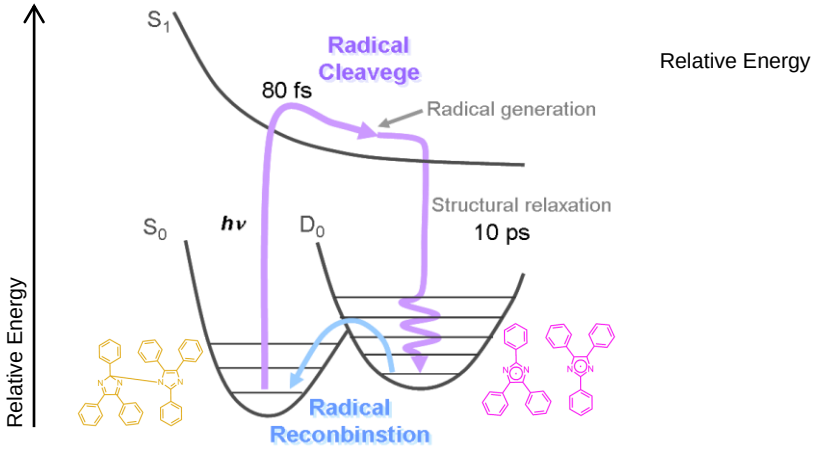

Figure 1.3.2. Potential energy surface for the radical cleavage of HABI.

HABI has several structural isomers depending on the manner of binding between the two imidazole rings (**Figure 1.3.3**). The 1,4′-isomer, which has the C–N bond between the 1- and 4′-positions of the two imidazole rings, exhibits photochromism similar to that of the 1,2′-isomer. The thermal back reaction of TPIR at high temperature affords the 2,4′-isomer, which exhibits thermochromism. Conversely, the 2,2′- and 4,4′-isomers, which have C–C bonds between the two imidazole rings, are obtained at low temperature.[91,104–106] The 2,2′-isomer of HABI exhibits piezochromism; the powdered 2,2′-isomer changes color from pale blue to purple when exposed to friction and under high-pressure conditions. The chemical properties of the 4,4′-isomer have not yet been investigated because of its thermal instability. It has been reported that the 2,2′- and 4,4′-isomers are thermally isomerized to the 1,2′-isomer via TPIR when dissolved in solvent at room temperature. The isomerization behaviors of HABI suggest that the activation energy for the dimerization reaction of two TPIR molecules to the 1,2′-isomer is greater than that for two TPIR molecules to the 2,2′- or 4,4′-isomers, because the 2,2′- and 4,4′-isomers are obtained at low temperatures.

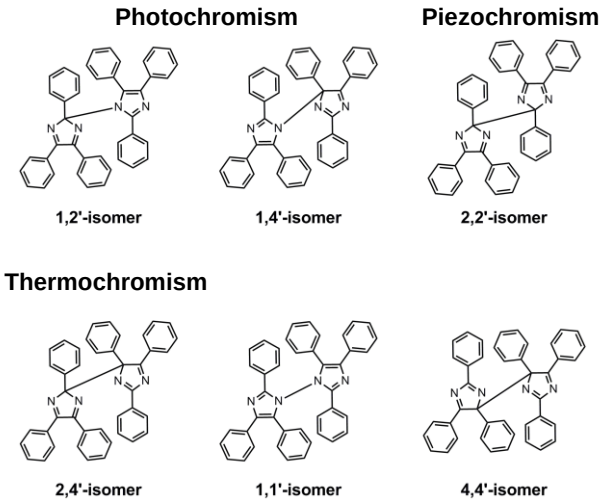

Figure 1.3.3. Structural isomers of HABI.

1.4. Bridged imidazole dimers

1.4.1. Photochromism of bridged imidazole dimers

As described in Section 1.3, the thermal back reaction of TPIR takes several minutes because of the diffusion of TPIR in the medium. Because it is a diffusion-limited reaction, the suppression of diffusion of two TPIR units by connecting them with a molecular linker accelerates the thermal back reaction. Thus, [2.2]paracyclophane ([2.2]PC)-bridged imidazole dimer, was developed (**Scheme 1.4.1**).[107] [2.2]PC-bridged imidazole dimer undergoes instantaneous coloration from colorless to blue upon UV light irradiation and rapid fading in the dark with a half-life of 33 ms in benzene solution at 25 °C (**Figures 1.4.1 and 1.4.2**), which is greatly accelerated compared to HABI systems. The absorption band in the NIR region is attributed to an intramolecular radical–radical interaction due to the spacial proximity of the two radicals. The fast photochromism of the [2.2]PC-bridged imidazole dimer demonstrates that suppression of the diffusion of two imidazolyl radicals is a rational strategy for accelerating the photochromism of HABI.

Scheme 1.4.1. Photochromism of *pseudogem*-bisDPI[2.2]PC.

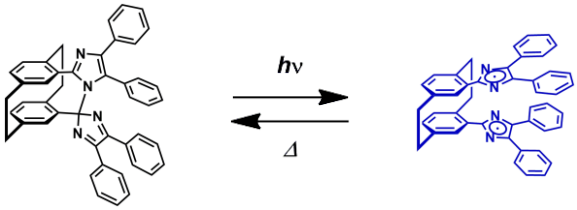

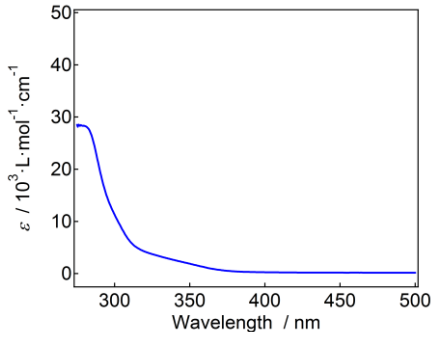

Figure 1.4.1. UV-vis absorption spectrum of *pseudogem*-bisDPI[2.2]PC in degassed benzene.

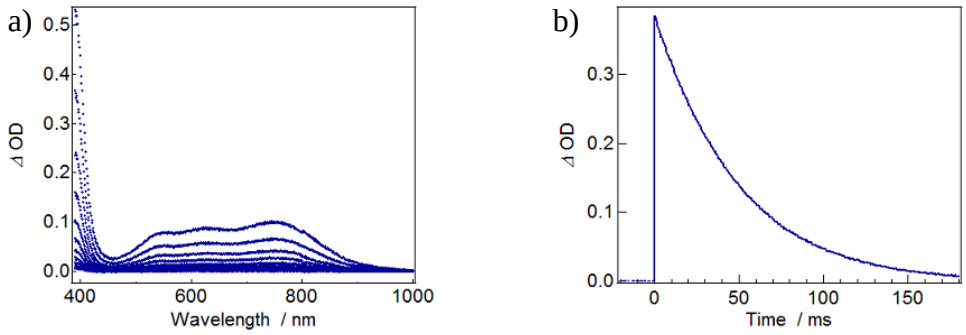

Figure 1.4.2. a) Transient absorption spectra and b) decay profile monitored at 400 nm for the biradical species generated from *pseudogem*-bisDPI[2.2]PC in degassed benzene (2.1×10^{-5} M) at 298 K after irradiation with 355 nm UV light.

Although the [2.2]PC-bridged imidazole dimer has excellent photochromic properties (i.e., a moderate rate constant for the thermal-back reaction, a high quantum yield, and high versatility as described in next section), six steps are required to synthesize only the [2.2]PC-bridging unit. On the other hand, the 1,1′-binaphthol (BINOL)-bridged imidazole dimer (bisTPI-BNE) can be synthesized in just three steps from BINOL as the starting material.[108] A benzene solution of bisTPI-BNE (**Scheme 1.4.2**) exhibits instantaneous coloration and rapid fading in the dark similar to that observed for the [2.2]PC-bridged imidazole dimer, despite the high degree of freedom in the biradical state (**Figure 1.4.4** and **1.4.5**). The biradical of bisTPI-BNE has a half-life of 38 ms at 25 °C, and its absorption spectrum includes intense and weak absorption bands near 600 and 800 nm, respectively. The presence of the weak absorption band in the NIR region suggests that the radical–radical interaction between the two imidazolyl radicals is weak compared to that in the [2.2]PC-bridged imidazole dimer.[109]

Scheme 1.4.2. Photochromism of bis-TPI-BNE.

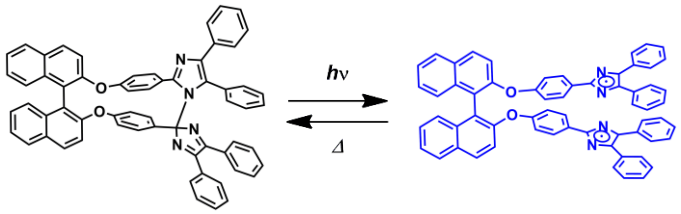

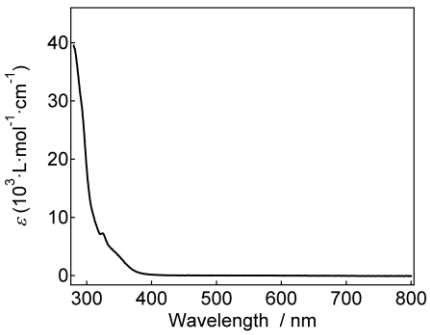

Figure 1.4.3 UV-Vis absorption spectrum of bisTPI-BNE in degassed benzene.

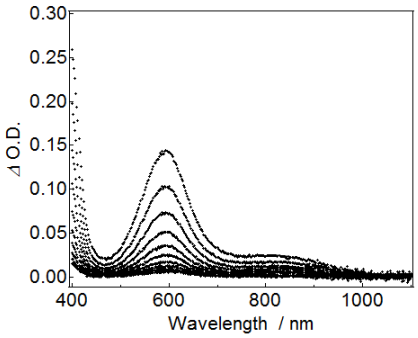

Figure 1.4.4 Transient absorption spectra of the biradical species generated from bisTPI-BNE in degassed benzene (2.1×10^{-5} M) at 298 K after irradiation with 355-nm UV light.

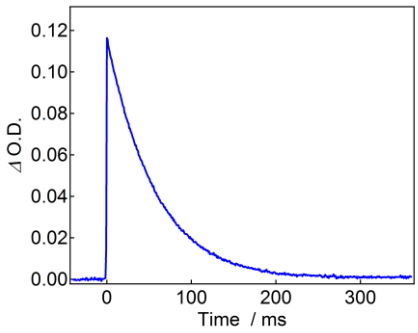

Figure 1.4.5 Decay profile at 400 nm of the biradical species generated from bisTPI-BNE in benzene (2.1×10^{-5} M) after irradiation with 355 nm UV light.

1.4.2. Functionalization of bridged imidazole dimers

A wide variety of [2.2]PC-bridged imidazole dimers have been reported, and it has been demonstrated that the color of the biradical species and the rate of the thermal back reaction can be controlled by introducing different substituents. For example, the thermal back reaction of the *pseudogem*-DPIPI[2.2]PC derivative, which has a phenanthroimidazole unit instead of a diphenyl imidazole unit, is greatly accelerated because of steric repulsion. The half-life of the biradical species generated from *pseudogem*-DPIPI[2.2]PC is 35 μs at 25 °C in benzene (**Scheme 1.4.3a**).[110] Conversely, the color of the biradical species can be modified from blue to black by substituting a pyrenyl group in the [2.2]PC-bridged imidazole dimer (**Scheme 1.4.3b**).[111] The origin of the color change is explained by intramolecular charge transfer (CT) from the electron donating pyrenyl moiety to the imidazole ring.

Scheme 1.4.3. Molecular structures of derivatives of the [2.2]PC-bridged imidazole dimer.

a) *pseudogem*-DPIPI[2.2]PC

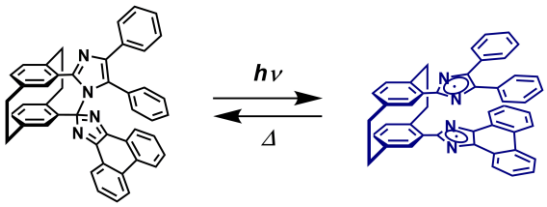

b) *pseudogem*-PPIDPI[2.2]PC

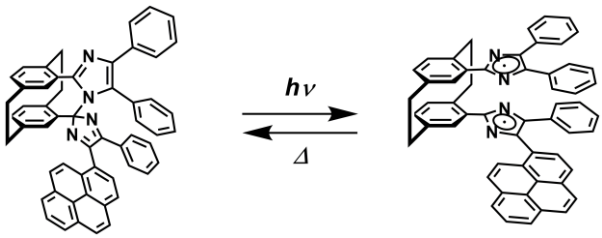

The BINOL-bridged imidazole dimer has axial chirality caused by the BINOL unit. BisCPDPI-BNE (**Scheme 1.4.4**) can be synthesized from the enantiomers of BINOL with retention of chirality (**Scheme 1.4.5**). The enantiomers of bisCPDPI-BNE exhibit large CD signals in the UV region in acetonitrile solution (**Figure 1.4.6a**). Moreover, the chirality of bisCPDPI-BNE is completely retained before and after the photochromic reaction (**Figure 1.4.6b**), and bisCPDPI-BNE has high fatigue resistance.

Scheme 1.4.4. Photochromism of bisCPDPI-BNE.

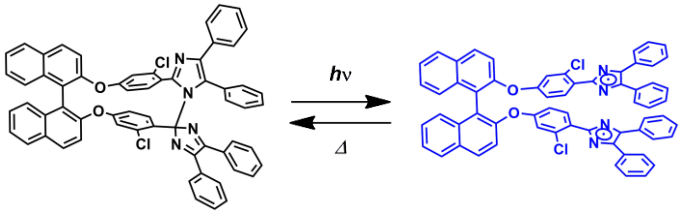

Scheme 1.4.5. Synthesis of the (S)-enantiomer of bisCPDPI-BNE with retention of the initial chirality.

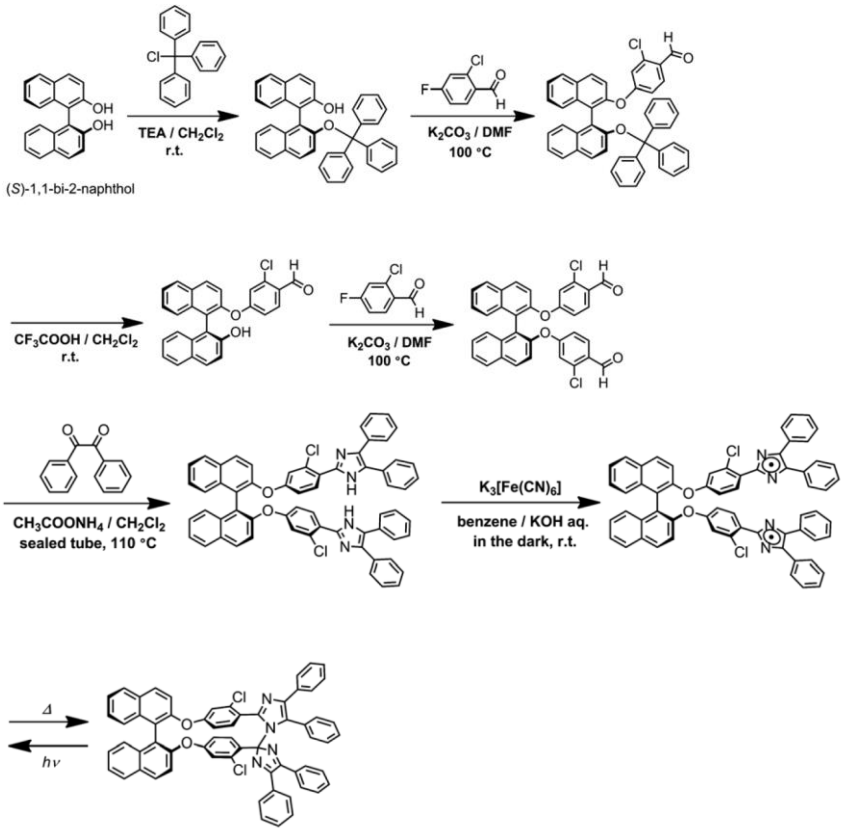

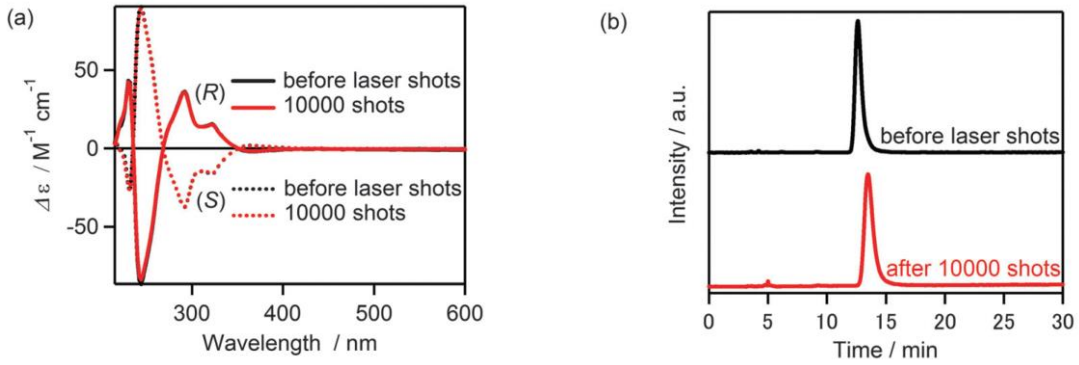

Figure 1.4.6 (a) CD spectra of (R)-bisCPDPI-BNE (solid lines) and (S)-bisCPDPI-BNE (dashed lines) in acetonitrile (3.3×10^{-5} M) at room temperature. The red and black lines indicate the spectra before and after laser shots, respectively. (b) Chiral HPLC chromatograms of (S)-bisCPDPI-BNE before (black) and after 10 000 shots (red) of nanosecond laser pulses (355 nm; pulse width, 5 ns; power, 4 mJ per pulse) at 25 °C. Both optical purities were 99% ee.

The fast photochromic properties of bridged imidazole dimers have been extended to polymeric and organogel materials (**Figure 1.4.7a and b**). Furthermore, real-time holography and fluorescence switching using bridged imidazole dimers have also been achieved (**Figure 1.4.7c and d**).[112–117] A polymer containing a fast photochromic bridged imidazole dimer enabled the real-time switching of the refractive index induced by the structural changes of the molecules following light irradiation. Real-time 3D holography was then achieved using the fast photochromic polymer film.[113,114] (**Figure 1.4.7c**). Separately, a fluorescence switch was achieved using Förster resonance energy transfer (FRET) from the fluorophore to the biradical species generated from a bridged imidazole dimer (**Figure 1.4.7d**).[115] These results demonstrate that fast photochromism using bridged imidazole dimers has the potential to contribute to various scientific and technological fields.

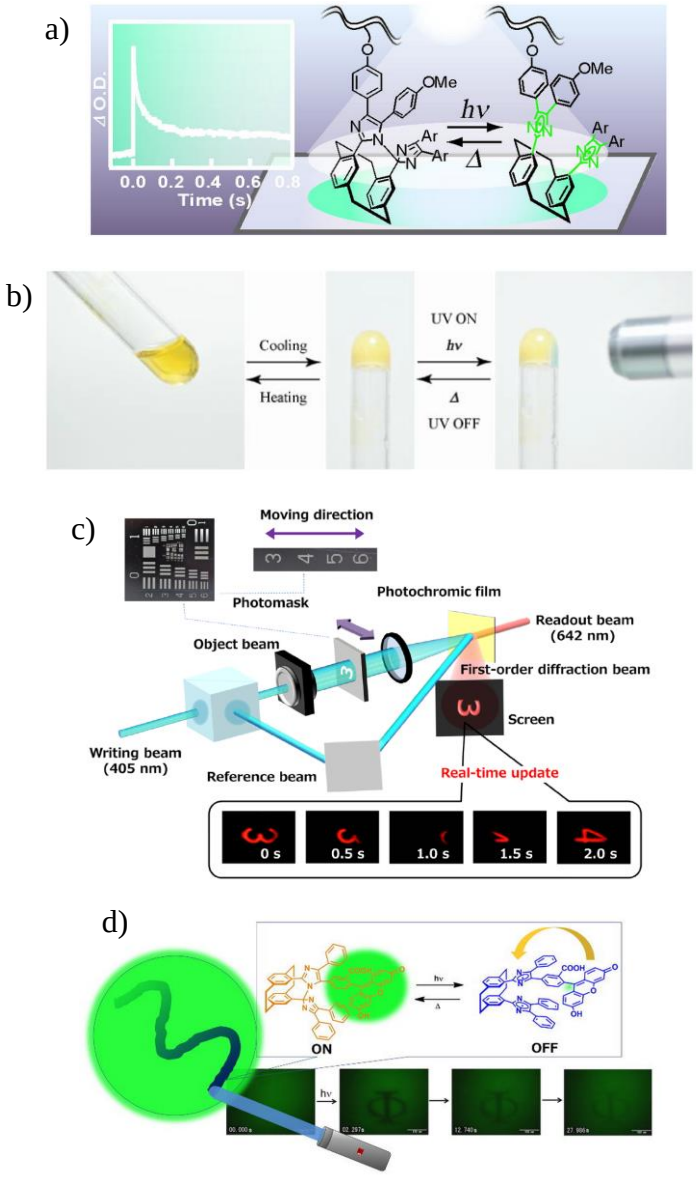

Figure 1.4.7 a) Illustration of a fast photochromic polymer (Kimoto, A.; Tokita, A.; Horino, T.; Oshima, T.; Abe, J. *Macromolecules* **2010**, *43*, 3764–3769; copyright (2011) American Chemical Society.) b) Photographic images of a fast photochromic gel system in cyclohexane. Reproduced from Ref. 116 with permission from Elsevier B. V. c) Optical setup for real-time holographic recording and development of 2D holographic images. d) Illustration of fast fluorescence switching (Mutoh, K.; Sliwa, M.; Abe, J. *J. Phys. Chem. C* **2013**, *117*, 4808–4814.).

1.4.3. Pentaarylbiimidazole and phenoxyl-imidazolyl radical complexes

Recently, pentaarylbiimidazole (PABI) was developed on the basis of the affinity of the reactivity of quinodimethane for the imidazolyl radical.[118,119] The molecular structure of PABI is similar to that of *o*-quinodimethane and contains a phenyl ring substituted by two imidazole rings at the *o*-positions (**Scheme 1.4.7**). The 1,2′-isomer isomer of PABI is the thermally stable, colorless isomer and exhibits photochromism. Solutions of PABI change from colorless to greenish-blue upon UV irradiation (**Figure 1.4.8**).[120] Transient spectra of several derivatives of PABI are shown in **Figure 1.4.8a**. These transient species have large absorption bands in the 700–800 nm range, and their spectral shapes are quite different from those reported for imidazole dimers. This absorption band is attributed to the radical–radical interaction according to DFT calculations. This result suggests that the radical–radical interactions of transient species of PABI are stronger than those of other bridged imidazole dimers.

Scheme 1.4.7. Photochromism of PABIs

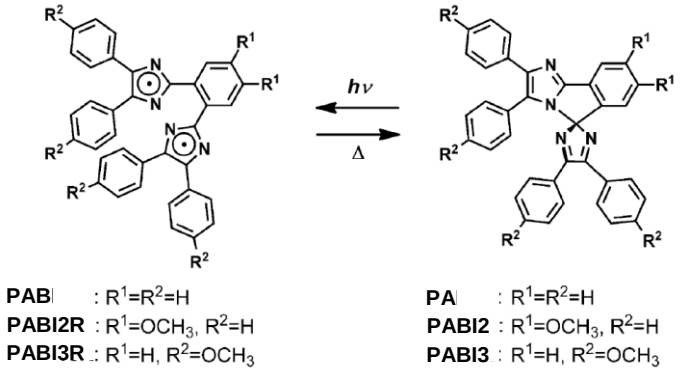

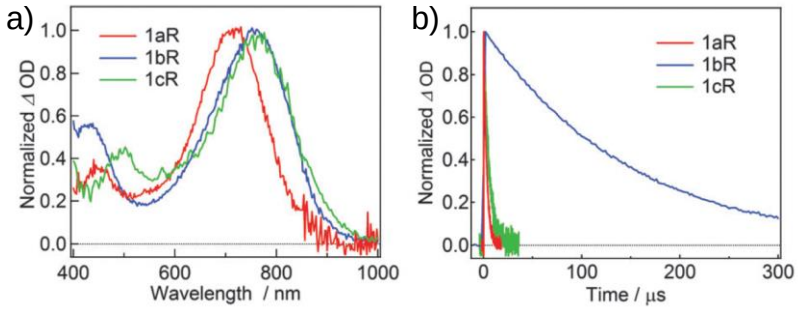

Figure 1.4.8. (a) Transient absorption spectra for the colored species 1a, 1b, and 1c in degassed benzene. The spectral shapes do not change during the decay processes. (b) Decay profiles for the colored species 1a, 1b, and 1c in degassed benzene at 25 °C (excitation wavelength, 355 nm; pulse width, 5 ns; power: 4 mJ per pulse; concentrations of 1a, 1b, and 1c: 3.1×10^{-4} M, 2.6×10^{-4} M, and 3.3×10^{-4} M, respectively).

On the other hand, phenoxyl imidazolyl radical complex (PIC), which has a phenoxyl radical unit instead of the diphenylimidazolyl radical unit of PABI, was developed by focusing on the similarity of the reactivities of imidazolyl and phenoxyl radicals (**Scheme 1.4.8 and 1.4.9**).[121] The colorless isomer of PIC has a C–N bond between the 1-position of the imidazole ring and the 4-position of the phenoxyl moiety. PIC also exhibits photochromism similar to that of PABI. In other words, solutions of PIC change from colorless to greenish-blue upon UV irradiation (**Figure 1.4.9a-d**). In addition, the rates of the thermal back reaction of PIC systems can be tuned from nanoseconds to seconds by varying the substituents (**Figure 1.4.9e**). This tunability may be useful in several applications. For example, photochromic lenses require thermal back reactions on the order of seconds, whereas security systems using fast photoswitches requires rates ranging from tens of μs to ms. Moreover, the imidazole ring of the colorless isomer of PIC is a 6π-electron system, whereas PABIs and bridged imidazole dimers have two structural isomers depending on which imidazole ring is the 6π-electron system and which is the 4π-electron system. Furthermore, PIC is the first example of a radical dissociation-type photochromic compound that generates two nonequivalent radicals.

Scheme 1.4.8. Oxidation and dimerization of imidazolyl and the phenoxyl radicals.

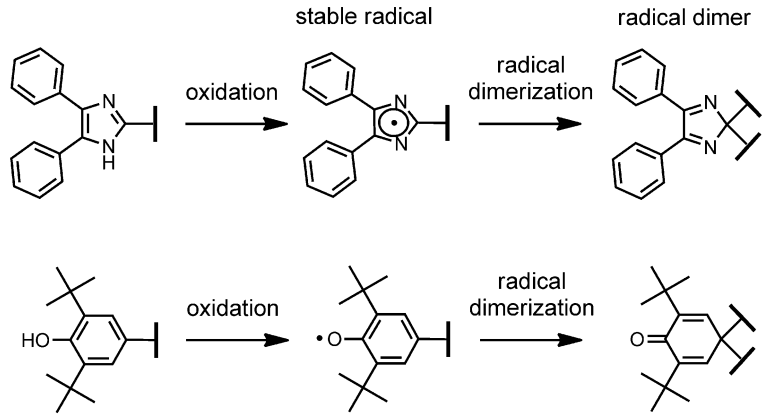

Scheme 1.4.9. Molecular structures of PIC derivatives

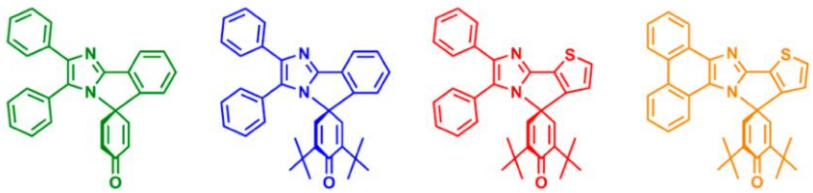

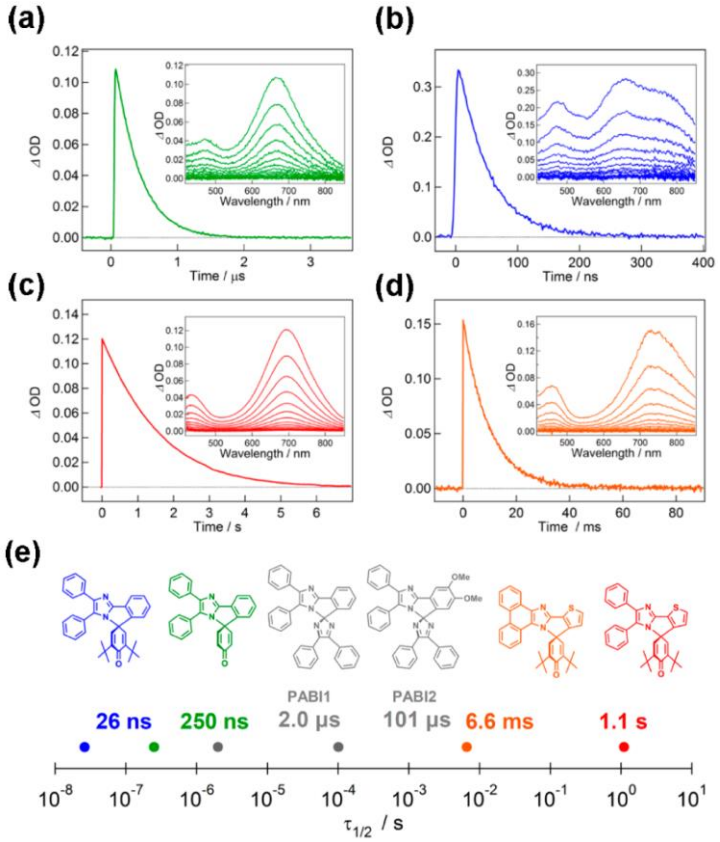

Figure 1.4.9. Decay profiles for the open-ring isomers of (a) PIC1, (b) PIC2, (c) PIC3, and (d) PIC4 in degassed benzene at 25 °C (excitation wavelength, 355 nm; pulse width, 5 ns; power, 4 mJ/pulse; concentrations of PIC1, PIC2, PIC3, and PIC4: 1.0×10^{-3}, 1.0×10^{-3}, 6.1×10^{-5}, and 2.4×10^{-5} M, respectively). Insets of panels a−d show transient absorption spectra for the open-ring isomers of PIC1−4, respectively. (e) Plot of the half-lives of the open-ring isomers of PIC and PABI derivatives on a logarithmic time scale.

1.5. Scope of this thesis

Although standard photochromic compounds have potential applications in the various fields of science and technology, the photochromism of macroscale structures, such as concentrated films, aggregates, and crystals, can be initiated only at the surface because of the reabsorption of the excitation light by photogenerated colored species. Conversely, negative photochromism can be initiated deeper inside these materials, which would greatly increase the contrast and eventually increase the total reaction efficiency. Therefore, negative photochromic molecules will open up novel potential applications for photochromic compounds. However, fast negative photochromic compounds have not yet been reported. To achieve fast negative photochromism, it is necessary to systematically understand negative photochromic compounds and their reactions. The colored isomers of BN-bridged imidazole dimers have unusual structures, and BN-bridged imidazole dimers exhibit unique negative photochromism. Although the half-lives of these colorless isomers are approximately 2 min at room temperature and longer than the half-lives of the colored isomer of another reported bridged imidazole dimer, we proposed that varying the functionality of BN-bridged imidazole dimers would allow tuning of the rate of the thermal back reaction through appropriate design of their molecular frameworks and enable fast negative photochromism.

The purpose of this study was therefore to develop fast negative photochromic molecules and investigate the photochromism of BN-bridged imidazole dimers. The photochromism of BN-bridged imidazole dimers is completely different from other bridged imidazole dimers because of the bridging unit. Thus, the use of similar types of bridging units, such as biphenyl unit and 1-phenylnaphthalene units, provides an opportunity for elucidation of the mechanism of photochromism in BN-bridged imidazole dimers. Furthermore, the acceleration of the thermal back reaction can be achieved through substitution of the phenyl groups at the 4- and 5-positions of the imidazole rings or introduction of phenoxyl units in place of the imidazole rings. The development of fast negative photochromic molecules would be advantageous for applications that require fast switching and high conversion efficiencies, such as a photomechanical materials and real-time holography.

This thesis comprises 4 chapters. Chapter 2 describes the photochromism of biphenyl (BP)-bridged imidazole dimer. When first synthesized, BP-bridged imidazole dimer was not considered to show photochromism because of the large reaction rate constants for its thermal back reaction. Femtosecond and nanosecond transient absorption spectroscopies revealed the photoresponsive property of BP-bridged imidazole dimer. Notably, this material is the first example which revealed of the 2,2′-isomer of imidazole dimer shows photochromism. The 2,2′-isomer of HABI is thermally unstable; therefore,

its photochromic property has not been observed.

Chapter 3 is concerned with the multistate photochromism of 1-phenylnaphthalene (PN)-bridged imidazole dimer. PN-bridged imidazole dimer has five isomers: the 2,2′-isomer, two types of 1,2′-isomers, the colored isomer, and the biradical. The 2,2′-isomer thermally isomerizes to the metastable colored isomer, and the colored isomer converts to the thermal stable 1,2′-isomer upon heating. The biradical is generated upon light irradiation of the 2.2′-isomer, the colored isomer, and the 1,2′-isomer. The main product of the thermal back reaction of the biradical is the 2,2′-isomer. Thus, the photochromism of PN-bridged imidazole dimer can be explained as sequential isomerization of 2,2′-isomer to 1,2′-isomer via metastable colored isomer, and this overall reaction can be reset using light irradiation.

Chapter 4 describes the fast photochromism of BN-bridged phenoxyl imidazolyl radical complexes (BN-PICs). BN-PICs have molecular structures with both phenoxyl and imidazole moieties, rather than two imidazole units and exhibit negative photochromism like BN-bridged imidazole dimers. The half-life of the BN-PIC derivative with a phenantroimidazole moiety is 1.9 s in benzene at 25 °C. This thermal back reaction is the fastest in reported negative photochromic molecules. In addition, BN-PICs have axial chirality derived from the BN unit. The enantiomers of BN-PICs exhibit large CD spectra in acetonitrile, and the rate constants for the thermal back reactions from the colorless to the colored isomers in (S)- and (R)-1-phenylethanol are different. These results suggest that BN-PICs undergo fast and high contrast changes in their CD spectra. The photochromism of BN-PICs may thus enable the development of new materials with fast switching and high conversion efficiencies in photostationary states.

1.6. References

(1) Bouas-Laurent, H.; Dürr, H. *Pure Appl. Chem.* **2001**, *73*, 639.

(2) Irie, M. *Chem. Rev.* **2000**, *100*, 1685.

(3) Yokoyama, Y. *Chem. Rev.* **2000**, *100*, 1717.

(4) Kose, M.; Shinoura, M.; Yokoyama, Y.; Yokoyama, Y. *J. Org. Chem.* **2004**, *69*, 8403.

(5) Irie, M.; Fukaminato, T.; Matsuda, K.; Kobatake, S. *Chem. Rev.* **2014**, 12174.

(6) Jean-Ruel, H.; Cooney, R. R.; Gao, M.; Lu, C.; Kochman, M. a.; Morrison, C. a.; Miller, R. J. D. *J. Phys. Chem. A* **2011**, *115*, 13158.

(7) Ishibashi, Y.; Umesato, T.; Kobatake, S.; Irie, M.; Miyasaka, H. *J. Phys. Chem. C* **2012**, *116*, 4862.

(8) Kobatake, S.; Takami, S.; Muto, H.; Ishikawa, T.; Irie, M. *Nature* **2007**, *446*, 778.

(9) Kitagawa, D.; Nishi, H.; Kobatake, S. *Angew. Chem. Int. Ed.* **2013**, *52*, 9320.

(10) Kitagawa, D.; Kobatake, S. *J. Phys. Chem. C* **2013**.

(11) Uchida, K.; Nishikawa, N.; Izumi, N.; Yamazoe, S.; Mayama, H.; Kojima, Y.; Yokojima, S.; Nakamura, S.; Tsujii, K.; Irie, M. *Angew. Chem. Int. Ed.* **2010**, *49*, 5942.

(12) Nishikawa, N.; Sakiyama, S.; Yamazoe, S.; Kojima, Y.; Nishihara, E. I.; Tsujioka, T.; Mayama, H.; Yokojima, S.; Nakamura, S.; Uchida, K. *Langmuir* **2013**, *29*, 8164.

(13) Nishikawa, N.; Kiyohara, H.; Sakiyama, S.; Yamazoe, S.; Mayama, H.; Tsujioka, T.; Kojima, Y.; Yokojima, S.; Nakamura, S.; Uchida, K. *Langmuir* **2012**, *28*, 17817.

(14) Nishikawa, N.; Mayama, H.; Nonomura, Y.; Fujinaga, N.; Yokojima, S.; Nakamura, S.; Uchida, K. *Langmuir* **2014**, *1*.

(15) Gilat, S. L.; Kawai, S. H.; Lehn, J.-M. *Chem. – Eur. J.* **1995**, *1*, 275.

(16) Matsuda, K.; Yamaguchi, H. *J. Phys. Chem. C* **2008**, *112*, 17005.

(17) Hayakawa, R.; Petit, M.; Higashiguchi, K.; Matsuda, K.; Chikyow, T.; Wakayama, Y. *Org. Electron.* **2015**, *21*, 149.

(18) Arai, K.; Kobayashi, Y.; Abe, J. *Chem. Commun.* **2015**, *51*, 3057.

(19) Kosa, T.; Sukhomlinova, L.; Su, L.; Taheri, B.; White, T. J.; Bunning, T. J. *Nature* **2012**, *485*, 347.

(20) Sousa, C. M.; Berthet, J.; Delbaere, S.; Coelho, P. J. *J. Org. Chem.* **2012**, *77*, 3959.

(21) Queiroz, M.-J. R. P.; Dubest, R.; Aubard, J.; Faure, R.; Guglielmetti, R. *Dye. Pigment.* **2000**, *47*, 219.

(22) Berkovic, G.; Krongauz, V.; Weiss, V. *Chem. Rev.* **2000**, *100*, 1741.

(23) Nerbonne, J. M.; Weiss, R. G. *J. Am. Chem. Soc.* **1978**, *100*, 5953.

(24) Cembran, A.; Bernardi, F.; Garavelli, M.; Gagliardi, L.; Orlandi, G. *J. Am. Chem. Soc.* **2004**, *126*, 3234.
(25) Crecca, C. R.; Roitberg, A. E. *J. Phys. Chem. A* **2006**, *110*, 8188.
(26) Fujino, T.; Arzhantsev, S. Y.; Tahara, T. *Bull. Chem. Soc. Jpn.* **2002**, *75*, 1031.
(27) Garcia-Amorós, J.; Bučinskas, A.; Reig, M.; Nonell, S.; Velasco, D. *J. Mater. Chem. C* **2014**, *2*, 474.
(28) Garcia-Amorós, J.; Reig, M.; Castro, M. C. R.; Cuadrado, A.; Raposo, M. M. M.; Velasco, D. *Chem. Commun.* **2014**, *50*, 6704.
(29) Garcia-Amorós, J.; Sánchez-Ferrer, A.; Massad, W. a; Nonell, S.; Velasco, D. *Phys. Chem. Chem. Phys.* **2010**, *12*, 13238.
(30) Kawamoto, M.; Shiga, N.; Takaishi, K.; Yamashita, T. *Chem. Commun.* **2010**, *46*, 8344.
(31) Yu, Y.; Nakano, M.; Ikeda, T. *Nature* **2003**, *425*, 145.
(32) Yamada, M.; Kondo, M.; Mamiya, J.-I.; Yu, Y.; Kinoshita, M.; Barrett, C. J.; Ikeda, T. *Angew. Chem. Int. Ed.* **2008**, *47*, 4986.
(33) Yamamoto, T.; Hasegawa, M.; Kanazawa, A.; Shiono, T.; Ikeda, T. *J. Phys. Chem. B* **1999**, *103*, 9873.
(34) Finkelmann, H.; Nishikawa, E.; Pereira, G. G.; Warner, M. *Phys. Rev. Lett.* **2001**, *87*, 015501.
(35) Meier, W.; Finkelmann, H. *Macromolecules* **1993**, *26*, 1811.
(36) Ichimura, K. *Chem. Rev.* **2000**, *100*, 1847.
(37) Seki, T.; Sakuragi, M.; Kawanishi, Y.; Tamaki, T.; Fukuda, R.; Ichimura, K.; Suzuki, Y. *Langmuir* **1993**, *9*, 211.
(38) Aoki, K.; Seki, T.; Suzuki, Y.; Tamaki, T.; Hosoki, A.; Ichimura, K. *Langmuir* **1992**, *8*, 1007.
(39) Kawanishi, Y.; Tamaki, T.; Seki, T.; Sakuragi, M.; Ichimura, K. *Mol. Cryst. Liq. Cryst. Sci. Technol. Sect. A. Mol. Cryst. Liq. Cryst.* **1992**, *218*, 153.
(40) Ichimura, K.; Seki, T.; Hosokit, A.; Aoki, K. *Langmuir* **1988**, *1216*, 1214.
(41) Seki, T.; Takashi Tamaki; Ichimura, K.; Aoki, K. *Macromolecules* **1989**, *22*, 3505.
(42) Ichimura, K.; Morino, S.; Akiyama, H. *Appl. Phys. Lett.* **1998**, *73*, 921.
(43) Denekamp, C.; Feringa, B. *Adv. Mater.* **1998**, 1080.
(44) Tanaka, D.; Ishiguro, H.; Shirasu, T.; Okuda, D. *Mol. Cryst. Liq. Cryst.* **2014**, *594*, 105.
(45) Hori, R.; Furukawa, D.; Yamamoto, K.; Kutsumizu, S. *Chem. – Eur. J.* **2012**, 7346.
(46) Kucharski, T. J.; Ferralis, N.; Kolpak, A. M.; Zheng, J. O.; Nocera, D. G.; Grossman, J. C. *Nat. Chem.* **2014**, *6*, 441.
(47) Uchida, E.; Azumi, R.; Norikane, Y. *Nat. Commun.* **2015**, *6*, 7310.

(48) Tamesue, S.; Takashima, Y.; Yamaguchi, H.; Shinkai, S.; Harada, A. *Angew. Chem. Int. Ed.* **2010**, *49*, 7461.
(49) Irie, M.; Kato, M. *J. Am. Chem. Soc.* **1985**, *107*, 1024.
(50) Kobayashi, M.; Takashima, A.; Ishii, T.; Naka, H.; Uchiyama, M. *Inorg. Chem. Commun.* **2007**, *46*, 1039.
(51) Safin, D. a.; Bolte, M.; Garcia, Y. *CrystEngComm* **2014**, *16*, 5524.
(52) Peng, P.; Strohecker, D.; Liao, Y. *Chem. Commun.* **2011**, *47*, 8575.
(53) Takase, M.; Inouye, M. *Chem. Commun.* **2001**, 2432.
(54) Andersson, J.; Li, S.; Lincoln, P.; Andréasson, J. *J. Am. Chem. Soc.* **2008**, *130*, 11836.
(55) Sunamoto, J.; Iwamoto, K.; Akutagawa, M.; Nagase, M.; Kondo, H. *J. Am. Chem. Soc.* **1982**, *104*, 4904.
(56) Ciardelli, F.; Fabbri, D.; Pieroni, O.; Fissi, A. *J. Am. Chem. Soc.* **1989**, *111*, 3470.
(57) Inoue, E.; Kokado, H.; Shimizu, I.; Kobayashi, H.; Takahashi, Y. *Bull. Chem. Soc. Jpn.* **1972**, *45*, 1951.
(58) Namba, K.; Suzuki, S. *Bull. Chem. Soc. Jpn.* **1975**, *48*, 1323.
(59) Yokoyama, Y.; Shiroyama, T. *Chem. Lett.* **1995**, *24*, 71.
(60) Keum, S. R.; Roh, S. J.; Kim, S. E.; Lee, S. H.; Cho, C. H.; Kim, S. H.; Koh, K. N. *Bull. Korean Chem. Soc.* **2006**, *27*, 187.
(61) Sakai, K.; Imaizumi, Y.; Oguchi, T.; Sakai, H.; Abe, M. *Langmuir* **2010**, *26*, 9283.
(62) Shimizu, I.; Kokado, H.; Inoue, E. *Bull. Chem. Soc. Jpn.* **1969**, *42*, 1730.
(63) Yagi, S.; Maeda, K.; Nakazumi, H. *J. Mater. Chem.* **1999**, *9*, 2991.
(64) Pieroni, O.; Fissi, a.; Angelini, N.; Lenci, F. *Acc. Chem. Res.* **2001**, *34*, 9.
(65) Shiraishi, Y.; Itoh, M.; Hirai, T. *Phys. Chem. Chem. Phys.* **2010**, *12*, 13737.
(66) Minami, M.; Taguchi, N. *Chem. Lett.* **1996**, 429.
(67) Ubukata, T.; Takahashi, K.; Yokoyama, Y. *J. Phys. Org. Chem.* **2007**, 981.
(68) Tomasulo, M.; Yildiz, I.; Raymo, F. M. *Inorganica Chim. Acta* **2007**, *360*, 938.
Tanaka, M.; Nakamura, M.; Salhin, M. a; Ikeda, T.; Kamada, K.; Ando, H.; Shibutani, Y.; Kimura, K. *J. Org. Chem.* **2001**, *66*, 1533.
(70) Tanaka, M.; Ikeda, T.; Xu, Q.; Ando, H.; Shibutani, Y.; Nakamura, M.; Sakamoto, H.; Yajima, S.; Kimura, K. *J. Org. Chem.* **2002**, *67*, 2223.
(71) Blattmann, H.-R.; Meuche, D.; Heilbronner, E.; Molyneux, R. J.; Boekelheide, V. *J. Am. Chem. Soc.* **1965**, *1339*, 4.
(72) Mitchell, R. H.; Ward, T. R.; Chen, Y.; Wang, Y.; Weerawarna, S. A.; Dibble, P. W.; Marsella, M. J.; Almutairi, A.; Wang, Z. *J. Am. Chem. Soc.* **2003**, *125*, 2974.
(73) Ayub, K.; Li, R.; Bohne, C.; Williams, R. V.; Mitchell, R. H. *J. Am. Chem. Soc.* **2011**, *133*, 4040.

(74) Ayub, K.; Mitchell, R. H. *J. Org. Chem.* **2014**, *79*, 664.
(75) Muratsugu, S.; Kume, S.; Nishihara, H. *J. Am. Chem. Soc.* **2008**, *130*, 7204.
(76) Kishida, M. A.; Kusamoto, T.; Nishihara, H. *J. Am. Chem. Soc.* **2014**, *136*, 4809.
(77) Roldan, D.; Cobo, S.; Lafolet, F.; Vilà, N.; Bochot, C.; Bucher, C.; Saint-Aman, E.; Boggio-Pasqua, M.; Garavelli, M.; Royal, G. *Chem. – Eur. J.* **2015**, *21*, 455.
(78) Ayub, K.; Zhang, R.; Robinson, S. G.; Twamley, B.; Williams, R. V.; Mitchell, R. H. *J. Org. Chem.* **2008**, *73*, 451.
(79) Williams, R. V.; Edwards, W. D.; Mitchell, R. H.; Robinson, S. G. *J. Am. Chem. Soc.* **2005**, *127*, 16207.
(80) Muratsugu, S.; Kishida, M. A.; Sakamoto, R.; Nishihara, H. *Chem. – Eur. J.* **2013**, *19*, 17314.
(81) Helmy, S.; Leibfarth, F. A.; Oh, S.; Poelma, J. E.; Hawker, C. J.; de Alaniz, J. R. *J. Am. Chem. Soc.* **2014**, *136*, 8169.
(82) Helmy, S.; Oh, S.; Leibfarth, F. A.; Hawker, C. J.; Alaniz, J. R. De. *J. Org. Chem.* **2014**, *79*, 11316.
(83) Fukaminato, T.; Tanaka, M.; Kuroki, L.; Irie, M. *Chem. Commun.* **2008**, 3924.
(84) Fukaminato, T.; Doi, T.; Tanaka, M.; Irie, M. *J. Phys. Chem. C* **2009**, *113*, 11623.
(85) Hatano, S.; Horino, T.; Tokita, A.; Oshima, T.; Abe, J. *J. Am. Chem. Soc.* **2013**, *135*, 3164.
(86) Hayashi, T.; Maeda, K. *Bull. Chem. Soc. Jpn.* **1960**, *33*, 565.
(87) Hayashi, T.; Maeda, K.; Morinaga, M. *Bull. Chem. Soc. Jpn.* **1964**, *37*, 1563.
(88) Maeda, K.; Hayashi, T. *Bull. Chem. Soc. Jpn* **1970**, *45*, 1474.
(89) White, D.; Sonnenberg, J. *J. Am. Chem. Soc.* **1966**, *16*, 3825.
(90) Ueda, H. *J. Phys. Chem.* **1963**, *68*, 1304.
(91) Hayashi, T.; Maeda, K. *Bull. Chem. Soc. Jpn.* **1965**, *45*, 685.
(92) Hayashi, T.; Maeda, K.; Takeuchi, M. *Bull. Chem. Soc. Jpn.* **1964**, *37*, 1717.
(93) Sathe, S. S.; Ahn, D.; Scott, T. F. *Ind. Eng. Chem. Res.* **2015**, *54*, 4203.
(94) WILKS, M. A. J.; WILLIS, M. R. *Nature* **1966**, *212*, 500.
(95) Wilks, M. A. J.; Willis, M. R. *J. Chem. Soc. B Phys. Org.* **1968**, 1526.
(96) Cescon, L. A.; Coraor, G. R.; Dessauer, R.; Silversmith, E. F.; Ueban, E. J. *J. Org. Chem.* **1971**, *36*, 2262.
(97) MacLachlan, A.; Riem, R. H. *J. Org. Chem.* **1971**, *36*, 2275.
(98) Cohen, R. L. *J. Org. Chem.* **1971**, *36*, 2280.
(99) BLANCHET, G. B.; DESSAUER, R. *J. imaging Sci. Technol. 37*, 238.
(100) Caspar, J. V.; Khudyakov, I. V.; Turro, N. J.; Weed, G. C. *Macromolecules* **1995**, *28*, 636.
(101) Dessauer, R. *Photochemistry, History and Commercial Applications of*

Hexaarylbiimidazoles: all about HABIs; Elsevier Ltd, 2006.

(102) Satoh, Y.; Ishibashi, Y.; Ito, S.; Nagasawa, Y.; Miyasaka, H.; Chosrowjan, H.; Taniguchi, S.; Mataga, N.; Kato, D.; Kikuchi, A.; Abe, J. *Chem. Phys. Lett.* **2007**, *448*, 228.

(103) Miyasaka, H.; Satoh, Y.; Ishibashi, Y.; Ito, S.; Nagasawa, Y.; Taniguchi, S.; Chosrowjan, H.; Mataga, N.; Kato, D.; Kikuchi, A.; Abe, J. *J. Am. Chem. Soc.* **2009**, *131*, 7256.

(104) Delbaere, S.; Orio, M.; Berthet, J.; Sliwa, M.; Hatano, S.; Abe, J. *Chem. Commun.* **2013**, *49*, 5841.

(105) Edkins, R. M.; Probert, M. R.; Robertson, C. M.; Howard, J. a. K.; Beeby, A. *RSC Adv.* **2014**, *4*, 5351.

(106) Kawano, M.; Sano, T.; Abe, J.; Ohashi, Y. *Chem. Lett.* **2000**, *9*, 1.

(107) Kishimoto, Y.; Abe, J. *J. Am. Chem. Soc.* **2009**, *131*, 4227.

(108) Iwasaki, T.; Kato, T.; Kobayashi, Y.; Abe, J. *Chem. Commun.* **2014**, *50*, 7481-7484.

(109) Mutoh, K.; Abe, J. *Phys. Chem. Chem. Phys.* **2014**, *16*, 17537.

(110) Harada, Y.; Hatano, S.; Kimoto, A.; Abe, J. *J. Phys. Chem. Lett.* **2010**, *1*, 1112.

(111) Yamashita, H.; Abe, J. *J. Phys. Chem. A* **2011**, *115*, 13332.

(112) Kimoto, A.; Tokita, A.; Horino, T.; Oshima, T.; Abe, J. *Macromolecules* **2010**, *43*, 3764.

(113) Ishii, N.; Kato, T.; Abe, J. *Sci. Rep.* **2012**, *2*, 819.

(114) Ishii, N.; Abe, J. *Appl. Phys. Lett.* **2013**, *102*, 163301.

(115) Mutoh, K.; Sliwa, M.; Abe, J. *J. Phys. Chem. C* **2013**, *117*, 4808.

(116) Takizawa, M.; Kimoto, A.; Abe, J. *Dye. Pigment.* **2011**, *89*, 254.

(117) Mutoh, K.; Abe, J. *Chem. Commun.* **2011**, *47*, 8868.

(118) Flynn, C. R. *J. Am. Chem. Soc.* **1974**, *2144*, 3280.

(119) Doehnert, D.; Koutecky, J. *J. Am. Chem. Soc.* **1980**, *102*, 1789.

(120) Yamashita, H.; Abe, J. *Chem. Commun.* **2014**, *50*, 8468.

(121) Yamashita, H.; Ikezawa, T.; Kobayashi, Y.; Abe, J. *J. Am. Chem. Soc.* **2015**, *137*, 4952.

Chapter 2

Biphenyl-bridged imidazole dimer

2.1 Introduction

Microsecond time scales cover various phenomena such as electronic relaxation processes of triplets and charge transfer states, molecular diffusion, enzyme reactions, folding of proteins, etc. To trigger and precisely control these phenomena by external stimuli, switches are necessary that respond faster than these time scales. Photochromic molecules are the best candidates for such switch molecules because they can modulate various properties such as color, conductivity,[1,2] chirality,[3,4] intermolecular interaction,[5] etc. As compared to the structural changes during the electronic relaxation pathways from the Frank-Condon state to the lowest excited state (S_1), photochromic reactions induce drastic structural changes repeatedly. Therefore, photochromic molecular switches have a potential to produce mechanical work[6–8] and to act as optical logic gate systems to control electronic relaxation processes such as charge transfer and coupling.[9–13] There are some reports on photochromic compounds whose switch cycles at ambient temperature are completed on sub-microsecond time scales such as certain oxazine and azo derivatives.[14,15] The switching materials that show fast photochromism on the ns time scale offer novel applications such as high speed optical actuators[16,17] with MHz repetition frequencies.

We have developed a series of bridged imidazole dimers which act as sub-second to microsecond fast molecular switches.[18–22] However, there are few compounds which act as sub-microsecond photochromic switches in bridged imidazole dimers.[23] In our previous study,[24] we reported that bisDMDPI-BP (Figure 2.1.1a and 2.1.1b) did not give any photochromic signals later than the microsecond time scale while other similar derivatives were reported to exhibit the characteristic negative photochromism. On the other hand, quantum chemical calculations of bisDMDPI-BP suggest a similarity of bisDMDPI-BP to the reported photochromic imidazole dimers. The quantum chemical calculations of the reported photochromic imidazole dimers suggest that the C–N bond between the two imidazole rings has an anti-bonding character in the LUMO (Figure 2.1.1b, DFT MPW1PW91/6-31G(d) level).[25] The calculations of bisDMDPI-BP also suggest that the C–C bond between the two imidazole rings has an anti-bonding character in the LUMO. This similarity implicitly suggests that bisDMDPI-BP is very likely to show photoinduced

bond cleavage of the C–C bond between the two imidazole rings as similar processes as the reported photochromic imidazole dimers.

In this Chapter, the author applies sub-picosecond and sub-microsecond transient absorption spectroscopy to reveal the photochromism of bisDMDPI-BP. The author found that bisDMDPI-BP indeed undergoes the expected ring opening (Figure. 2.1.1a) and is one of the fastest photochromic compounds, with the ring opening within 1 ps and a thermal lifetime of the open form of ~100 ns. The fast and large conformational change of bisDMDPI-BP offers great potential for a molecular device to produce large mechanical work and for a trigger to induce a local conformational change to macromolecular and biological organizations.

Imidazole dimers are categorized into several isomers depending on the binding manner between two imidazole rings. BisDMDPI-BP is the 2,2′-isomer, in which the C–C bond is formed between the 2-position of an imidazole ring and the 2′-position of the other imidazole ring,[24] while almost all reported bridged imidazole dimers are the 1,2′- or the 1,4′-isomers, in which a C–N bond is formed between the two imidazole rings.[18,20,21,26] While there are several reports on the 2,2′-isomers of hexaarylbiimidazole (HABI) derivatives,[27,28] they are sensitive to temperature and pressure, and easily converted to the photochromic 1,2′-isomers via the imidazolyl radical formed by thermochromism or piezochromism. Therefore, the stable 2,2′-isomer of bisDMDPI-BP offers a unique opportunity to reveal the photochromism of a representative 2,2′-isomer.

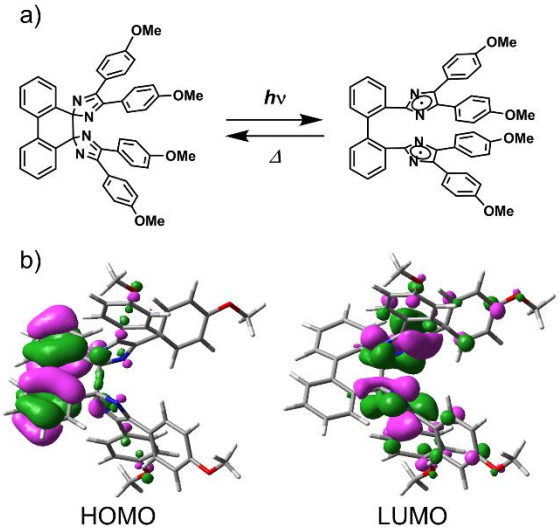

Figure 2.1.1. (a) Photochromism and (b) the relevant molecular orbitals of bisDMDPI-BP obtained by the MPW1PW91/6-31G(d) level of theory.

2.2 UV-vis absorption spectrum

The steady-state absorption spectrum of bisDMDPI-BP is shown in Figure 2.2.1. The absorbance of bisDMDPI-BP increases rapidly at wavelengths shorter than ~370 nm. Prior to time-resolved experiments, the author examined the durability of bisDMDPI-BP by repetitive exposures to ns laser pulses. The absorption spectra and HPLC analyses reveal that bisDMDPI-BP almost does not decompose even after 10,000 laser shots under an O_2 atmosphere (Figure 2.2.2 and 2.2.3). It shows that bisDMDPI-BP has high durability and the decomposition during the laser experiments is negligible. The author set the excitation wavelength to 305 nm for ns and 310 nm for fs transient absorption measurements. The details of the experimental setup were reported previously[29,30]

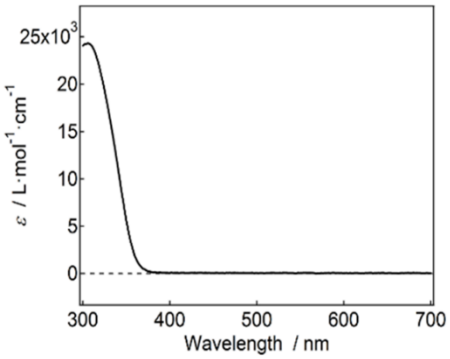

Figure 2.2.1. UV-vis absorption spectrum of bisDMDPI-BP in benzene at room temperature.

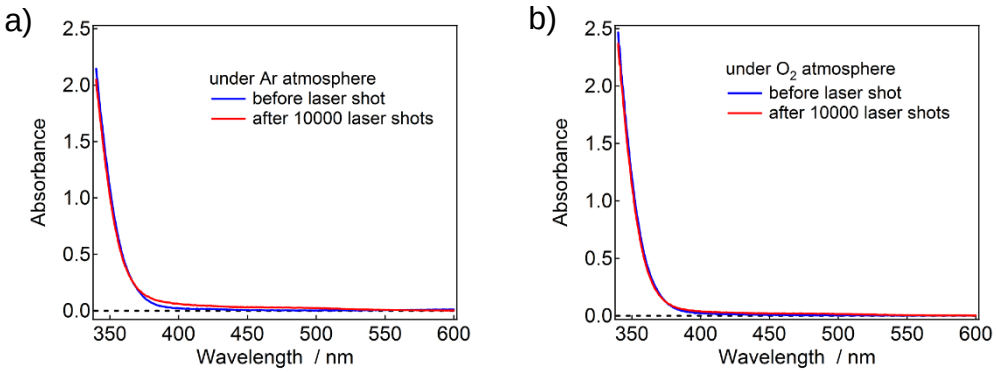

Figure 2.2.2. UV-vis absorption spectra of bisDMDPI-BP in benzene before and after 10,000 laser shots (355 nm, pulse duration, 5 ns; power, 8 mJ) under a) Ar (1.9×10^{-4} M) and b) O_2 atmospheres (2.2×10^{-4} M). The blue and red lines show the spectra before and after laser irradiation, respectively.

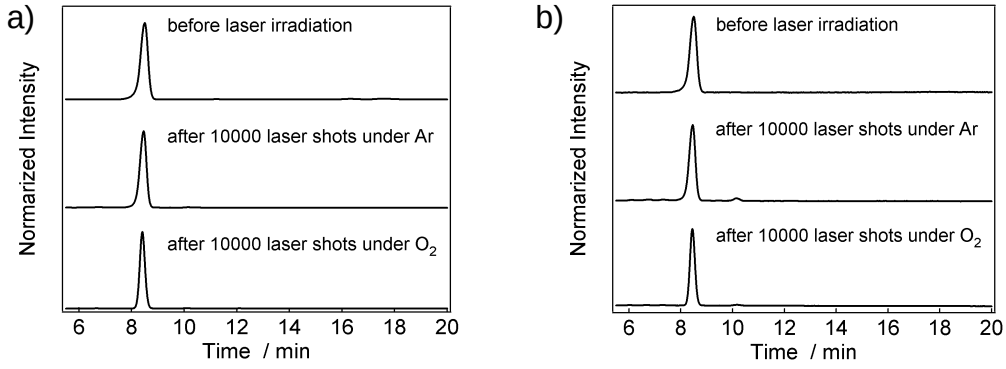

Figure 2.2.3. HPLC chromatograms of bisDMDPI-BP before 355 nm laser shot (upper line), after 10,000 laser shots in Ar (middle line) and O_2 atmospheres (bottom line) in benzene. The HPLC analysis was performed using a reverse phase column (eluent, H_2O/acetonitrile = 1/4; flow rate, 1 mL/min; detected at a) 254 and b) 365 nm.

2.3 Nanosecond transient absorption spectra

Figure 2.3.1a shows ns transient absorption spectra of bisDMDPI-BP at different time delays at room temperature (~20 °C). The author observed two absorption bands at ~380 and 595 nm superimposed on a broad background, and the whole spectrum decays exponentially. The transient spectrum is very similar to those of the radical species of bridged imidazole dimers reported previously.[21,24] The quantum chemical calculations suggest that the absorption band at 550–650 nm can be attributed to the π–π* like transition (Figure 2.3.4 and 2.3.5). In addition, the calculations also suggest that the dihedral angle of the biphenyl moiety changes from 20 to 91° by the photochromic reaction (Figure 2.3.2 and 2.3.3). The ns transient absorption experiment shows that the biradical of bisDMDPI-BP has a weak and broad background at >700 nm, where the absorption band due to the radical–radical interaction was observed in the previously studied bridged imidazole dimers.[20,21,26] Our previous work demonstrated that the absorption band due to the radical–radical interaction decreases, becomes broad, and shifts to longer wavelengths with decreasing radical–radical interactions.[21] Since bisDMDPI-BP has little transient absorption at >700 nm as compared to that of reported bridged imidazole dimers,[20,21] it indicates that the radical–radical interaction of the biradical of bisDMDPI-BP is weak because of the large dihedral angle of the bridging biphenyl. The calculations and experimental results show that the photochromism of bisDMDPI-BP induces a large conformational change due to the rotation of the biphenyl moiety.

Figure 2.3.1b shows the decay profile of the colored species of bisDMDPI-BP observed at 400 nm at room temperature. The decay is fitted with a single exponential function and the lifetime and the rate constant are 103 ns and 9.7×10^6 s^{-1} at room temperature, respectively. This lifetime shows that bisDMDPI-BP exhibits the fastest thermal back reaction in all reported imidazole dimers. The decays at other wavelengths are quite similar (Figure 2.3.6), indicating that there is a single transient species that decays with first order kinetics, as expected for the biradical.

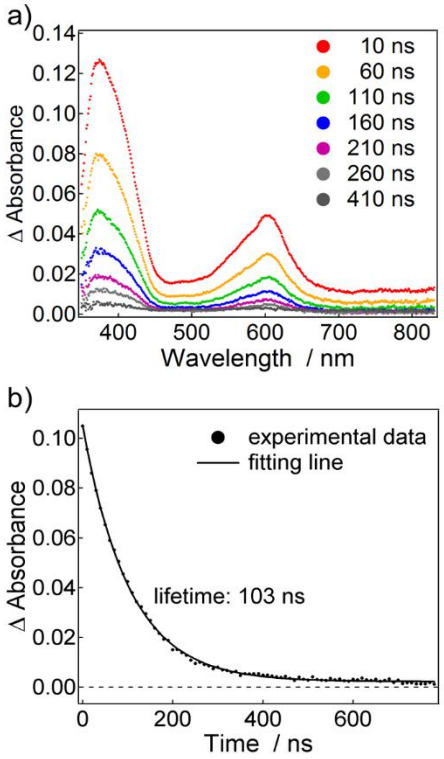

Figure 2.3.1. (a) Transient absorption spectra on the ns time scale and (b) the decay profile of the biradical of bisDMDPI-BP observed at 400 nm in degassed benzene (1.1×10^{-4} M, excitation wavelength: 305 nm, pulse duration: 5 ns, and excitation intensity: 1.8 mJ).

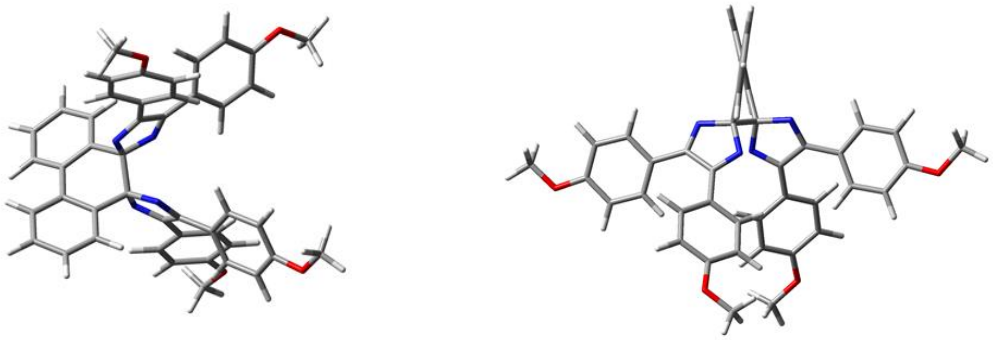

Figure 2.3.2. Optimized structure of the 2,2′-isomer of bisDMDPI-BP at MPW1PW91/6-31G(d) level of theory.

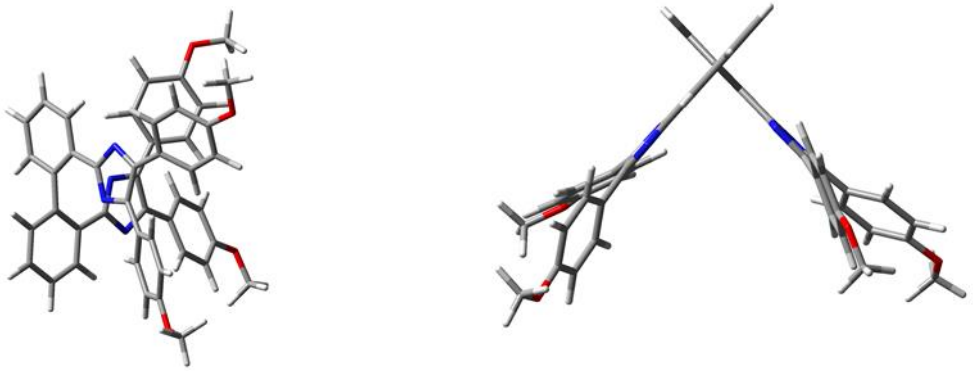

Figure 2.3.3. Optimized structure of the biradical of bisDMDPI-BP at UMPW1PW91/6-31G(d) level of theory.

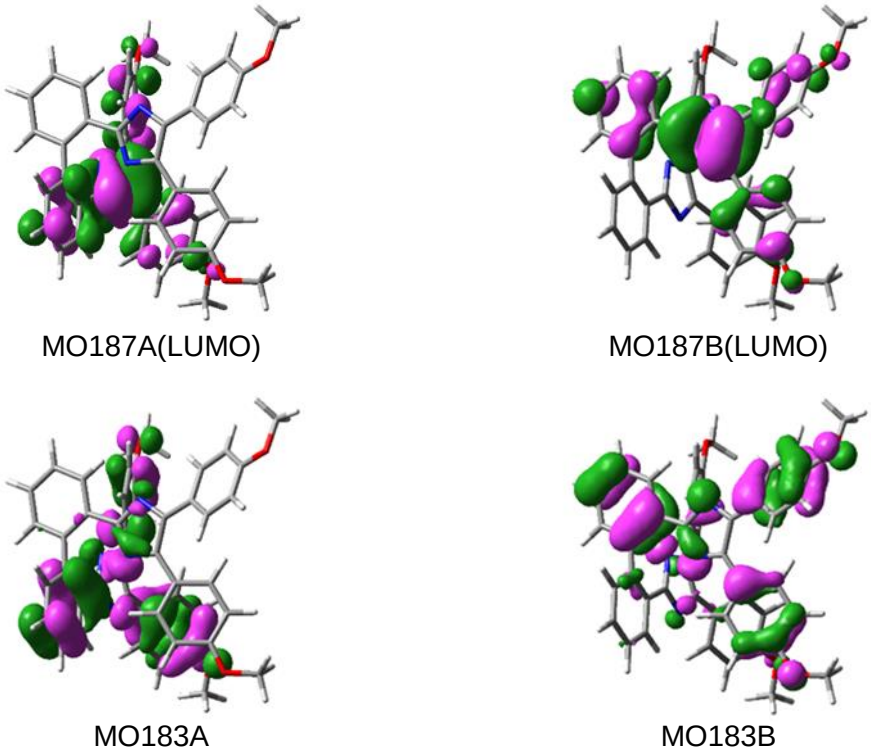

Figure 2.3.4. Relevant molecular orbitals of the biradical of bisDMDPI-BP obtained by the UMPW1PW91/6-31G(d) level.

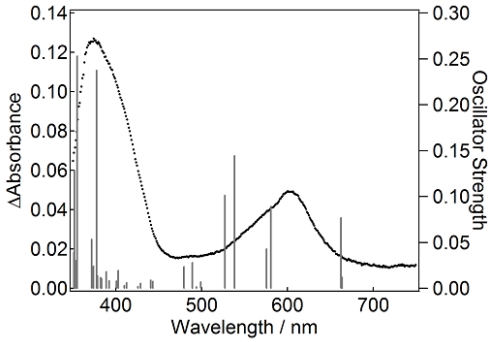

Figure 2.3.5. Transient absorption spectrum (dotted line) and the oscillator strength (vertical lines) obtained by the TDDFT calculations (UMPW1PW91/6-31G(d) //UMPW1PW91/6-31G(d)).

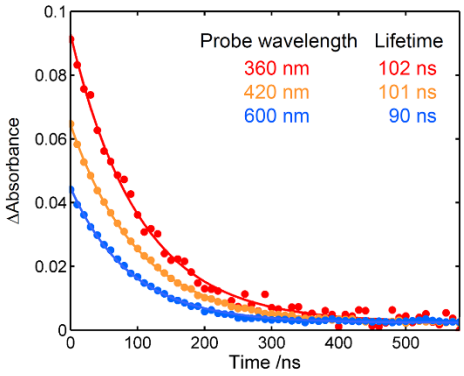

Figure 2.3.6. Decay profiles of the colored species of bisDMDPI-BP in degassed benzene at room temperature (1.1×10^{-4} M, excitation wavelength: 305 nm, pulse duration: 5 ns, excitation intensity: 1.8 mJ). The dots and solid line are experimental data and fittings, respectively.

2.4 Femtosecond transient absorption spectra

To reveal the details of the bond cleavage process of bisDMDPI-BP, the author conducted sub-picosecond transient absorption spectroscopy in which the sample was excited at 310 nm with a pulse duration of ~200 fs. Figure 2.4.1 shows a time evolution of the transient absorption spectrum. Color represents ΔAbsorbance. Figure 2.4.4a and 2.4.4b show the transient absorption spectra and dynamics of bisDMDPI-BP at different time delays, respectively. The grey dots and solid red curves show the experimental data and fitted spectra (and dynamics) obtained by the global analyses as explained later. The author found that the transient absorption spectra until 1 ps are quite broadened and the spectra after 3 ps look very similar to those in the ns transient absorption experiments (Figure 2.3.1a). As was seen in the Figure. 2.4.4a, the initial transient absorption spectra at 0.3-1.0 ps are obviously broadened. Two possibilities are conceivable for the broadening: transient absorption from the precursor states of the biradical and/or the vibrational cooling from hot states. Interestingly, although the spectral width earlier than 1 ps is quite broadened, the peak positions are almost identical, which indicates that the radical component is already generated on sub-picosecond time scales.

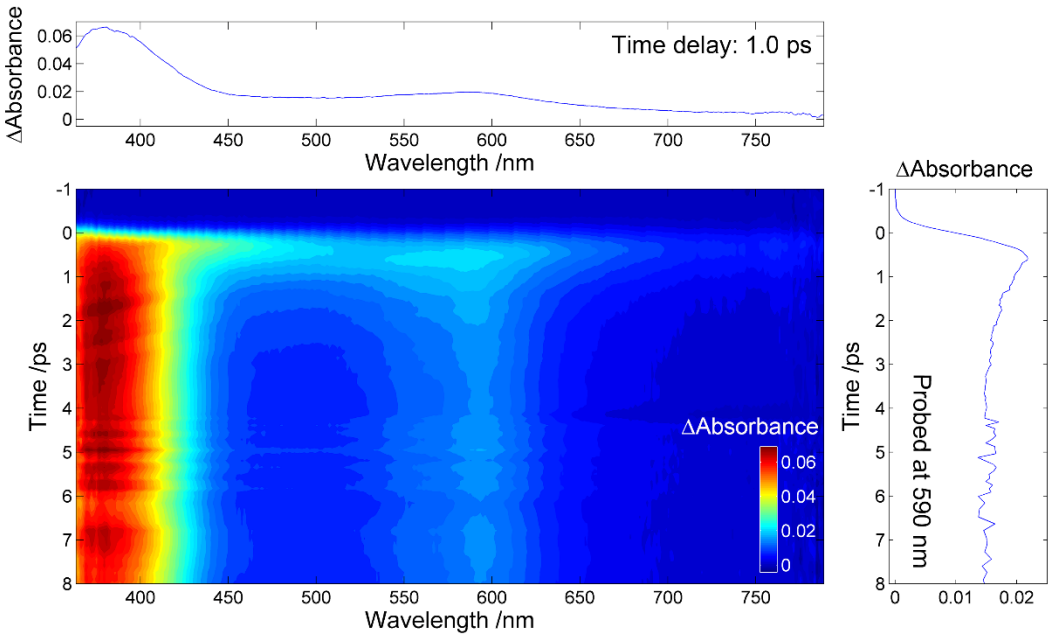

Figure 2.4.1. Time-evolution of the chirp corrected transient absorption spectrum of bisDMPI-BP from 0 to 8 ps in benzene at room temperature (5.5×10^{-4} M, excitation wavelength: 305 nm, pulse duration: 200 fs and laser intensity: 1.8 μJ).

The author applied global analyses to reveal the multiwavelength kinetics of bisDMDPI-BP. These analyses were done by using the TIMP package with the graphical interface program Glotaran, version 1.0.1 (http://glotaran.org).[31] The instrument response function (IRF) was set to 200 fs. The author proposes that the kinetics follows a sequential model because the initial relaxation pathways of HABI derivatives can be expected as follows (Figure 2.4.2):[32,33] 1) the vibrational relaxation from the Franck-Condon state to the S_1 state, 2) the transition from the S_1 state to the hot state of the biradical, and 3) the vibrational cooling to the ground state of the biradical. In addition to the process 3), the higher excited states of the biradical may also contribute to the generation process of the radicals. All processes are completed within a ps. In addition to the transition from the S_1 state to the higher vibrational state of the biradical, the higher excited state of the biradical may also contribute to the bond cleavage process through the coupling with the S_1 state of the colorless species. Therefore, the author applies sequential kinetic models for the global analyses. After the photoexcitation, the dynamics from 430 to 750 nm show a fast decay and a very slow decay. On the other hand, the transient absorption at 380 nm only shows a fast rise and a very slow decay. The slow decay is attributed to the colored photoproduct, which is almost stationary on this time scale. Firstly, the author applied the two-state sequential model as follows:

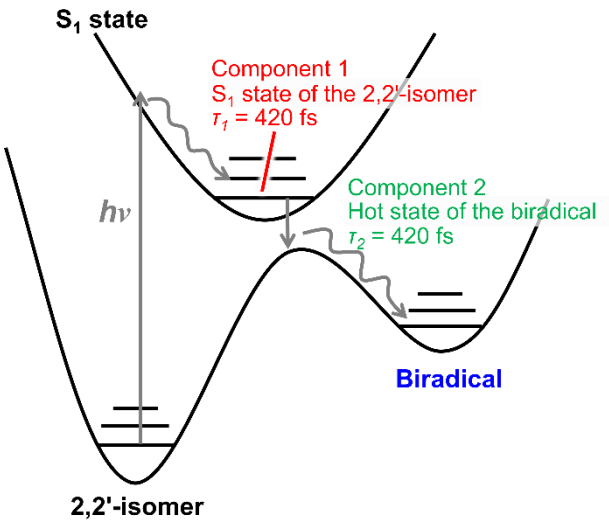

Figure 2.4.2. Plausible energy relaxation pathway of photochromic reaction of bisDMPI-BP.

a) Two-state sequential model analysis

$$[S_0] \xrightarrow{h\nu} [\text{Component 1}] \xrightarrow{\tau_1} [\text{biradical}]$$

Firstly, the kinetics were fitted with the two-state sequential model with convolution by the IRF. Figures 2.4.3a and 2.4.3b show evolution associated spectra (EAS) and decays of two components. The component 1 has a broad absorption band and it is quickly converted to the biradical state. It is assigned to the transient absorption from the precursor state of the biradical, which is most probably the transient absorption from the S_1 state and/or the vibrationallly hot state of the colored species. The component which rises while component 1 decreases is assigned to the biradical of bisDMDPI-BP because of the strong similarity of the spectral shape to that observed in the ns experiments. The time constants of the decay of the component 1 (τ_1) and biradical are estimated to be 760 fs and >50 ps, respectively. Fitted spectra at different delay times and fitted decays probed at different wavelengths are shown in Figure 2.4.4. The gray dots and red solid lines indicate the raw data and fitted spectra, respectively. While the simulated transient absorption spectra obtained from the global analyses qualitatively fit with the data (except the spectrum at 0.3 ps), the simulated transient absorption dynamics obviously cannot reproduce the experimental data at 540, 580, and 590 nm (indicated as black arrows). These results suggest that another rise component is necessary to explain the kinetics of bisDMDPI-BP.

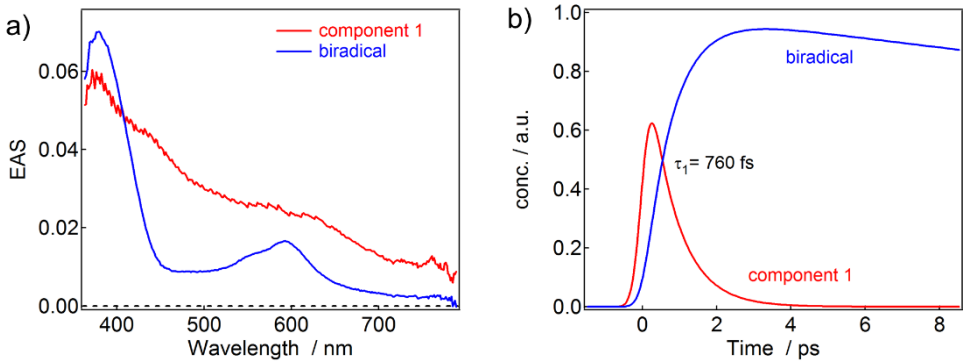

Figure 2.4.3. (a) Evolution associated spectra (EAS) and time profiles of the concentration changes of two components obtained from the global analysis of the two-state sequential model.

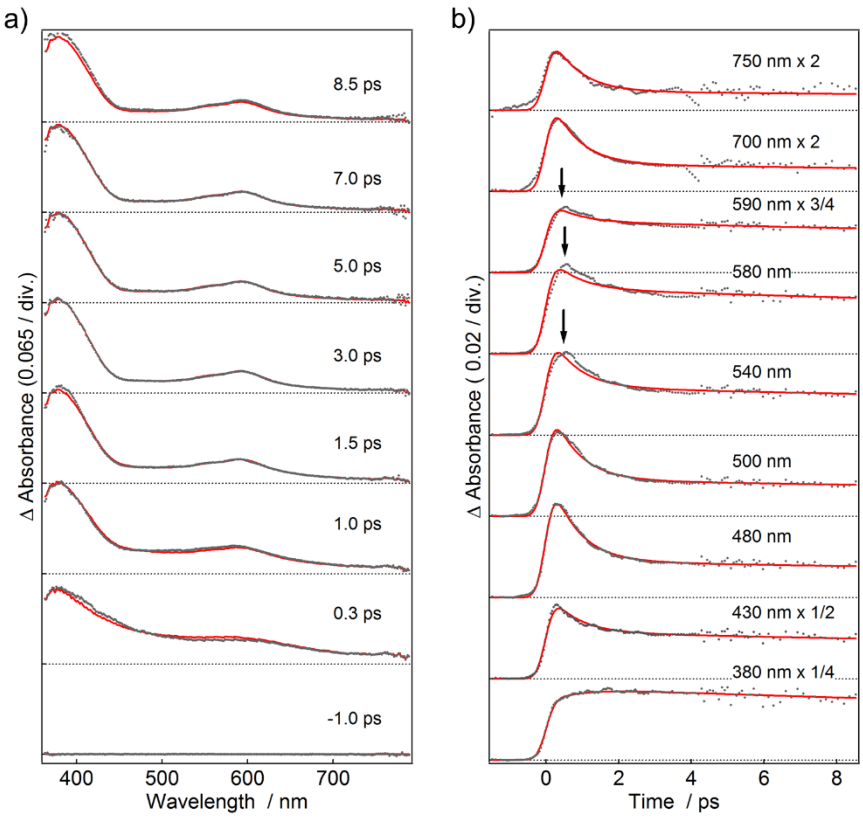

Figure 2.4.4. (left) Transient absorption spectra and (right) dynamics of bisDMDPI-BP. The red curves represent the simulated spectra and decays obtained by global analysis with the two-state sequential model.

b) Three-state sequential model analysis

$$[\text{Ground state}] \xrightarrow{h\nu} [\text{Component 1}] \xrightarrow{\tau_1} [\text{Component 2}] \xrightarrow{\tau_2} [\text{biradical}]$$

The two-state sequential model assumes that the precursor of the biradical is described as a single component. However, the two-state sequential model does not reproduce the experimental data well. Next, the author assumes that the precursor state can be split into two states and the author fits the kinetics with the three-state sequential model convoluted by the IRF. Figures 2.4.5a and 2.4.5b show EAS and time profiles of each component. Component 1 has a broad absorption band and it is quickly converted to component 2. The spectrum of component 2 has sharp and broad peaks at ~390 and 550 nm and component 2 decays within 2 ps. By following to the relaxation energy diagram shown in Figure 2.4.2, the author assigned component 1 to the transient absorption from the S_1 state. Since the spectrum of component 2 is similar to that of the biradical and the spectrum is somewhat shifted and more broadened, component 2 can be assigned to the hot state of the biradical. The component which generates with decreasing the component 2 is assigned to the

biradical of bisDMDPI-BP because of the similarity of the spectral shape. The time constants of the decay of the components 1, 2 (τ_1 and τ_2), and biradical are estimated to be 420 fs, 420 fs and >50 ps, respectively. Fitted transient absorption spectra at different delay times and fitted transient absorption dynamics probed at different wavelengths are shown in Figure 2.4.6. The striking difference from the two-state sequential model is that the addition of component 2 satisfactorily reproduces the rise around 520-600 nm.

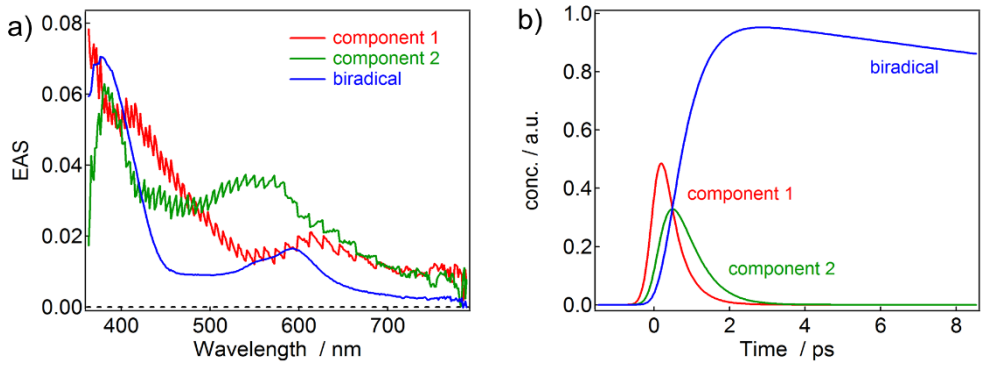

Figure 2.4.5. (a) Evolution Associated Spectra and time profiles of the concentration changes of three components obtained from the global analysis of the three-state sequential model. The τ_1, τ_2, and biradical are 420 fs, 420 fs and >50 ps, respectively.

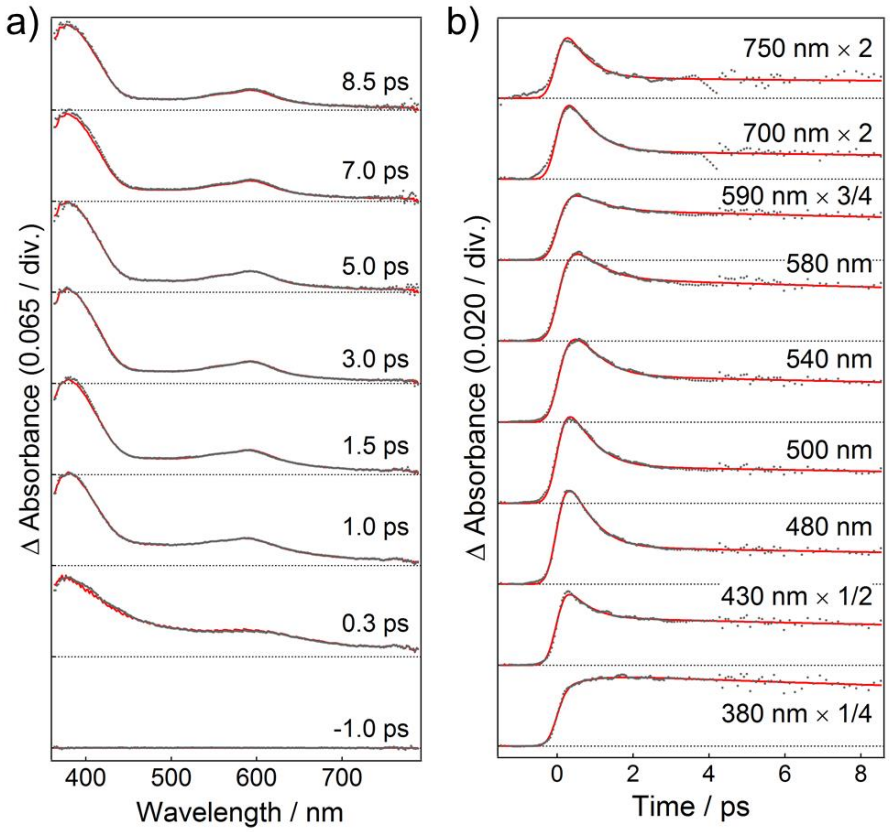

Figure 2.4.6. (left) Transient absorption spectra and (right) dynamics of bisDMDPI-BP. The red curves represent the simulated spectra and decays obtained by global analysis with the three-state sequential model.

2.5 Conclusion

In conclusion, sub-picosecond to sub-microsecond transient absorption spectroscopy reveals that bisDMDPI-BP exhibits extremely fast photochromism with a large conformational change. The biradical of bisDMDPI-BP forms within 1 ps after the excitation and the thermal back reaction of the biradical takes only ~100 ns. As compared to other ns-scale switching molecules, the advantage of using bisDMDPI-BP is the easy functionalization with sustained fast photochromic properties because the rates of the photochromic properties in bridged imidazole dimers are mostly dominated by the bridging unit: biphenyl in the present case. These properties of the imidazole dimer support the potential of bisDMDPI-BP as nanosecond-time scale photoswitching materials.

2.6 References

(1) Gilat, S. L.; Kawai, S. H.; Lehn, J.-M. *Chem. –Eur. J.* **1995**, *1*, 275–284.

(2) Matsuda, K.; Yamaguchi, H.; Sakano, T.; Ikeda, M.; Tanifuji, N.; Irie, M. *J. Phys. Chem. C* **2008**, *112*, 17005–17010.

(3) Denekamp, C.; Feringa, B. L. *Adv. Mater.* **1998**, *10*, 1080–1082.

(4) Hashim, P. K.; Tamaoki, N. *Angew. Chem. Int. Ed.* **2011**, *50*, 11729–11730.

(5) Yagai, S.; Nakajima, T.; Kishikawa, K.; Kohmoto, S.; Karatsu, T.; Kitamura, A. *J. Am. Chem. Soc.* **2005**, *127*, 11134–11139.

(6) Eelkema, R.; Pollard, M. M.; Katsonis, N.; Vicario, J.; Broer, D. J.; Feringa, B. L. *J. Am. Chem. Soc.* **2006**, *128*, 14397–14407.

(7) Kobatake, S.; Takami, S.; Muto, H.; Ishikawa, T.; Irie, M. *Nature* **2007**, *446*, 778–781.

(8) Kitagawa, D.; Nishi, H.; Kobatake, S. *Angew. Chem. Int. Ed.* **2013**, *52*, 9320–9322.

(9) Raymo, F. M. *Adv. Mater.* **2002**, *14*, 401–414.

(10) Castellanos, S.; Vieira, A. A.; Illescas, B. M.; Sacchetti, V.; Schubert, C.; Moreno, J.; Guldi, D. M.; Hecht, S.; Martín, N. *Angew. Chem. Int. Ed.* **2013**, *52*, 13985–13990.

(11) Szaciłowski, K. *Chem. Rev.* **2008**, *108*, 3481–3548.

(12) Andréasson, J.; Pischel, U.; Straight, S. D.; Moore, T. A.; Moore, A. L.; Gust, D. *J. Am. Chem. Soc.* **2011**, *133*, 11641–11648.

(13) Yagai, S.; Iwai, K.; Karatsu, T.; Kitamura, A. *Angew. Chem. Int. Ed.* **2012**, *51*, 9679–9683.

(14) Tomasulo, M.; Sortino, S.; Raymo, F. M. *Org. Lett.* **2005**, *7*, 1109–1112.

(15) Garcia-Amorós, J.; Bučinskas, A.; Reig, M.; Nonell, S.; Velasco, D. *J. Mater. Chem. C* **2014**, *2*, 474.

(16) White, T. J.; Tabiryan, N. V.; Serak, S. V.; Hrozhyk, U. A.; Tondiglia, V. P.; Koerner, H.; Vaia, R. A.; Bunning, T. J. *Soft Matter* **2008**, *4*, 1796–1798.

(17) Serak, S.; Tabiryan, N.; Vergara, R.; White, T. J.; Vaia, R. A.; Bunning, T. J. *Soft Matter* **2010**, *6*, 779–783.

(18) Harada, Y.; Hatano, S.; Kimoto, A.; Abe, J. *J. Phys. Chem. Lett.* **2010**, *1*, 1112–1115.

(19) Iwasaki, T.; Kato, T.; Kobayashi, Y.; Abe, J. *Chem. Commun.* **2014**, *1*, 10–13.

(20) Kishimoto, Y.; Abe, J. *J. Am. Chem. Soc.* **2009**, *131*, 4227–4229.

(21) Shima, K.; Mutoh, K.; Kobayashi, Y.; Abe, J. *J. Am. Chem. Soc.* **2014**, *136*, 3796–3799.

(22) Yamashita, H.; Abe, J. *Chem. Commun.* **2014**, 3–6.

(23) Yamaguchi, T.; Hatano, S.; Abe, J. *J. Phys. Chem. A* **2013**.

(24) Hatano, S.; Horino, T.; Tokita, A.; Oshima, T.; Abe, J. *J. Am. Chem. Soc.* **2013**, *135*, 3164–3172.

(25) Frisch, M. J.; Trucks, G. W.; Schlegel, H. B.; Scuseria, G. E.; Robb, M. A.; Cheeseman, J. R.; Scalmani, G.; Barone, V.; Mennucci, B.; Petersson, G. A.; Nakatsuji, H.; Caricato, M.; Li, X.; Hratchian, H. P.; Izmaylov, A. F.; Bloino, J.; Zheng, G.; Sonnenberg, J. L.; Hada, M.; Ehara, M.; Toyota, K.; Fukuda, R.; Hasegawa, J.; Ishida, M.; Nakajima, T.; Honda, Y.; Kitao, O.; Nakai, H.; Vreven, T.; Montgomery, J. A., J.; Peralta, J. E.; Ogliaro, F.; Bearpark, M.; Heyd, J. J.; Brothers, E.; Kudin, K. N.; Staroverov, V. N.; Kobayashi, R.; Normand, J.; Raghavachari, K.; Rendell, A.; Burant, J. C.; Iyengar, S. S.; Tomasi, J.; Cossi, M.; Rega, N.; Millam, N. J.; Klene, M.; Knox, J. E.; Cross, J. B.; Bakken, V.; Adamo, C.; Jaramillo, J.; Gomperts, R.; Stratmann, R. E.; Yazyev, O.; Austin, A. J.; Cammi, R.; Pomelli, C.; Ochterski, J. W.; Martin, R. L.; Morokuma, K.; Zakrzewski, V. G.; Voth, G. A.; Salvador, P.; Dannenberg, J. J.; Dapprich, S.; Daniels, A. D.; Farkas, Ö.; Foresman, J. B.; Ortiz, J. V.; Cioslowski, J.; Fox, D. J. Gaussian 09 Citation http://www.gaussian.com/g_tech/g_ur/m_citation.htm (accessed Aug 18, 2015).

(26) Mutoh, K.; Shima, K.; Yamaguchi, T.; Kobayashi, M.; Abe, J. *Org. Lett.* **2013**, *15*, 2938–2941.

(27) Maeda, K.; Hayashi, T. *Bull. Chem. Soc. Jpn.* **1970**, *45*, 1474–1480.

(28) Edkins, R. M.; Probert, M. R.; Robertson, C. M.; Howard, J. a. K.; Beeby, A. *RSC Adv.* **2014**, *4*, 5351.

(29) Jacquart, A.; Williams, R. M.; Brouwer, A. M.; Ishow, E. *Chem. –Euro. J.* **2012**, *18*, 3706–3720.

(30) Kumpulainen, T.; Bakker, B. H.; Hilbers, M.; Brouwer, A. M. *J. Phys. Chem. B* **2015**, *119*, 2515–2514.

(31) Snellenburg, J.; Laptenok, S.; Seger, R.; Mullen, K.; Stokkum, I. Van. *J. Stat. Softw.* **2012**, *49*.

(32) Satoh, Y.; Ishibashi, Y.; Ito, S.; Nagasawa, Y.; Miyasaka, H.; Chosrowjan, H.; Taniguchi, S.; Mataga, N.; Kato, D.; Kikuchi, A.; Abe, J. *Chem. Phys. Lett.* **2007**, *448*, 228–231.

(33) Miyasaka, H.; Satoh, Y.; Ishibashi, Y.; Ito, S.; Nagasawa, Y.; Taniguchi, S.; Chosrowjan, H.; Mataga, N.; Kato, D.; Kikuchi, A.; Abe, J. *J. Am. Chem. Soc.* **2009**, *131*, 7256–7263.

Chapter 3
1-Phenylnaphthalene-bridged imidazole dimer

3.1 Introduction

Almost all photochromic molecules including HABI derivatives change their molecular structures from a thermally stable colorless isomer to a thermally metastable colored isomer upon UV light irradiation. The metastable colored isomer can be reversed to the original colorless isomer either by thermal means or by subsequent irradiation with a specific light wavelength. On the other hand, only a few molecules have been reported to show negative photochromism that is observed with several photochromic molecules where the absorption spectrum of the molecule after irradiation is blue-shifted relative to that before irradiation.[1–27] The colored isomer of a negative photochromic molecule is more stable than the colorless isomer, and the colored isomer becomes colorless upon exposure to visible light. By changing the bridging unit with a 1,1′-binaphthyl moiety, we have recently developed the 1,1′-binaphthyl-bridged imidazole dimer (bisDMDPI-BN) that shows unusual negative photochromism as described in Chapter 1 (Scheme 3.1.1a).[28] On the other hand, the biphenyl-bridged imidazole dimer (bisDMDPI-BP) is obtained as the colorless photochromic 2,2′-isomer (Scheme 3.1.1b) that shows fast photochromic molecular switching as described Chapter 2.[29]

Scheme 3.1.1. (a) Photochromism of bisDMDPI-BN and Molecular Structures of (b) bisDMDPI-BP and (c) bisDPI-PN

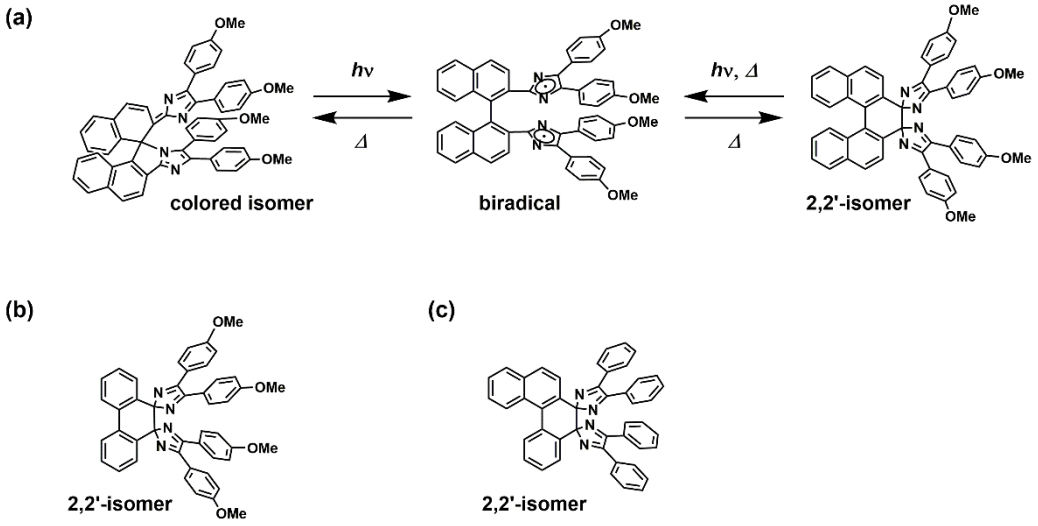

Thus the author expected that negative photochromism of the biaryl-bridged imidazole dimers could be controlled by changing the bridging unit. Herein, the author reports the unique photochromic and thermochromic behavior of the 1-phenylnaphthalene-bridged imidazole dimer (bisDPI-PN) shown in Scheme 3.1.1c. The author found that this molecule has three kinds of colorless isomers and one colored isomer other than the short-lived colored biradical and successfully isolated four kinds of isomers, i.e., the 1,2′-isomer A, the 1,2′-isomer B, the 2,2′-isomer, and the colored isomer, leading to the determination of the molecular structures by X-ray crystallographic analysis.

3.2 Synthesis

Commercially available reagents and solvents for syntheses were of reagent grade and used without further purification. All reactions were monitored by thin-layer chromatography carried out on 0.2 mm E. Merck silica gel plates (60F-254). Column chromatography was performed on silica gel (Silica Gel 60N (spherical, neutral), 40−50 μm, Kanto Chemical Co., Inc.). ^{1}H and ^{13}C NMR spectra were recorded with a NMR spectrometer (Bruker, Avance III 400 NanoBay). DMSO-d_6 (0.03% TMS) and $CDCl_3$ (0.03% TMS) were used as deuterated solvents. Chemical shifts are reported in parts per million (ppm) relative to tetramethylsilane, and the coupling constants (J) are reported in Hertz (Hz). ESI-TOF MS spectra were recorded on a Bruker Daltonics micrOTOFII-AGA1 instrument using positive-ion mode.

BisDPI-PN was prepared as shown in Scheme 3.2.1.

Scheme 3.2.1. Synthesis of bisDPI-PN

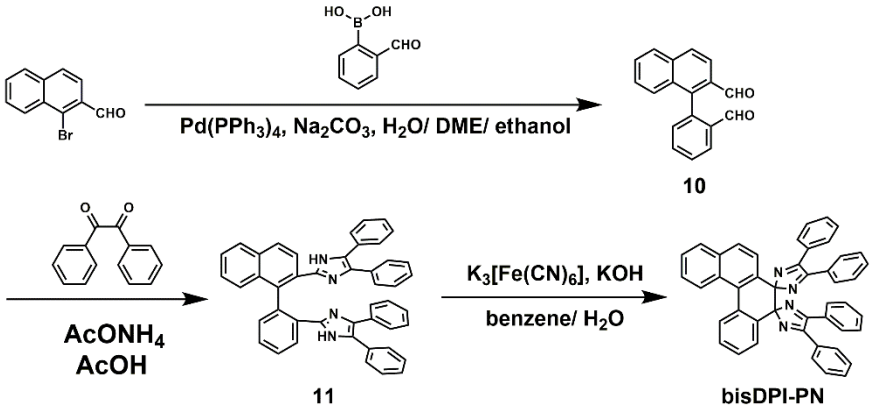

1-(formylphenyl)-2-naphthaldehyde (10)[30]

Under a N_2 atmosphere, 1-bromo-2-naphthaldehyde (202 mg, 0.86 mmol) and 2-formyl-1-phenylboronic acid (202 mg, 1.35 mmol) were added to degassed DME (3 mL), EtOH (2 mL), and 2 M Na_2CO_3 aq. (3.8 mL). The reaction mixture was stirred at 60 °C, and tetrakis(triphenylphosphine)palladium (0) (112 mg, 0.097 mmol) was added. The mixture was stirred at 80 °C for 28 h. After cooling to room temperature, the resulting mixture was washed with water and extracted with CH_2Cl_2. The crude sample was purified by silica gel column chromatography using CH_2Cl_2/hexane = 2/1 as eluent to give a white powder of **10**.

^{1}H NMR (400 MHz, $CDCl_3$), δ: 9.84 (s, 1H), 9.57 (s, 1H), 8.18 (d, 1H, J = 7.67 Hz), 8.12 (d, 1H, J = 8.52 Hz), 8.03 (d, 1H, J = 8.94 Hz), 7.97 (d, 1H, J = 8.52 Hz), 7.78 (t, 1H, J = 7.51 Hz), 7.72 (t, 1H, J = 7.51 Hz), 7.65 (t, 1H, J = 7.51 Hz), 7.51−7.42 (m, 2H), 7.38 (d, 1H, J = 8.51 Hz).

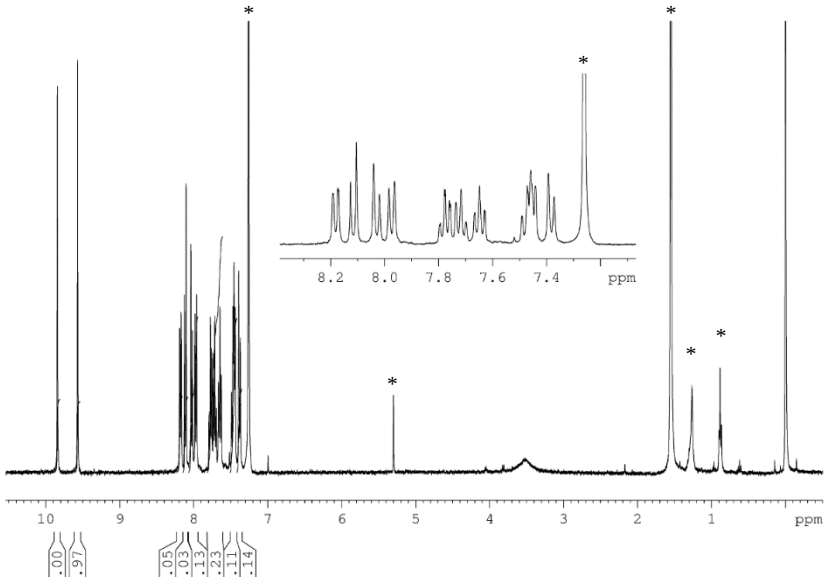

Figure 3.2.1. ^{1}H NMR spectrum of 1-(Formylphenyl)-2-naphthaldehyde **10** in $CDCl_3$ (* solvent peaks).

bisDPIH-PN (11)

1-(Formylphenyl)-2-naphthaldehyde **10** (30 mg, 0.115 mmol), benzil (54 mg, 0.260 mmol), and ammonium acetate (118 mg, 1.34 mmol) were dissolved in $CHCl_3$ (0.6 mL). The mixture was refluxed at 110 °C for 2 days. After cooling to room temperature, the resulting mixture was extracted with CH_2Cl_2 and washed with water. The crude mixture was purified by silica gel column chromatography using AcOEt/hexane = 1/2 as eluent to give white powder of **11**.

^{1}H NMR (400 MHz, DMSO-d_6), δ: 13.83 (s, 1H), 13.66 (s, 1H), 8.07 (d, 1H, J = 7.99 Hz), 7.99 (d, 1H, J = 8.31 Hz), 7.92 (d, 1H, J = 8.63 Hz), 7.87 (d, 1H, J = 7.35 Hz), 7.61 (t, 1H, J = 7.70 Hz), 7.50 (d, 1H, J = 7.34 Hz), 7.43−7.06 (m, 23H). ESI-TOF-MS, m/z: calcd, 640.263 ($C_{46}H_{32}N_4$); found, 663.3150 $[M + Na]^+$.

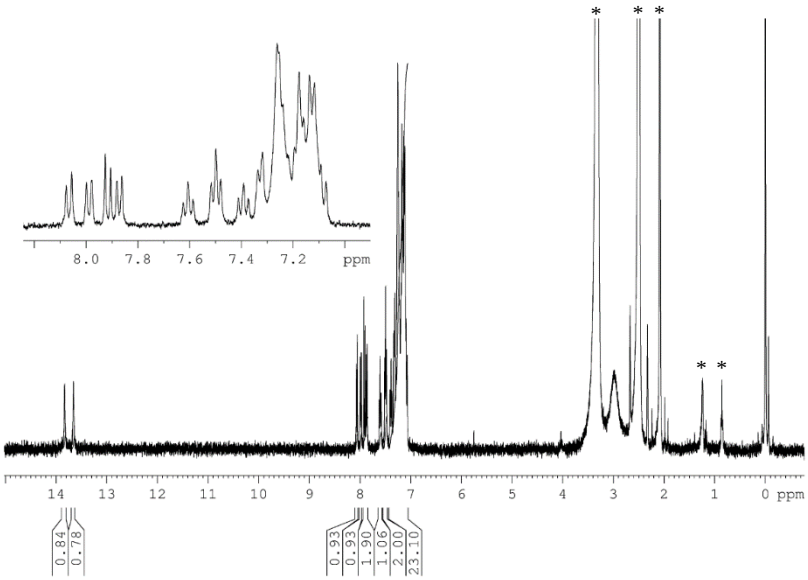

Figure 3.2.2. ^{1}H NMR spectrum of compound **11** in DMSO-d_6 (* solvent peaks).

bisDPI-PN

All manipulations were carried out with exclusion of light. BisDPIH-PN **11** (25 mg, 0.039 mmol) was dissolved in degassed benzene (12 mL) and $K_3[Fe(CN)_6]$ (627 mg, 2.33 mmol) aqueous solution containing KOH bilayer, and the solution was stirred for 18 h. After the reaction was completed, the reaction product was extracted with benzene, and washed with water. The crude mixture was purified by silica gel column chromatography using AcOEt/hexane = 1/2 as eluent to give reddish white powder. The slow evaporation of an acetonitrile solution of bisDPI-PN gave colorless, plate single crystal suitable for X-ray crystallographic analysis.

^{1}H NMR (400 MHz, $CDCl_3$), δ: 8.79 (d, 1H, J = 8.42 Hz), 8.26 (d, 1H, J = 7.73 Hz), 7.86 (d, 1H, J = 7.73 Hz), 7.69 (d, 1H, J = 8.42 Hz), 7.56−7.38 (m, 14H), 7.38−7.14 (m, 11H), 7.00 (d, 1H, J = 8.42 Hz). HR-ESI-TOF-MS, m/z: calcd, 638.247 ($C_{46}H_{30}N_4$); found, 661.239 $[M+Na]^+$.

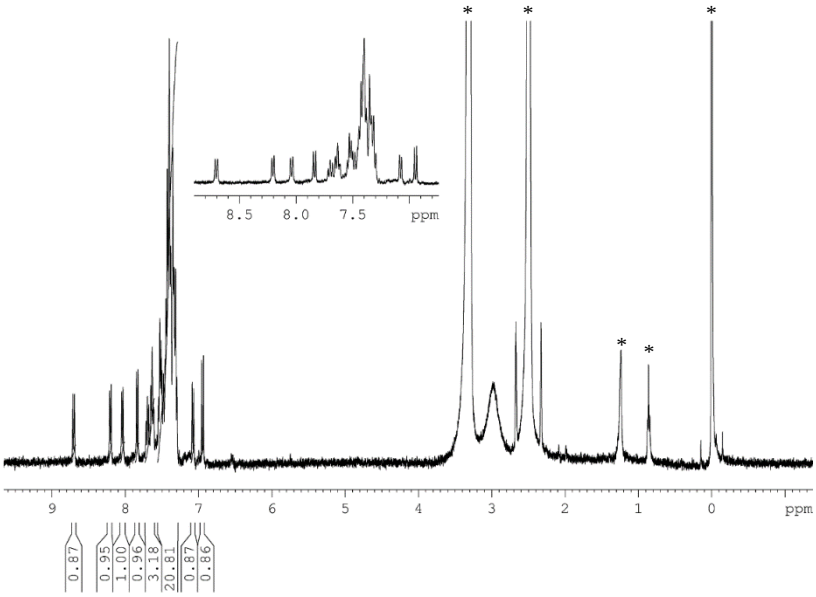

Figure 3.2.3. ^{1}H NMR spectrum of the 2,2′-isomer of bisDPI-PN in DMSO-d_6 (* solvent peaks).

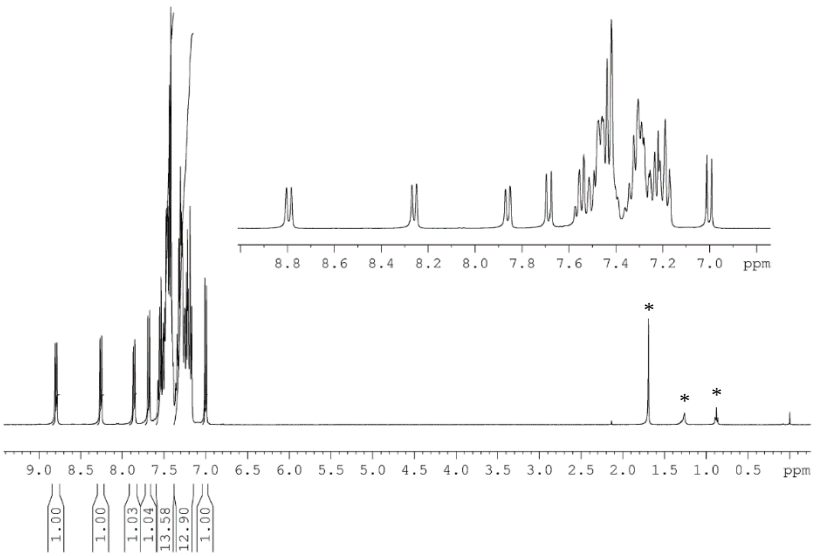

Figure 3.2.4. ^{1}H NMR spectrum of the 2,2′-isomer of bisDPI-PN in $CDCl_3$ (* solvent peaks).

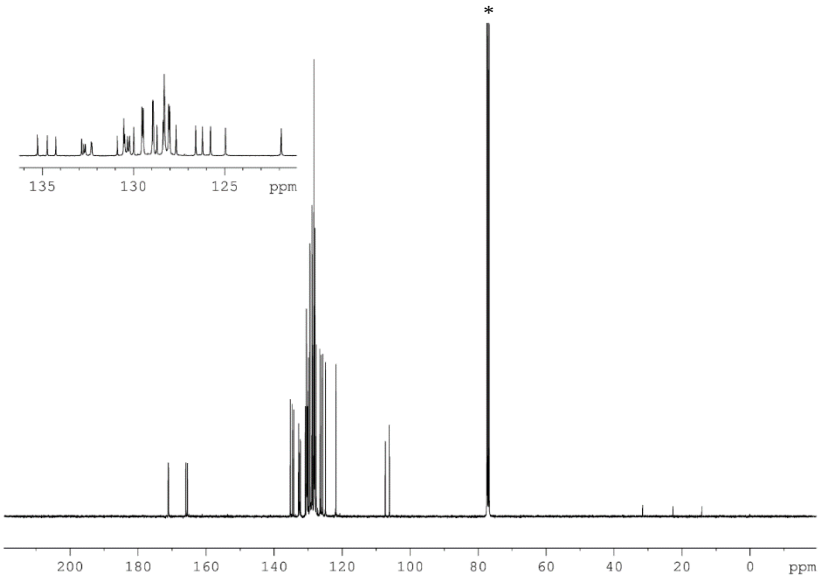

Figure 3.2.5. ^{13}C NMR spectrum of the 2,2′-isomer of bisDPI-PN in $CDCl_3$ (* solvent peaks).

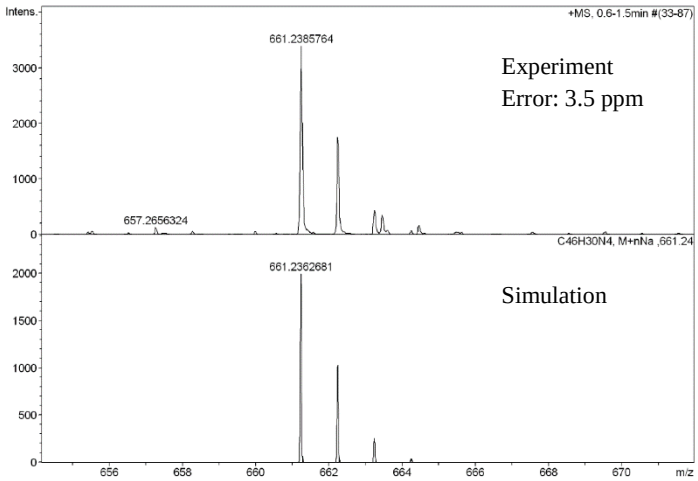

Figure 3.2.6. HR-ESI-TOF-MS spectra of the 2,2′-isomer of bisDPI-PN.

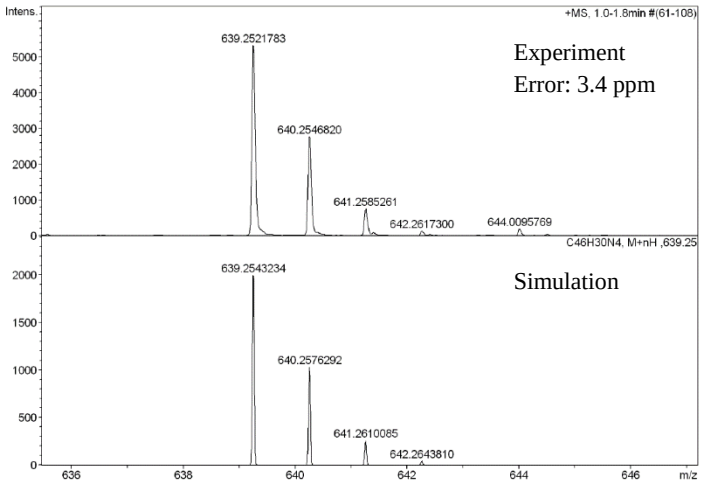

Figure 3.2.7. HR-ESI-TOF-MS spectra of the colored isomer of bisDPI-PN.

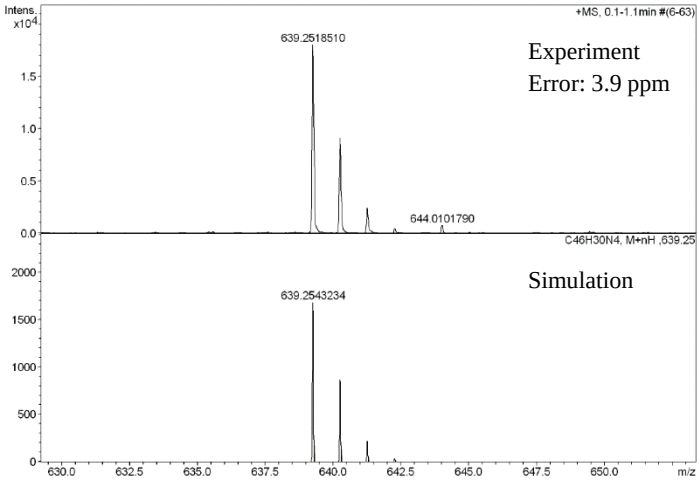

Figure 3.2.8. HR-ESI-TOF-MS spectra of the 1,2′-isomer A of bisDPI-PN.

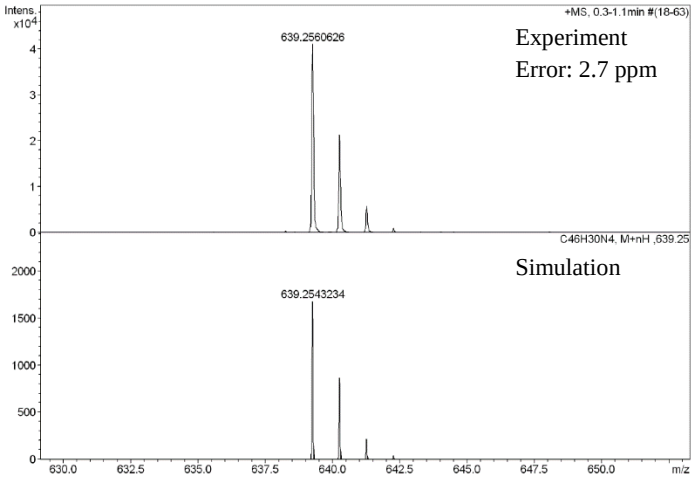

Figure 3.2.9. HR-ESI-TOF-MS spectra of the 1,2′-isomer B of bisDPI-PN.

3.3 Photochromic and thermochromic behavior

Colorless crystals are formed from the acetonitrile solution of the reddish white powder of bisDPI-PN. Though the oxidation of the lophine precursor of bisDMDPI-BN gives only the colored isomer, the major oxidation product of the lophine precursor of bisDPI-PN is colorless isomer as well as the oxidation of the lophine precursor of bisDMDPI-BP. The molecular structure of the colorless isomer of bisDPI-PN was determined by X-ray crystallographic analysis as shown in Figure 3.3.1a. It is revealed that the colorless isomer is the 2,2′-isomer with the C−C bond (1.5775(18) Å) between the imidazole rings as well as bisDMDPI-BP. The 2,2′-isomer of bisDPI-PN is stable at room temperature contrary to that of bisDMDPI-BN that thermally returns to the colored isomer within 20 min in benzene at room temperature. Though the 2,2′-isomers of the classical HABI derivatives show piezochromism, the 2,2′-isomer of bisDPI-PN does not show the color change by grinding at room temperature The solution of the 2,2′-isomer of bisDPIPN changes its color from colorless to yellow by UV light irradiation and returns to the original colorless state by visible light irradiation. This reversible color change can be repeated many times by alternating UV and visible light irradiation. This photoisomerization behavior was followed by HPLC analysis. As shown in Figure 3.3.2, the UV light irradiation to the benzene solution of the 2,2′-isomer results in the appearance of a small peak other than the peak of the 2,2′-isomer. Upon visible light irradiation to the yellow solution, the small peak completely disappears and the solution color returns to colorless. The UV−vis absorption spectrum of the fraction of the small peak has an intense absorption band in visible light region, suggesting that the fraction of the small peak is the colored isomer in analogy with bisDMDPI-BN. The colored fraction is stable at room temperature to allow for recrystallization. The X-ray crystallographic analysis of the single crystal of the colored fraction revealed the molecular structure as shown in Figure 3.3.1b. As would be expected, the colored isomer forms the structure similar to the colored isomer of bisDMDPI-BN. The photostationary state of the benzene solution was reached after 1 min of irradiation at 365 nm at room temperature and the fraction of the colored isomer at the photostationary state is 0.01, indicating low conversion efficiency from the 2,2′-isomer to the colored isomer upon UV light irradiation.

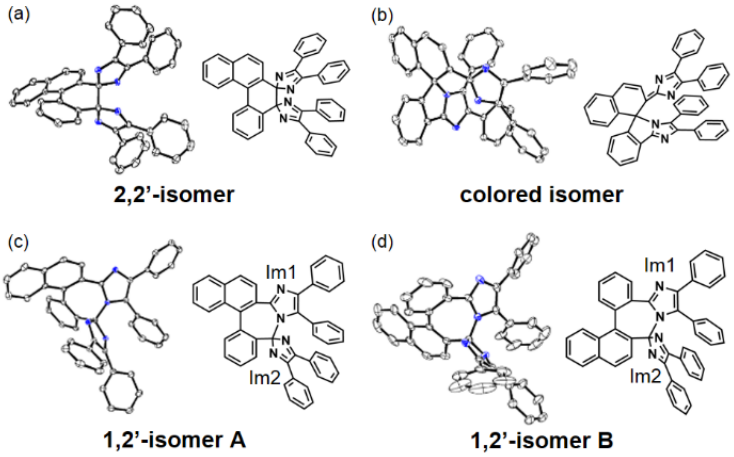

Figure 3.3.1. ORTEP representations of the molecular structures of (a) the 2,2′-isomer, (b) the colored isomer, (c) the 1,2′-isomer A, and (d) the 1,2′-isomer B of bisDPI-PN with thermal ellipsoid. The hydrogen atoms and the solvent molecule are omitted. Nitrogen atoms are highlighted in blue.

Table 3.3.1. X-ray crystallographic data of the 2,2′-isomer of bisDPI-PN.

Identification code	The 2,2′-isomer of bisDPI-PN	
Empirical formula	$C_{46}H_{30}N_4$	
Formula weight	638.74	
Temperature	90 K	
Wavelength	0.71073 Å	
Crystal system	Triclinic	
Space group	P-1	
Unit cell dimensions	a = 9.512(6) Å	α= 96.062(6)°.
	b = 11.533(7) Å	β= 94.541(6)°.
	c = 16.990(10) Å	γ = 104.431(6)°.
Volume	1784.0(19) $Å^3$	
Z	2	
Density (calculated)	1.189 Mg/m^3	
Absorption coefficient	0.070 mm^{-1}	
F(000)	668	
Crystal size	0.58 x 0.22 x 0.15 mm^3	
Theta range for data collection	1.21 to 25.31°.	
Index ranges	-11<=h<=11, -13<=k<=13, -20<=l<=20	
Reflections collected	17239	
Independent reflections	6411 [R(int) = 0.0236]	
Completeness to theta = 25.31°	98.4 %	
Absorption correction	Empirical	
Max. and min. transmission	0.9898 and 0.9607	
Refinement method	Full-matrix least-squares on F^2	
Data / restraints / parameters	6411 / 0 / 479	
Goodness-of-fit on F^2	1.031	
Final R indices [I>2sigma(I)]	R1 = 0.0351, wR2 = 0.0867	
R indices (all data)	R1 = 0.0446, wR2 = 0.0919	
Largest diff. peak and hole	0.192 and -0.198 $e.Å^{-3}$	

Table 3.3.2. X-ray crystallographic data of the colored isomer of bisDPI-PN.

Identification code	The colored isomer of bisDPI-PN	
Empirical formula	C_{46} H_{30} N_4	
Formula weight	638.74	
Temperature	93(2) K	
Wavelength	0.71073 Å	
Crystal system	Monoclinic	
Space group	P2(1)/n	
Unit cell dimensions	a = 10.145(8) Å	α= 90°.
	b = 25.68(2) Å	β= 94.357(9)°.
	c = 12.867(10) Å	γ = 90°.
Volume	3342(4) $Å^3$	
Z	4	
Density (calculated)	1.269 Mg/m^3	
Absorption coefficient	0.075 mm^{-1}	
F(000)	1336	
Crystal size	0.62 x 0.34 x 0.34 mm^3	
Theta range for data collection	1.59 to 28.10°.	
Index ranges	-13<=h<=11, -33<=k<=33, -16<=l<=14	
Reflections collected	18392	
Independent reflections	7547 [R(int) = 0.0716]	
Completeness to theta = 28.10°	92.6 %	
Absorption correction	Empirical	
Max. and min. transmission	0.9753 and 0.9551	
Refinement method	Full-matrix least-squares on F^2	
Data / restraints / parameters	7547 / 0 / 451	
Goodness-of-fit on F^2	1.069	
Final R indices [I>2sigma(I)]	R1 = 0.0473, wR2 = 0.1188	
R indices (all data)	R1 = 0.0651, wR2 = 0.1323	
Largest diff. peak and hole	0.339 and -0.278 e.$Å^{-3}$	

Table 3.3.3. X-ray crystallographic data of the 1,2′-isomer A of bisDPI-PN.

Identification code	The 1,2′-isomer A of bisDPI-PN	
Empirical formula	C_{47} H_{32} Cl_2 N_4	
Formula weight	723.67	
Temperature	90 K	
Wavelength	0.71073 Å	
Crystal system	Monoclinic	
Space group	P2(1)/n	
Unit cell dimensions	a = 9.3295(16) Å	α= 90°.
	b = 21.719(4) Å	β= 98.470(2)°.
	c = 17.834(3) Å	γ = 90°.
Volume	3574.3(11) $Å^3$	
Z	4	
Density (calculated)	1.345 Mg/m^3	
Absorption coefficient	0.223 mm^{-1}	
F(000)	1504	
Crystal size	0.49 x 0.24 x 0.20 mm^3	
Theta range for data collection	1.49 to 26.45°.	
Index ranges	-10<=h<=11, -27<=k<=20, -22<=l<=22	
Reflections collected	18821	
Independent reflections	7351 [R(int) = 0.0254]	
Completeness to theta = 26.45°	99.5 %	
Absorption correction	Empirical	
Max. and min. transmission	0.9565 and 0.8977	
Refinement method	Full-matrix least-squares on F^2	
Data / restraints / parameters	7351 / 0 / 478	
Goodness-of-fit on F^2	1.038	
Final R indices [I>2sigma(I)]	R1 = 0.0476, wR2 = 0.1179	
R indices (all data)	R1 = 0.0616, wR2 = 0.1263	
Largest diff. peak and hole	0.460 and -0.816 e.$Å^{-3}$	

Table 3.3.4. X-ray crystallographic data of the 1,2′-isomer B of bisDPI-PN.

Identification code	The 1,2′-isomer B bisDPI-PN	
Empirical formula	$C_{46}H_{30}N_4$	
Formula weight	638.74	
Temperature	183 K	
Wavelength	0.71073 Å	
Crystal system	Triclinic	
Space group	P-1	
Unit cell dimensions	a = 9.720(4) Å	α= 82.640(5)°.
	b = 11.606(5) Å	β= 87.985(5)°.
	c = 15.241(6) Å	γ = 75.216(5)°.
Volume	1648.8(12) $Å^3$	
Z	2	
Density (calculated)	1.287 Mg/m^3	
Absorption coefficient	0.076 mm^{-1}	
F(000)	668	
Crystal size	0.45 x 0.36 x 0.12 mm^3	
Theta range for data collection	1.35 to 25.55°.	
Index ranges	-11<=h<=11, -14<=k<=14, -18<=l<=18	
Reflections collected	16466	
Independent reflections	6123 [R(int) = 0.0454]	
Completeness to theta = 25.55°	99.2 %	
Absorption correction	Empirical	
Refinement method	Full-matrix least-squares on F^2	
Data / restraints / parameters	6123 / 0 / 452	
Goodness-of-fit on F^2	0.993	
Final R indices [I>2sigma(I)]	R1 = 0.0508, wR2 = 0.1239	
R indices (all data)	R1 = 0.0790, wR2 = 0.1403	
Extinction coefficient	0.0036(13)	
Largest diff. peak and hole	0.365 and -0.410 e.$Å^{-3}$	

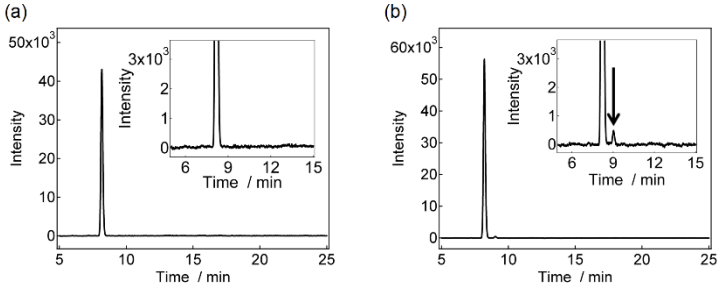

Figure 3.3.2. HPLC chromatograms of the benzene solution of the 2,2′-isomer of bisDPI-PN (a) before and (b) after UV irradiation. The HPLC analysis was performed using a reverse phase column (eluent, H_2O/acetonitrile = 1/9; flow rate, 1 mL/min; λ_{obs} = 344 nm).

The thermal stability at room temperature of the colored isomer and the colorless 2,2′-isomer of bisDPI-PN makes it possible to isolate these isomers, whereas the thermal coloration of the 2,2′-isomer is observed at elevated temperatures. The heated colorless solution of the 2,2′-isomer once becomes yellow, and the color of the solution subsequently changes to colorless very slowly with time. These color changes take longer in benzene as compared with those in cyclohexane (Figure 3.3.3). Therefore, the author carried out the thermal isomerization experiment for the cyclohexane solution of the 2,2′-isomer. Figure 3.3.4 shows the HPLC chromatograms for the cyclohexane solution of the 2,2′-isomer kept at 70 °C for 3 days in the dark. The HPLC peak of the 2,2′-isomer decreases and that of the colored isomer increases by heating. Thus the 2,2′-isomer is thermally converted to the colored isomer. The rate of disappearance of the 2,2′-isomer follows the first-order kinetics, and the rate constant is 2.70×10^{-5} s^{-1} at 70 °C in cyclohexane (Figures 3.3.5 and 3.3.6, Supporting Information). Other than the peak for the colored isomer, new peaks (peak A and peak B) are observed with a retention time of 17−19 min, as shown in Figure 3.3.4b. These fractions are not detected for the light irradiated solution of the 2,2′-isomer or the colored isomer. After another 15 days at 70 °C, the peaks for the 2,2′-isomer and the colored isomer completely disappeared and the peaks A and B increased (Figure 3.3.4c). Taking into account the thermal conversion from the colorless 2,2′-isomer to the colored isomer of bisDMDPI-BN at room temperature, it is plausible to assume that the 2,2′- isomer of bisDPI-PN is thermally converted to the colored isomer and the resultant colored isomer also thermally isomerizes to the two new constituents of peaks A and B. These two constituents are also stable at room temperature and can be isolated by preparative HPLC. The single crystals were grown from the solution of the constituent of peak A in the CH_2Cl_2/MeOH mixture and that of peak B in CH_3CN. The X-ray crystallographic analysis revealed that the constituents of peak A and peak B are the 1,2′-isomer A and the 1,2′-

isomer B, respectively (Figure 3.3.1c, d). The 1,2′-isomer has two types of imidazole rings, Im1 and Im2, as indicated in Figure 3.3.1c, d.[31,32] Im1 is a resonant planar structure that has a typical bond length for a 6π-electron system with an electron-donating characteristic, whereas Im2 has two localized C=N double bonds and one sp^3 carbon atom connecting Im1, consistent with a 4π-electron system with an electron-withdrawing characteristic. Thus the 1,2′-dimer A and the 1,2′-dimer B can be distinguished in a bonding manner between the imidazole ring and the aryl moiety. Im1 of the 1,2′-dimer A is bonded to a naphthyl ring whereas that of the 1,2′-dimer B is bonded to a phenyl ring. The bond lengths of the C−N bonds between two imidazole rings of 1,2′-isomers A and B are 1.478(2) and 1.486(2) Å, respectively. These bond lengths are approximately equal to that of 1,2′-isomers of the other bridged imidazole dimers.

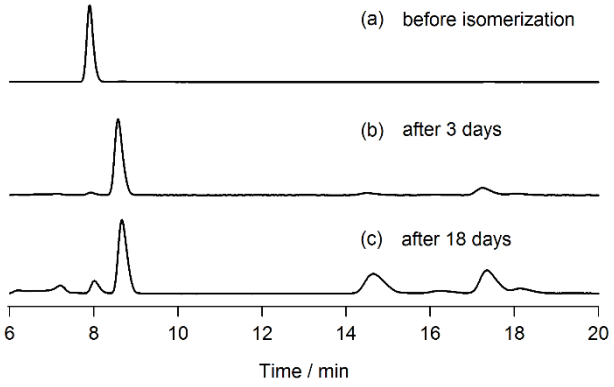

Figure 3.3.3. HPLC chromatograms of the benzene solution of bisDPI-PN. (a) the 2,2′-isomer, (b) the solution after kept 3 days at 70 °C and (d) the solution after kept 18 days at 70 °C. HPLC analysis was performed using reverse phase column (eluent; H_2O/acetonitrile = 9/1, flow rate; 1 mL/min, λ_{obs} = 344 nm).

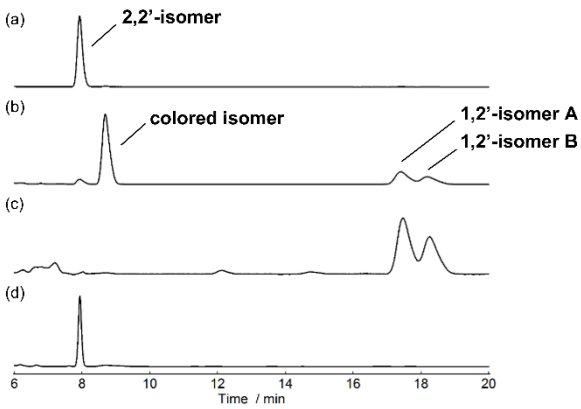

Figure 3.3.4. HPLC chromatograms of the cyclohexane solution of bisDPI-PN: (a) the 2,2′-isomer, (b) the solution after kept 3 days at 70 °C, (c) the solution after kept 18 days at 70 °C, and (d) the solution after visible light (400−700 nm) irradiation. HPLC analysis was performed using reversed phase column (eluent, H_2O/acetonitrile = 9/1; flow rate, 1 mL/min; λ_{obs} = 344 nm).

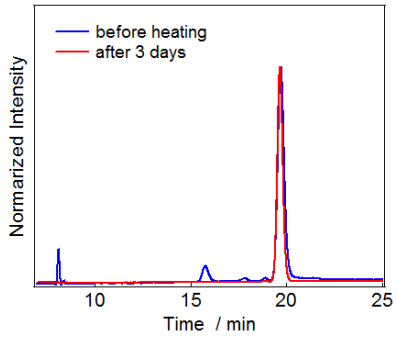

Figure 3.3.5. HPLC chromatograms of cyclohexane solution of the 1,2′-isomer B of bisDPI-PN. (blue line) Before heating the solution, (red line) after heating the solution at 70 °C for 3 days. HPLC analysis was performed using reversed phase column (eluent, H_2O/acetonitrile = 9/1; flow rate, 1 mL/min; λ_{obs} = 344 nm).

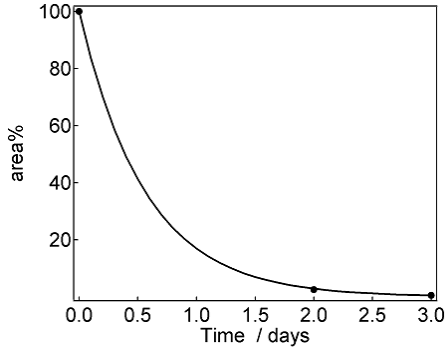

Figure 3.3.6. Decay profiles of the 2,2′-isomer of bisDPI-PN monitored at 334 nm in benzene at 70 °C.

Moreover, the author found that the 1,2′-isomers A and B are converted to the 2,2′-isomer not only by UV light irradiation but also by visible light irradiation. The UV light irradiation to the solution of 1,2′-isomers forms both the 2,2′-isomer and the colored isomer and causes the color change of the solution from colorless to yellow, whereas the visible light irradiation does not change the color of the solution and forms only the 2,2′- isomer, as shown in Figure 3.3.4d. As will be described below, this behavior can be attributable to the photoconversion of the colored isomer to the 2,2′-isomer through the biradical with the irradiation of visible light that is not absorbed by the 2,2′-isomer. As shown in Figure 3.3.7, the absorption tails of the 1,2′- isomers A and B extending into the visible light region of the spectra as well as the other 1,2′-dimers including the classical HABI derivatives[33] make it possible to form the biradical by visible light irradiation. The mechanism of this unique photoisomerization will be discussed later.

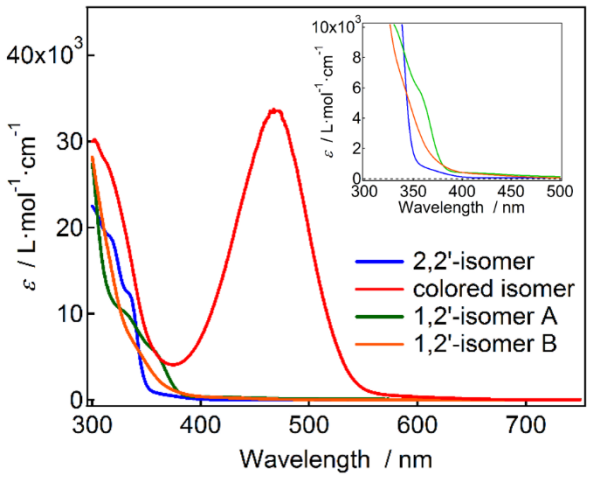

Figure 3.3.7. UV−vis absorption spectra of each isomer of bisDPI-PN in benzene at 25 °C. The inset is the enlargement of the spectra.

3.4 Laser flash photolysis

Because all bridged imidazole dimers except for bisDMDPI-BP have been reported to generate biradicals by light irradiation, the four kinds of structural isomers of bisDPI-PN could be also expected to generate the biradical by light irradiation. The author investigated the possible presence of the short-lived biradical in the photochemical process of bisDPI-PN by nanosecond laser flash photolysis. Figure 3.4.1a shows the transient vis−NIR absorption spectrum of the 2,2′-isomer of bisDPI-PN in benzene at room temperature, excited with a nanosecond laser pulse at 355 nm. The identical transient absorption spectra were also obtained for the other isomers. A sharp absorption band around at 400 nm and a broad absorption band ranging from 500 to 800 nm can be ascribed to the biradical because its spectrum shape is similar to those of the colored biradicals observed for the other bridged imidazole dimers. Figure 3.4.1b shows the decay profile of the transient absorbance at 400 nm of the biradical. The decay profile of the biradical obeys first-order kinetics with a half-life of 180 ns at 25 °C, which is the fastest among the reported half-lives of the imidazolyl radicals of HABI derivatives. The author also confirmed that the shape of the transient absorption spectra and the decay kinetics are not affected by the presence of molecular oxygen as shown in Figure 3.4.2.

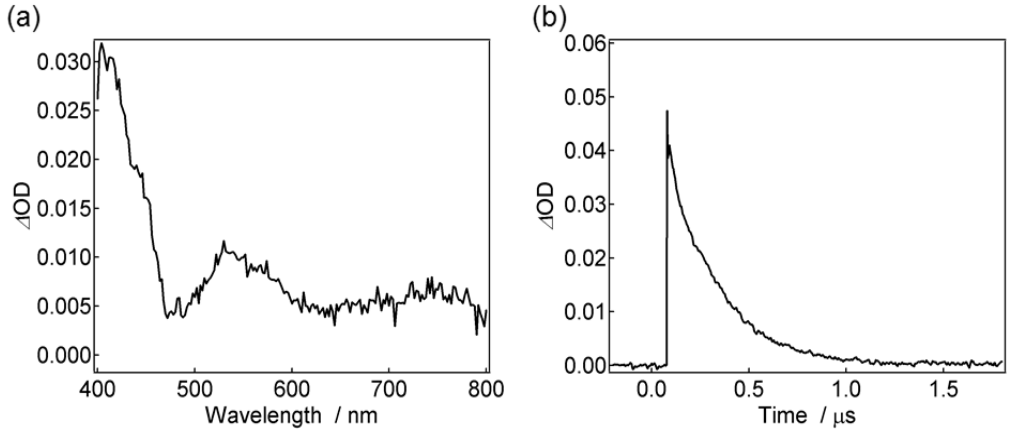

Figure 3.4.1. (a) Transient vis−NIR absorption spectra of the 2,2′-isomer of bisDPI-PN in deaerated benzene (1.1×10^{-4} M) at 25 °C. The spectrum was recorded at 100 ns after excitation with a nanosecond laser pulse (excitation wavelength, 355 nm; pulse width, 5 ns; power, 3 mJ/pulse). (b) Decay profile of the biradical monitored at 400 nm in deaerated benzene (1.1×10^{-4} M) at 25 °C (excitation wavelength, 355 nm; pulse width, 5 ns; power, 3 mJ/pulse).

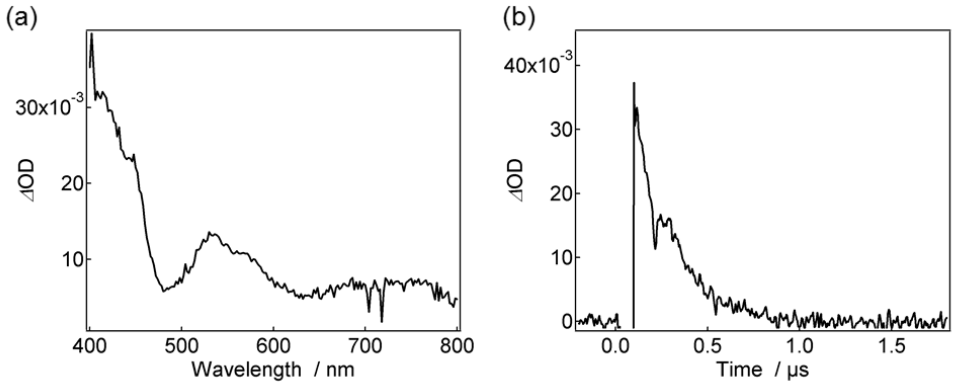

Figure 4.3.2. (a) Transient vis–NIR absorption spectra of the benzene solution of the 2,2′-isomer of bisDPI-PN in oxygen atmosphere (1.1×10^{-4} M) at 25 °C. The spectrum was recorded at 100 ns after excitation with a nanosecond laser pulse (excitation wavelength; 355 nm, pulse width; 5 ns, power; 3 mJ/pulse). (b) Decay profile of the biradical monitored at 400 nm of benzene solution in oxygen atmosphere (1.1×10^{-4} M) at 25 °C (excitation wavelength: 355 nm, pulse width: 5 ns, power: 3 mJ/pulse).

3.5 Radical recombination reaction of biradical

The significant question to be solved as to the photochemical isomerizations is to elucidate the products formed by the radical recombination reaction of the photogenerated biradical. As already mentioned, the 2,2′-isomer is converted to the colored isomer by UV light irradiation, and the colored isomer mainly returns to the 2,2′-isomer by visible light irradiation. The 1,2′-isomers A and B mainly return to the 2,2′-isomer by UV or visible light irradiation. These observations can raise the assumption that the major product by the radical recombination reaction of the biradical is the 2,2′-isomer. The photochemical conversion of the colored isomer was investigated by HPLC analysis for the benzene solution irradiated with the laser pulses of the wavelength of 550 nm at 70 °C, at which temperature the experiment of the thermal conversion of the 2,2′-isomer shown in Figure 3.3.4 was conducted. As shown in Figure 3.5.1, the peak intensity of the colored isomer with a retention time around 9 min decreases with increasing the irradiation times of the visible laser pulses, whereas that of the 2,2′-isomer with a retention time around 8 min increases. It is worth noting that the negligibly small HPLC peaks attributable to the 1,2′-isomers A and B appear after the light irradiation. Thus, it can be concluded that the radical recombination reaction of the biradical affords the 2,2′-isomer as a major product and the colored isomer as a minor product. The observation of the photochemical conversion from the 2,2′-isomer to the colored isomer by UV light irradiation as shown in Figure 3.3.2 would be the direct evidence for the formation of the colored isomer by the radical recombination reaction of the biradical. It is considered that the activation energy barriers toward the formation of the 2,2′-isomer is smaller than those of the colored isomer and the 1,2′-isomers A and B.

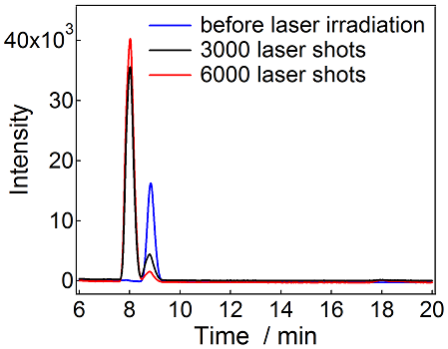

Figure 3.5.1. HPLC chromatograms of the benzene solutions of the colored isomer of bisDPI-PN. The solution was irradiated with the laser pulses (3 mJ/pulse) of the wavelength of 550 nm at 70 °C. HPLC analysis was performed using reverse phase column (eluent, H_2O/acetonitrile = 9/1; flow rate, 1 mL/min; λ_{obs} = 344 nm).

3.6 Photochemical conversion efficiency

The photochemical conversion efficiency from the colored isomer to the 2,2′-isomer was investigated with the intention to evaluate the negative photochromic property of bisDPI-PN. The conversion efficiency was estimated by nanosecond laser flash photolysis by using 1,2-bis(2-methylbenzo[*b*]thiophen-3-yl)perfluorocyclopentene (DAE) as a standard.[28,34] The colorless open-ring isomer of DAE can undergo cyclization in a conrotatory fashion to the colored closed-ring isomer upon UV light irradiation. The thermal back-reaction is symmetry-forbidden, giving excellent thermal stability to the closed-ring isomer. The cycloreversion reaction from the closed-ring isomer to the open-ring isomer occurs only by irradiating with a visible light. The solutions of the colored isomer of bisDPI-PN in benzene and the closed-ring isomer of DAE in hexane with matched absorbances at the excitation wavelength of 517 nm were irradiated at various laser energies (Figure 3.6.1). The absorbance changes, ΔOD(DAE), before and after a laser pulse irradiation at 517 nm for the closed-ring isomer of DAE were plotted against those, ΔOD(S), for the colored isomer of bisDPI-PN. The conversion efficiency was estimated from the slope of the fit of the data to the following equation,[35,36]

$$\Delta OD(DAE) = \frac{\varphi_{DAE}\varepsilon_{DAE}}{\varphi_s\varepsilon_s}\Delta OD(S) \qquad \text{(eq. 3.1)}$$

where φ_{DAE} (0.35) is the quantum yield of cycloreversion reaction of DAE excited at 517 nm,[37] φ_s is the conversion efficiency from the colored isomer to the 2,2′-isomer of bisDPI-PN, and ε_{DAE} (0.91 × 104 M^{-1} cm^{-1}) and ε_s (0.98 × 104 M^{-1} cm^{-1}) are the absorptivity coefficients of DAE[37] and the colored isomer of bisDPI-PN at 517 nm, respectively. As shown in Figure 3.6.3, φ_s was obtained from the slope of the fit of the data to eq. 3.1 and was determined to be 0.14, which is about 5 times larger than that of bisDMDPI-BN reported in our previous paper.[28]

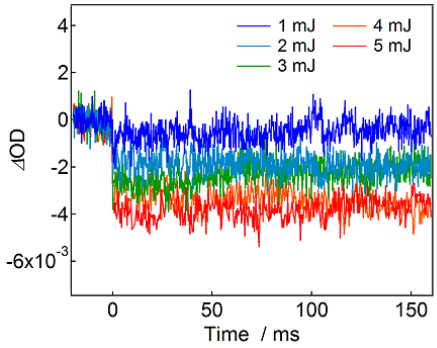

Figure 3.6.1. Laser intensity dependence of the time profiles of transient absorbance of the colored isomer of bisDPI-PN in benzene (1.4×10^{-6} M) at 293 K monitored at 517 nm (excitation wavelength: 517 nm, pulse width: 5 ns).

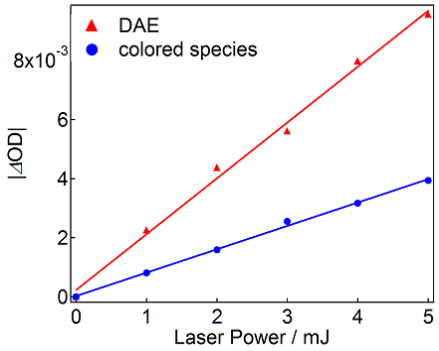

Figure 3.6.2. Laser power dependence of the absorbance change, |⊿OD|, before and after a laser pulse irradiation at 517 nm for the closed-ring isomer of DAE in hexane (5.49×10^{-6} M) and the colored isomer of bisDPI-PN in benzene (1.4×10^{-6} M) at 293 K.

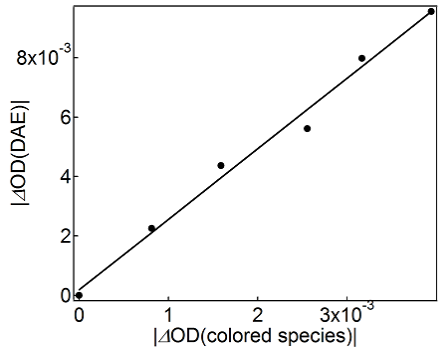

Figure 3.6.3. |⊿OD(DAE)| vs. |⊿OD(s)|. The photochemical conversion efficiency from the colored isomer to the 2,2′-isomer of bisDPI-PN was obtained from the slope of the fit of the data to eq. 3.1.

3.7 DFT calculations for isomers

By comparing the photochemical and thermochemical properties of bisDMDPI-BP, bisDMDPI-BN, and bisDPI-PN, the author found that the biaryl moiety that bridges a set of DPIs would have a significant effect on the stability of the isomers. BisDPI- PN has four kinds of stable isomers, i.e., the 2,2′-isomer, the colored isomer, and the 1,2′-isomers A and B, and a short-lived biradical, whereas bisDMDPI-BN has two kinds of stable isomers, i.e., the 2,2′-isomer and the colored isomer, and a short-lived biradical. On the other hand, only the 2,2′-isomer is the stable form of bisDMDPI-BP. The author carried out the DFT calculations to investigate the relative energies for the isomers of bisDMDPI-BP, bisDMDPI-BN, and bisDPI-PN. As shown in Figure 3.7.1, the most stable isomer for these biaryl-bridged imidazole dimers is the 1,2′-isomer. However, the 1,2′-isomers are not formed from the biradicals that is generated by the oxidation of the lophine precursors or by the photochemical reaction in the case of bisDMDPI-BN and the negligibly small amount of the 1,2′-isomera A and B are given from biradical in the case of bisDPI-PN. This incomprehensible behavior leads to the idea that the activation energy barriers toward the formation of the 1,2′-isomers from the biradicals are significantly higher than those toward the formation of the 2,2′-isomers and the colored isomers. The author considered that the major products of the radical recombination reaction of the biradicals are not the colored isomers but the 2,2′-isomers. This idea can be supported by the two experimental results. The first basis is that the 1,2′-isomers A and B of bisDPI-PN are converted to the 2,2′-isomer by UV light irradiation, and the second basis is that the oxidation of the lophine precursor of bisDMDPI-BN at room temperature initially forms the colorless solution that gradually changes to the red solution by forming the colored isomer.

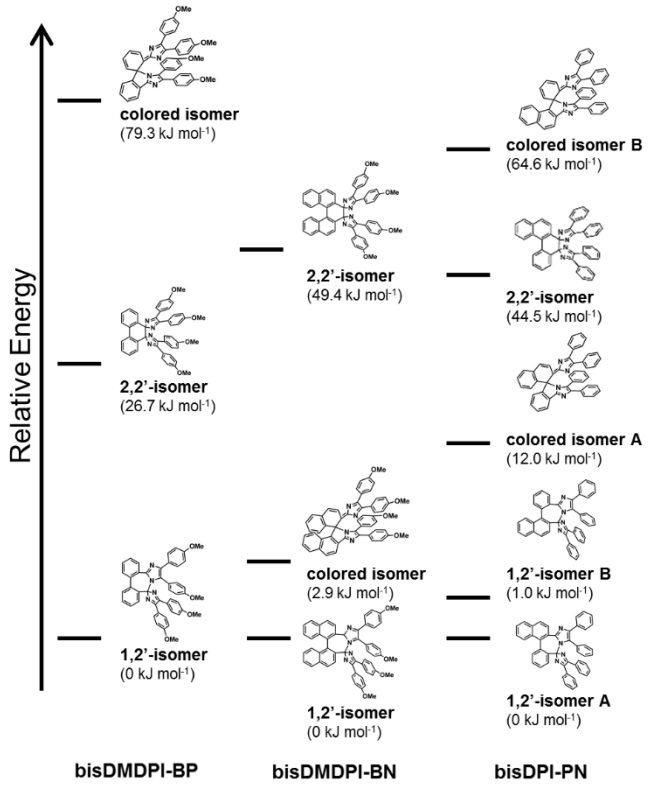

Figure 3.7.1. Schematic drawing of the energy level diagrams of the isomers of bisDMDPI-BP, bisDMDPI-BN, and bisDPI-PN calculated by the DFT M052X/6-31G(d) level of the theory. The energy levels of the 1,2′-isomers of all the molecules are set to zero for comparing the energy differences for each molecule.

The stability of the colored isomers can be accounted for by the resonance energy of the phenyl ring in the biaryl-bridging moiety. Both the colored isomer of bisDMDPI-BP and the colored isomer B of bisDPI-PN described in Figure 3.7.1 are unstable due to the loss of aromaticity of the phenyl ring in the biaryl-bridging moiety. On the other hand, the colored isomer of bisDMDPI-BN and the colored isomer A of bisDPI-PN, which is identical to the colored isomer isolated in this work, have the same diazafulvene substructure connected to the naphthyl moiety. Thus it is considered that these colored isomers are relatively stable compared with the colored isomers that lose the aromaticity of the phenyl rings.

By combining the above-described considerations, the author assumes the thermal conversion from the 2,2′-isomers to the colored proceeds by the thermally generated biradical. The 2,2′-isomer of classical HABI is known to show thermochromism that gives triphenylimidazolyl radicals by homolytic cleavage of the C−C bond between the imidazole

rings.[38–41] The oxidation of triphenylimidazole at lower than 5 °C gives the 2,2′-isomer, whereas the 1,2′-isomer is obtained at room temperature. This behavior can be accounted for by the difference in the activation energy barriers toward the formation of the imidazole dimers. That is, the activation energy barrier for the dimerization path to form the 2,2′-isomer is lower than that for the 1,2′-isomer. However, the 2,2′-isomer consisting of a couple of 4π-electron imidazole rings is less stable than the 1,2′-isomer consisted of a 6π-electron imidazole ring and a 4π-electron imidazole ring because of the lack of resonance effect in imidazole ring for the 2,2′-isomer. Thus the thermochemical instability of the 2,2′-isomer causes the thermochromism by forming the thermally stable 1,2′-isomer through the biradical by increasing the temperature. We already reported the in situ direct observation of the thermal isomerization from the 2,2′-isomer to the 1,2′-isomer of HABI in crystal by X-ray crystallographic analysis.[42,43] Therefore, it seems reasonable to assume that the 2,2′-isomer of bisDPI-PN also shows thermochromism at elevated temperature to form the biradical that would dimerize to form the more stable colored isomer A than the 2,2′-isomer by overcoming the activation energy barrier toward the formation of the colored isomer A. However, an attempt to detect the biradical of bisDPI-PN at elevated temperature by EPR measurement was unsuccessful due to the low concentration of the biradical with extremely short half-life (180 ns at 25 °C) as described above.

On the other hand, almost reported bridged imidazole dimers were obtained as the 1,2′-isomers. Thus it can be considered that the small amount of the 1,2′-isomers A and B of bisDPI-PN are also formed from the biradical. This indicates that thermal generation of the biradical from the colored isomer, because the generation of the 1,2′-isomers proceeds from the colored isomer. The rate constant for the thermal generation of the biradical from the 2,2′-isomer of bisDPI-PN would be larger than that of the colored isomer due to the instability of the 2,2′-isomer. Therefore, it is believed that the concentration of the 2,2′ -isomer does not increase after the thermal equilibrium moves from the 2,2'-isomer to the colored isomer. As a result, the colored isomer appears to directly isomerizes to the 1,2′-isomer. As a whole, the photochemical and thermochemical transformations between the isomers of bisDPI-PN can be summarized as shown in Figure 3.7.2.

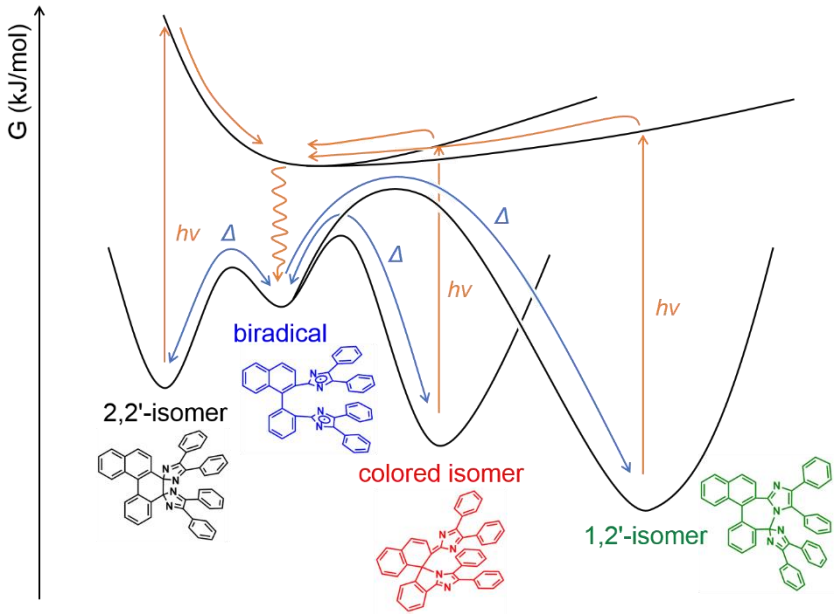

Figure 3.7.2. Schematic drawing of the potential energy surfaces for the excited state (upper) and the ground state (lower) of bisDPI-PN accounting for the photochemical and thermochemical transformation between the isomers.

3.8 Conclusion

The author investigated the photochemical and the thermochemical behavior of bisDPI-PN with a 1-phenylnaphthalene moiety that bridges two diphenylimidazole units at the 2- and 2′-positions. This molecule shows unique multistate photochromism, in which the stable colorless 1,2′-isomers A and B photochemically isomerize to the colorless 2,2′-isomer. Although the 2,2′-isomer is stable at room temperature, it thermally returns to the initial 1,2′-isomers A and B through the biradical and usually the colored isomer at elevated temperatures. The colored isomer consists of the diazafulvene structure formed by the C−N bond between the nitrogen atom of the imidazole ring bonded at the 2′-position and the carbon atom at the 2-position of the 1-phenylnaphthalene moiety. The molecular structures of these four kinds of structural isomers were determined by X-ray crystallographic analysis. It should be emphasized that these isomers are stable at room temperature and can be almost fully converted to the 2,2′-isomer by light irradiation. The photochemical conversion can be accounted for by the radical recombination reaction of the short-lived biradical with a half-life of 180 ns at 25 °C that is generated from all isomers by light irradiation. The reason the 2,2′-isomer is mainly formed from the biradical would be attributable to the low activation energy barrier toward the formation of the 2,2′-isomer by comparing the activation energy barriers toward the formation of the other isomers. The theoretical considerations of the mechanisms for the thermal isomerization and the radical

recombination reaction are important problems left for future study. Thus the aryl-bridged imidazole dimers are attractive multistate photochromic molecules with negative and positive photochromic properties. As described at the beginning, only a few molecules have been reported to show negative photochromism. The development of unique photochromic molecules with negative photochromism would open a new field in the photoresponsive materials. This study serves the useful strategy for the molecular design of a new type of negative photochromic molecules applicable to switch molecular properties by visible light irradiation. The rational molecular design to prevent the formation of the colorless 1,2′-dimer from the colored isomer and to destabilize the colorless 2,2′-isomer will lead to the development of an unknown fast negative photochromic molecule that enables us to change and reset the molecular properties by simply turning a visible light source on and off.

3.9 References

(1) Hayashi, T.; Maeda, K. *Bull. Chem. Soc. Jpn.* **1960**, *33*, 565−566.
(2) White, D. M.; Sonnenberg, J. *J. Am. Chem. Soc.* **1966**, *88*, 3825−3829.
(3) Maeda, K.; Hayashi, T. *Bull. Chem. Soc. Jpn.* **1969**, *42*, 3509−3514.
(4) Shida, T.; Maeda, K.; Hayashi, T. *Bull. Chem. Soc. Jpn.* **1970**, *43*, 652−657.
(5) Cohen, R. L. *J. Org. Chem.* **1971**, *36*, 2280−2284.
(6) Riem, R. H.; MacLachlan, A.; Coraor, G. R.; Urban, E. J. *J. Org. Chem.* **1971**, *36*, 2272−2275.
(7) Cescon, L. A.; Coraor, G. R.; Dessauer, R.; Silversmith, E. F.; Urban, E. J. *J. Org. Chem.* **1971**, *36*, 2262−2267.
(8) Tanino, H.; Kondo, T.; Okada, K.; Goto, T. *Bull. Chem. Soc. Jpn.* **1972**, *45*, 1474−1480.
(9) Qin, X.-Z.; Liu, A.-D.; Trifunac, A. D.; Krongauz, V. V. *J. Phys. Chem.* **1991**, *95*, 5822−5826.
(10) Liu, A.-D.; Trifunac, A. D.; Krongauz, V. V. *J. Phys. Chem.* **1992**, *96*, 207−211.
(11) Kawano, M.; Sano, T.; Abe, J.; Ohashi, Y. *J. Am. Chem. Soc.* **1999**, *121*, 8106−8107.
(12) Kawano, M.; Sano, T.; Abe, J.; Ohashi, Y. *Chem. Lett.* **2000**, *29*, 1372−1373.
(13) Abe, J.; Sano, T.; Kawano, M.; Ohashi, Y.; Matsushita, M. M.; Iyoda, T. *Angew. Chem., Int. Ed.* **2001**, *40*, 580−582.
(14) Kikuchi, A.; Iyoda, T.; Abe, J. *Chem. Commun.* **2002**, *38*, 1484−1485.
(15) Kikuchi, A.; Iwahori, F.; Abe, J. *J. Am. Chem. Soc.* **2004**, *126*, 6526−6527.
(16) Miyamoto, Y.; Kikuchi, A.; Iwahori, F.; Abe, J. *J. Phys. Chem. A* **2005**, *109*, 10183−10188.
(17) Miyasaka, H.; Satoh, Y.; Ishibashi, Y.; Ito, S.; Nagasawa, Y.; Taniguchi, S.; Chosrowjan, H.; Mataga, N.; Kato, D.; Kikuchi, A.; et al. *J. Am. Chem. Soc.* **2009**, *131*, 7256−7263.

(18) Kimoto, A.; Niitsu, A.; Iwahori, F.; Abe, J. *New J. Chem.* **2009**, *33*, 1339.
(19) Kikuchi, A.; Harada, Y.; Yagi, M.; Ubukata, T.; Yokoyama, Y.; Abe, J. *Chem. Commun.* **2010**, *46*, 2262−2264.
(20) Kishimoto, Y.; Abe, J. A *J. Am. Chem. Soc.* **2009**, *131*, 4227−4229.
(21) Harada, Y.; Hatano, S.; Kimoto, A.; Abe, J. *J. Phys. Chem. Lett.* **2010**, *1*, 1112−1115.
(22) Kimoto, A.; Tokita, A.; Horino, T.; Oshima, T.; Abe, J. *Macromolecules* **2010**, *43*, 3764−3769.
(23) Mutoh, K.; Hatano, S.; Abe, J. *J. Photopolym. Sci. Technol.* **2010**, *23*, 301−306.
(24) Hatano, S.; Sakai, K.; Abe, J. *Org. Lett.* **2010**, *12*, 4152−4155.
(25) Takizawa, M.; Kimoto, A.; Abe, J. *Dyes Pigm.* **2011**, *89*, 254−259.
(26) Mutoh, K.; Abe, J. *J. Phys. Chem. A* **2011**, *115*, 4650−4646.
(27) Mutoh, K.; Abe, J. *Chem. Commun.* **2011**, *47*, 8868−8870.
(28) Yamashita, H.; Abe, J. *J. Phys. Chem. A* **2011**, *115*, 13332−13337.
(29) Mutoh, K.; Nakano, E.; Abe, J. *J. Phys. Chem. A* **2011**, *116*, 6792−6797.
(30) Ishii, N.; Kato, T.; Abe, J. *Sci. Rep.* **2012**, *2*, 819−824.
(31) Kawai, S.; Yamaguchi, T.; Kato, T.; Hatano, S.; Abe, J. *Dyes Pigm.* **2012**, *92*, 872−876.
(32) Mutoh, K.; Sliwa, M.; Abe, J. *J. Phys. Chem. C* **2013**, *117*, 4808−4814.
(33) Iwahori, F.; Hatano, S.; Abe, J. *J. Phys. Org. Chem.* **2007**, *20*, 857−863.
(34) Fujita, K.; Hatano, S.; Kato, D.; Abe, J. *Org. Lett.* **2008**, *10*, 3105−3108.
(35) Hatano, S.; Abe, J. *J. Phys. Chem. A* **2008**, *112*, 6098−6103.
(36) Hatano, S.; Fujita, K.; Tamaoki, N.; Kaneko, T.; Nakashima, T.; Naito, M.; Kawai, T.; Abe, J. *J. Phys. Chem. Lett.* **2011**, *2*, 2680−2682.
(37) Hatano, S.; Abe, J. *Phys. Chem. Chem. Phys.* **2012**, *14*, 5855−5860.
(38) Mutoh, K.; Shima, K.; Yamaguchi, T.; Kobayashi, M.; Abe, J. *Org. Lett.* **2013**, *15*, 2938−2941.
(39) Shimizu, I.; Kokado, H.; Inoue, E. *Bull. Chem. Soc. Jpn.* **1969**, *42*, 1730−1734.
(40) Inoue, E.; Kokado, H.; Shimizu, I.; Kobayashi, H. *Bull. Chem. Soc. Jpn.* **1972**, *45*, 1951−1956.
(41) Namba, K.; Shimizu, I. *Bull. Chem. Soc. Jpn.* **1975**, *48*, 1323−1324.
(42) Sunamoto, J.; Iwamoto, K.; Akutagawa, M.; Nagase, M.; Kondo, H. *J. Am. Chem. Soc.* **1982**, 104, 4904−4907.
(43) Ciardelli, F.; Fabbri, D.; Pieroni, O.; Fissi, A. *J. Am. Chem. Soc.* **1989**, *111*, 3470−3472.
(44) Inouye, M.; Ueno, M.; Kitao, T. Alkali *J. Am. Chem. Soc.* **1990**, *112*, 8977−8979.
(45) Hirano, M.; Miyashita, A.; Shitara, H.; Nohira, H. *Chem. Lett.* **1991**, *20*, 1873−1876.
(46) Takagi, K.; Kurematsu, T.; Sawaki, Y. *J. Chem. Soc., Perkin Trans. 2* **1991**, *10*, 1517−1522.
(47) Nakano, S.; Miyashita, A.; Nohira, H. *Chem. Lett.* **1993**, *22*, 13−16.

(48) Yokoyama, Y.; Shiroyama, T. *Chem. Lett.* **1995**, *24*, 71−72.
(49) Fissi, A.; Pieroni, O.; Ruggeri, G.; Ciardelli, F. *Macromolecules* **1995**, *28*, 302−309.
(50) Takagi, K.; Kurematsu, T.; Sawaki, Y. *J. Chem. Soc., Perkin Trans. 2* **1995**, *8*, 1667−1671.
(51) Minami, M.; Taguchi, N. *Chem. Lett.* **1996**, *25*, 429−430.
(52) Suzuki, T.; Lin, F.-T.; Priyadashy, S.; Weber, S. G. *Chem. Commun.* **1998**, *24*, 2685−2686.
(53) Tanaka, M.; Nakamura, M.; Salhin, M. A. A.; Ikeda, T.; Kamada, K.; Ando, H.; Shibutani, Y.; Kimura, K. *J. Org. Chem.* **2001**, *66*, 1533−1537.
(54) Pieroni, O.; Fissi, A.; Angelini, N.; Lenci, F. *Acc. Chem. Res.* **2001**, *34*, 9−17.
(55) Tanaka, M.; Ikeda, T.; Xu, Q.; Ando, H.; Shibutani, Y.; Nakamura, M.; Sakamoto, H.; Yajima, S.; Kimura, K. *J. Org. Chem.* **2002**, *67*, 2223−2227.
(56) Yokoyama, Y.; Hara, W.; Inoue, T.; Ubukata, T.; Sakomura, M.; Tukada, H. *Chem. Lett.* **2005**, *34*, 1622−1623.
(57) Keum, S.-R.; Roh, S.-J.; Kim, S.-E.; Lee, S.-H.; Cho, C.-H.; Kim, S.-H.; Koh, K.-N. *Bull. Korean Chem. Soc.* **2006**, *27*, 187−188.
(58) Tomasulo, M.; Yildiz, I.; Raymo, F. M. *Inorg. Chim. Acta* **2007**, *360*, 938−944.
(59) Zhang, C.; Zhang, Z.; Fan, M.; Yan, W. *Dyes Pigm.* **2008**, *76*, 832−835.
(60) Sakai, K.; Imaizumi, Y.; Oguchi, T.; Sakai, H.; Abe, M. *Langmuir* **2010**, *26*, 9283−9288.
(61) Mitchell, R. H.; Ward, T. R.; Chen, Y.; Wang, Y.; Weerawarna, S. A.; Dibble, P. W.; Marsella, M. J.; Almutairi, A.; Wang, Z.-Q. *J. Am. Chem. Soc.* **2003**, *125*, 2974−2988.
(62) Kobayashi, M.; Takashima, A.; Ishii, T.; Naka, H.; Uchiyama, M.; Yamaguchi, K. *Inorg. Chem.* **2007**, *46*, 1039−1041.
(63) Irie, M.; Fukaminato, T.; Tanaka, M. Japan Patent JP 2009-062344 A, **2009**.
(64) Fukaminato, T.; Doi, T.; Tanaka, M.; Irie, M. *J. Phys. Chem. C* **2009**, *113*, 11623−11627.
(65) Ayub, K.; Li, R.; Bohne, C.; Williams, R. V.; Mitchell, R. H. *J. Am. Chem. Soc.* **2011**, *133*, 4040−4045.
(66) Peng, P.; Strohecker, D.; Liao, Y. *Chem. Commun.* **2011**, *47*, 8575−8577.
(67) Hatano, S.; Horino, T.; Tokita, A.; Oshima, T.; Abe, J. *J. Am. Chem. Soc.* **2013**, *135*, 3164−3172.
(68) Hanazawa, M.; Sumiya, R.; Horikawa, Y.; Irie, M. *J. Chem. Soc., Chem. Commun.* **1992**, 206−207.
(69) Wintgens, V.; Johnston, L. J.; Scaiano, J. C. *J. Am. Chem. Soc.* **1988**, *110*, 511−517.
(70) Sheepwash, M. A. L.; Ward, T. R.; Wang, Y.; Bandyopadhyay, S.; Mitchell, R. H.; Bohne, C. *Photochem. Photobiol. Sci.* **2003**, *2*, 104−112.

(71) Yamaguchi, T.; Uchida, K.; Irie, M. *Bull. Chem. Soc. Jpn.* **2008**, *81*, 644−652.
(72) Moleele, S. S.; Michael, J. P.; de Koning, C. B. *Tetrahedron* **2008**, *64*, 10573−10580.
(73) Sheldrick, G. M. SHELXS-97 and SHELXL-97; University of Gottingen: Gottingen, Germany, **1997**.
(74) Sheldrick, G. M. SADABS; University of Gottingen: Gottingen, Germany, **1996**.
(75) Frisch, M. J.; Trucks, G. W.; Schlegel, H. B.; Scuseria, G. E.; Robb, M. A.; Cheeseman, J. R.; Scalmani, G.; Barone, V.; Mennucci, B.; Petersson, G. A.; *et al*. Gaussian 09, Revision D.01; Gaussian, Inc.: Wallingford, CT, **2009**.

Chapter 4
Binaphthyl-bridged phenoxyl-imidazolyl radical complex

4.1 Introduction

Photochromic compounds have been applied to various fields of science and technologies because of their high functionalities and versatilities.[1–4] In conventional T-type photochromic compounds, the colorless or less colored form is a stable isomer and it isomerizes to the thermally unstable colored form upon UV light irradiation. Although conventional T-type photochromic compounds have been demonstrated as a promising materials for various applications, one of the serious issues is reabsorption of the excitation UV light by the photogenerated colored form. That is, the photochromic reaction can be occurred only near the surface of the materials. This issue becomes prominent in bulk materials such as crystal, film, and liquid crystal. If the photogenerated species does not absorb the excitation light, the light goes into the deep inside of the materials and induces the photochromic reactions at the inside of the materials. One of the best candidates for overcoming this subject is the use of negative photochromic compounds. Negative photochromism is a photochromic reaction in which the thermally stable colored form isomerizes to the metastable colorless form upon visible light irradiation and the generated colorless form thermally returns to the initial colored form.[5–8] There are several reports on negative photochromic compounds such as spiropyran derivatives,[9–11] dimethyldihydropyrenes,[12,13] Stenhouse salts,[14,15] and 1,1´-binaphthyl-bridged imidazole dimer.[16] The time scales of the thermal back reaction of these negative photochromic reactions range from minutes through hours to days, and no fast-response negative photochromic compounds have been demonstrated until today.

The potentials of the acceleration of the thermal back reaction in T-type photochromic compounds have been demonstrated by bridged imidazole dimers,[17–19] pentaarylbiimidazole (PABI),[20] phenoxyl-imidazolyl radical complex (PIC)[21] and so on.[22–24] By accelerating the thermal back reaction from seconds to sub-microseconds, the potential applications of these photochromic compounds have expanded from photochromic lenses to dynamic holography,[25,26] security systems and fast fluorescence switching for super-resolution microscope.[27,28] As already demonstrated by the fast photochromic molecules, the acceleration of the thermal back reaction of negative photochromism is expected to initiate novel potentials of negative photochromic materials.

In this chapter, the author report the fast photoswitchable negative photochromism of 1,1´-binaphthyl-bridged phenoxyl-imidazolyl radical complex (BN-PIC, Scheme 4.1). The strategy for the molecular design of BN-PIC was inspired by the molecular frameworks of PIC and 1,1´-binaphthyl-bridged imidazole dimer. Upon light irradiation, the colored and colorless forms of BN-PICs give the short-lived biradical species that forms either colored or colorless forms by the intramolecular radical coupling reaction. **BN-PIC1** shows slow thermal back reaction from the photogenerated colorless form to the thermally stable colored form via the thermally accessible biradical species while **BN-PIC2**, in which the diphenylimidazole moiety is replaced with the phenanthroimidazole moiety, greatly accelerates the thermal back reaction to second time scales. In addition to the negative photochromic properties of BN-PICs, the unique chiroptical properties are also demonstrated.

Scheme 4.1.1 Photochromic reaction of (a) **BN-PIC1** and (b) **BN-PIC2**

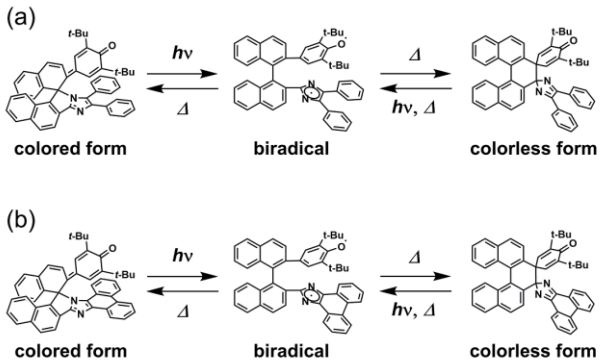

4.2 Experimental Section

4.2.1 Synthesis

Materials: All reactions were monitored by thin-layer chromatography carried out on 0.2 mm E. Merck silica gel plates (60F-254). Column chromatography was performed on silica gel (Wakogel® C-300). All reagents and solvents were obtained from commercial suppliers (Sigma-Aldrich, Wako Chemicals, TCI, Kanto Chemical Company, Inc., and Acros Organics) and the reagents were used without further purification. All reaction solvents were distilled on the appropriate drying reagents prior to use. ^{1}H NMR spectra and ^{13}C NMR spectra were recorded on a Bruker AVANCE III 400NanoBay at 400 and 100 MHz, respectively. Chemical shifts (δ) are recorded in parts per million (ppm) relative to tetramethylsilane, and the coupling constants (J) are reported in Hertz (Hz). DMSO-d_6 and $CDCl_3$ were used as deuterated solvents. Mass spectra (ESI-TOF-MS) were recorded on a Bruker micrOTOF II-AGA1.

Scheme 4.2.1 Synthetic scheme of **BN-PIC1** and **BN-PIC2**

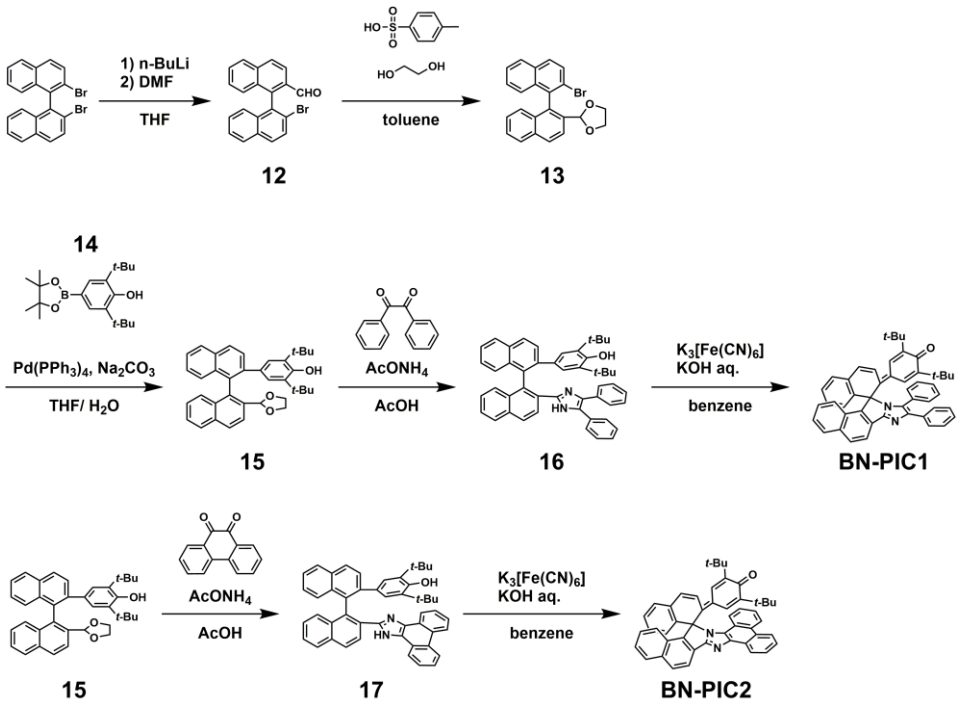

2´-bromo-[1,1´-binaphthalene]-2-carbaldehyde (12)

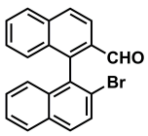

12

2,2´-Dibromo-1,1´-binaphthyl (995 mg, 2.4 mmol) was dissolved in dry THF 13.4 mL and cooling to −78 °C. *n*-Butyllithium (1.6 M, 1.6 mL) was added dropwise to the reaction mixture and stirred for 1 h. After addition of the dry DMF, the mixture was stirred for 1 h and another 2.5 h

at room temperature. 1 N HCl was added and stirred for 1 h. The reaction mixture was washed with water and extracted with ethyl acetate. The organic extracts were evaporated and purified using column chromatography on silica gel (CH_2Cl_2/hexane = 1/1) to yield **12** as a pale yellow solid (483 mg, 55 %). ^{1}H NMR (400 MHz, $CDCl_3$), δ: 9.63 (s, 1H), 8.18 (d, *J*= 8.7 Hz, 1H), 8.08 (d, *J*= 8.6 Hz, 2H), 8.00 (d, *J*= 8.3 Hz, 1H), 7.95 (d, *J*= 8.2 Hz, 1H), 7.93 (d, *J*= 9.0 Hz, 1H), 7.84 (d, *J*= 8.8 Hz, 1H), 7.63 (t, *J*= 7.4 Hz, 1H), 7.52 (t, *J*= 7.4 Hz, 1H), 7.37 (t, *J*= 7.6 Hz, 1H), 7.30 (t, *J*= 7.7 Hz, 1H), 7.25 (d, *J*= 7.4 Hz, 1H), 7.04 (d, *J*= 8.5Hz, 1H); m/Z (HR-ESI-TOF-MS): calculated for $C_{21}H_{13}BrO$ $[M+Na]^+$: 383.0042, found: 383.0035.

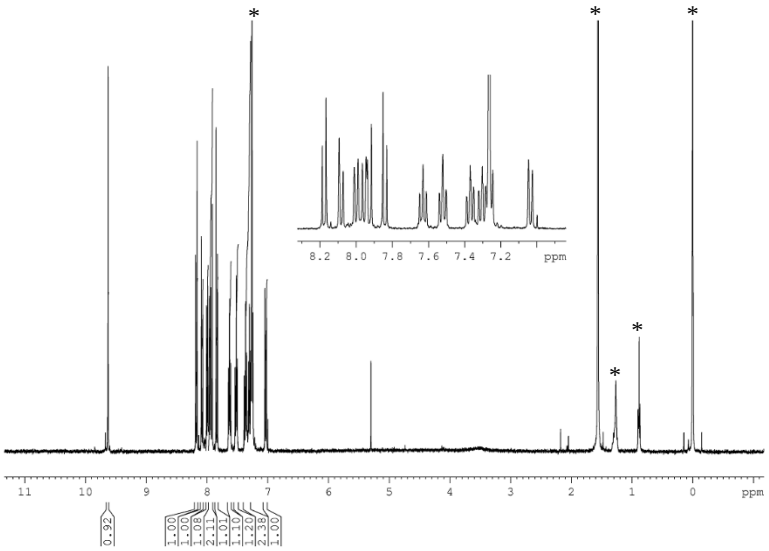

Figure 4.2.1. ^{1}H NMR spectrum of compound **12** in $CDCl_3$ (* solvent peaks).

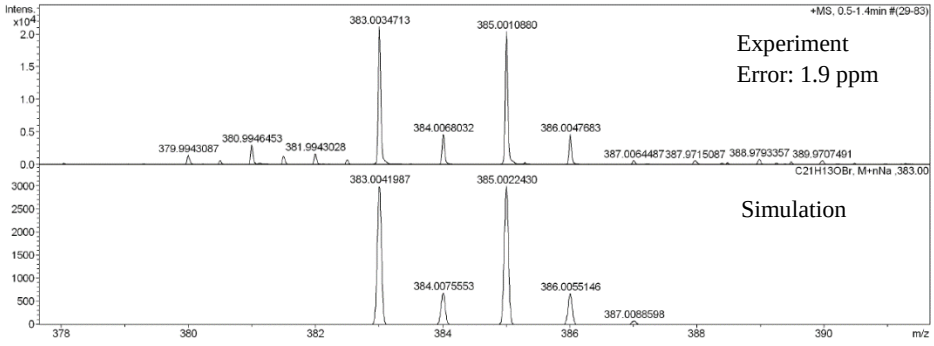

Figure 4.2.2. HR-ESI-TOF MS spectra of compound **12**.

2-(2´-bromo-[1,1´-binaphthalen]-2-yl)-1,3-dioxolane (13)

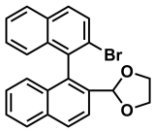

13

2´-Bromo-[1,1´-binaphthalene]-2-carbaldehyde (**12**) (203 mg, 0.56 mmol), *p*-toluenesulfonic acid (5 mg, 0.028 mmol), ethylene glycol (0.080 mL, 1.4 mmol) and toluene (5.6 mL) were added and refluxed for 2 days. After cooling to room temperature, the reaction mixture was washed with water and extracted with ethyl acetate and concentrated. The residue was purified using column chromatography on silica gel (CH_2Cl_2/hexane = 1/1) to yield **13** as a pale yellow solid (136 mg, 60 %). ^{1}H NMR (400 MHz, $CDCl_3$), δ: 8.06 (d, *J*= 8.6 Hz, 1H), 7.95 (d, *J*= 8.0 Hz, 1H) , 7.92 (d, *J*= 8.2 Hz, 1H), 7.88–7.79 (m, 3H), 7.50 (t, *J*= 7.6 Hz, 2H), 7.32–7.27 (m, 2H), 7.13 (d, *J*= 8.4 Hz, 1H), 7.05 (d, *J*= 8.2 Hz, 1H), 5.36 (s, 1H), 4.18–4.04 (m, 2H), 3.90–3.70 (m, 2H); m/Z (HR-ESI-TOF-MS): calculated for $C_{23}H_{17}O_2BrNa$ $[M+Na]^+$: 427.0304, found: 427.0285.

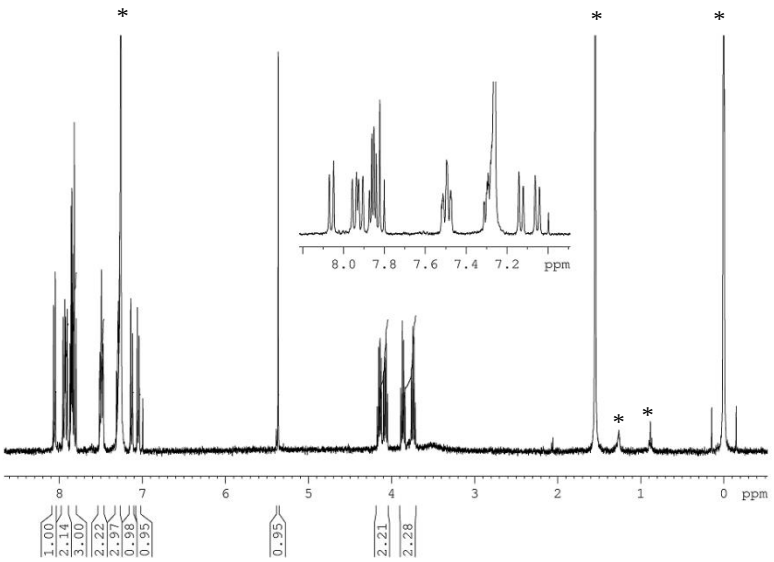

Figure 4.2.3. ^{1}H NMR spectrum of compound **13** in $CDCl_3$ (* solvent peaks).

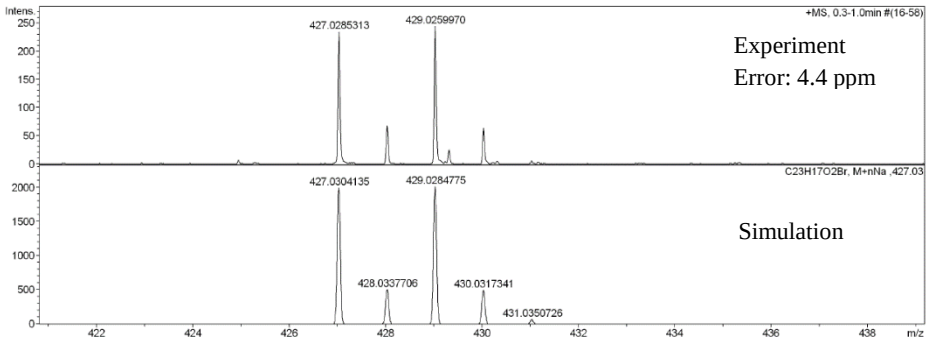

Figure 4.2.4. HR-ESI-TOF MS spectra of compound **13**.

4-(2´-(1,3-dioxolan-2-yl)-[1,1´-binaphthalen]-2-yl)-2,6-di-tert-butylphenol (14)

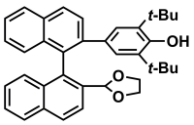

14

2-(2´-Bromo-[1,1´-binaphthalen]-2-yl)-1,3-dioxolane (**13**) (52 mg, 0.13 mmol), 2,6-di-*tert*-butyl-4-(4,4,5,5-tetramethyl-1,3,2-dioxaborolan-2-yl)phenol (**13**)[21] (59 mg, 0.18 mmol), sodium carbonate (63 mg, 0.59 mmol), tetrakis(triphenylphosphine)palladium (0) (13 mg, 0.011 mmol), THF (0.65 mL) and water (0.26 mL) were added to a sealed tube. The reaction mixture was degassed by three freeze-pump-thaw cycles and refluxed for overnight. After Celite filtration, the filtrate was washed with water and extracted with ethyl acetate. The organic layer was dried in vacuo and the residue was purified using column chromatography on silica gel (CH_2Cl_2/hexane = 1/1) to yield **14** as a white solid (58 mg, 89 %). ^{1}H NMR (400 MHz, $CDCl_3$), δ: 8.03 (d, J= 8.5 Hz, 1H), 7.94 (d, J= 8.4 Hz, 1H), 7.82 (t, J= 8.6 Hz, 2H), 7.69 (d, J= 8.5 Hz, 1H), 7.61 (d, J= 8.7 Hz, 1H), 7.45 (t, J= 7.3 Hz, 1H), 7.39 (t, J= 7.3 Hz, 1H), 7.25–7.20 (m, 5H), 6.79 (s, 2H) , 4.90 (s, 1H), 4.05–3.92 (m, 2H), 3.73–3.64 (m, 2H), 1.09 (s, 18H); m/Z (HR-ESI-TOF-MS): calculated for $C_{37}H_{38}O_3Na$ $[M+Na]^+$: 553.2713, found: 553.2811.

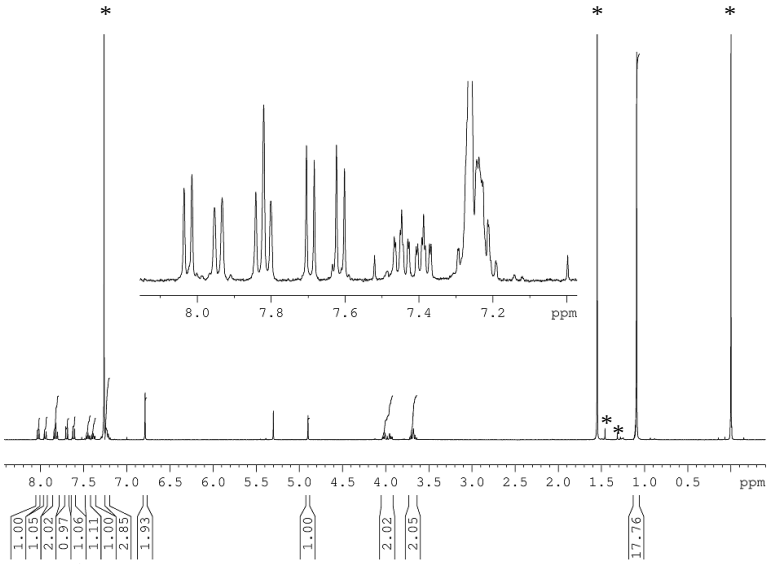

Figure 4.2.5. ^{1}H NMR spectrum of compound **14** in $CDCl_3$ (* solvent peaks).

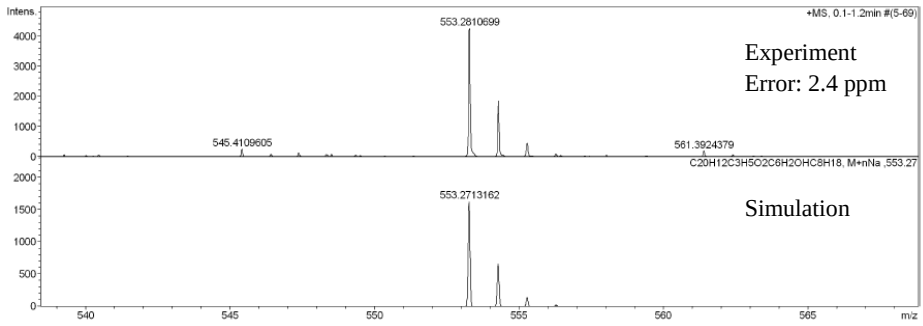

Figure 4.2.6. HR-ESI-TOF MS spectra of compound **14**.

2,6-di-tert-butyl-4-(2´-(4,5-diphenyl-1H-imidazol-2-yl)-[1,1´-binaphthalen]-2-yl)phenol (15)

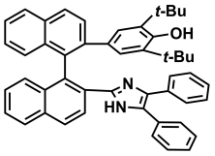

15

4-(2´-(1,3-Dioxolan-2-yl)-[1,1´-binaphthalen]-2-yl)-2,6-di-*tert*-butylphenol (**14**) (58 mg, 0.11 mmol), benzil (29 mg, 0.14 mmol), ammonium acetate (207 mg, 2.66 mmol) and acetic acid (1.5 mL) were added to a sealed tube and refluxed for 1 day. The resulting mixture was cooled to room temperature and neutralized with NH_3 aq. The residue was filtered and dried in vacuo. The crude product was purified using column chromatography on silica gel (CH_2Cl_2/hexane = 3/1) to yield **15** as a pale yellow solid (24 mg, 32 %). ^{1}H NMR (400 MHz, DMSO-d_6), δ: 11.48 (s, 1H), 8.16 (d, J= 8.5 Hz, 1H), 8.11 (d, J= 8.9 Hz, 1H), 8.06 (d, J= 8.5 Hz, 1H), 8.01 (d, J= 8.3 Hz, 1H), 7.99 (d, J= 6.8 Hz, 1H), 7.64 (d, J= 8.3 Hz, 1H), 7.49 (t, J= 7.1 Hz, 1H), 7.43 (t, J= 7.3 Hz, 1H), 7.40–7.33 (m, 3H), 7.32–7.26 (m, 4H), 7.23 (t, J= 7.5 Hz, 1H), 7.10–7.06 (m, 4H), 7.05–7.00 (m, 2H), 6.60 (s, 2H), 6.51 (s, 1H), 0.88 (s, 18H); m/Z (HR-ESI-TOF-MS): calculated for $C_{49}H_{45}N_2O$ $[M+H]^+$: 677.3526, found: 677.3523.

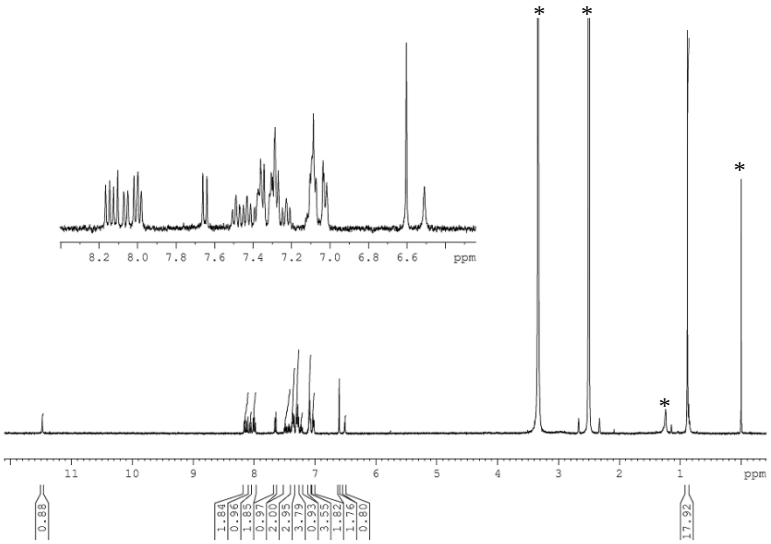

Figure 4.2.7. ^{1}H NMR spectrum of compound **15** in DMSO-d_6 (* solvent peaks).

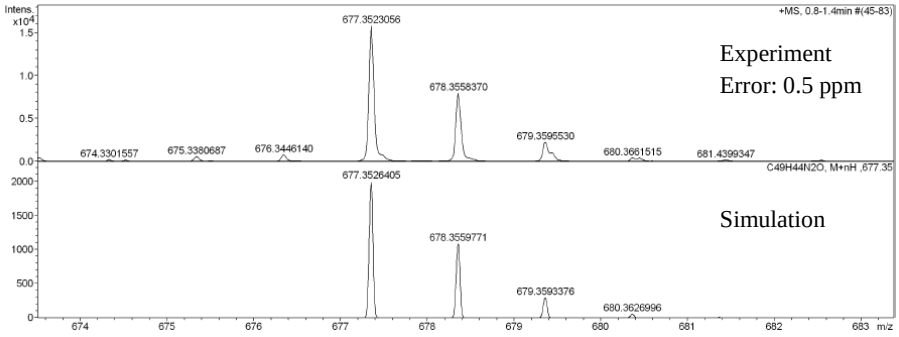

Figure 4.2.8. HR-ESI-TOF MS spectra of compound **15**.

BN-PIC1

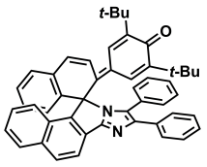

BN-PIC1

A water solution (4.0 mL) contained potassium ferricyanide (416 mg, 1.3 mmol) and KOH (135 mg, 2.4 mmol) was added to a benzene solution (4.0 mL) of 2,6-di-*tert*-butyl-4-(2´-(4,5-diphenyl-1*H*-imidazol-2-yl)-[1,1´-binaphthalen]-2-yl)phenol (**15**) (24 mg, 0.035 mmol). After stirring for 1.5 h at room temperature, the resultant mixture was then extracted with benzene and the organic extract was washed with water. After removal of the solvents, the crude product was purified by reverse phase HPLC using CH_3CN as the eluent, to yield **BN-PIC1** as an orange solid (23 mg, 96 %). ^{1}H NMR (400 MHz, $CDCl_3$), δ: 8.25 (d, *J*= 8.3 Hz, 1H), 8.02 (d, *J*= 8.3 Hz, 1H), 7.88 (d, *J*= 8.2 Hz, 1H), 7.54 (t, *J*= 8.5 Hz, 3H), 7.39 (t, *J*= 7.2 Hz, 1H), 7.30 (t, *J*= 7.2 Hz, 1H), 7.27–7.00 (m, 11H), 6.84 (d, *J*=

10.2 Hz, 1H), 6.79 (d, *J*= 8.0 Hz, 1H), 6.50 (d, *J*= 4.87 Hz, 3H), 1.20 (s, 9H), 0.93 (s, 9H); ^{13}C NMR (100 MHz, $CDCl_3$) δ: 185.97, 151.31, 150.83, 148.91, 147.73, 142.76, 140.67, 137.33, 134.56, 134.00, 133.12, 130.81, 130.66, 130.63, 130.28, 130.07, 129.69, 129.48, 128.65, 128.15, 128.12, 128.07, 128.05, 127.78, 127.27, 126.93, 126.58, 126.54, 126.44, 126.33, 126.21, 123.84, 122.85, 118.28, 68.44, 35.77, 35.48, 29.61, 29.48; m/Z (HR-ESI-TOF-MS): calculated for $C_{49}H_{43}N_2O$ $[M+H]^+$: 675.3370, found: 675.3363.

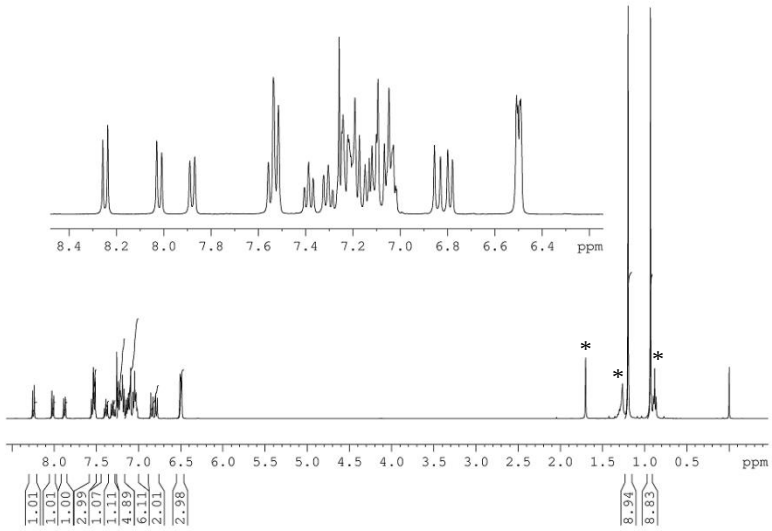

Figure 4.2.9. ^{1}H NMR spectrum of the colored isomer of **BN-PIC1** in $CDCl_3$ (* solvent peaks).

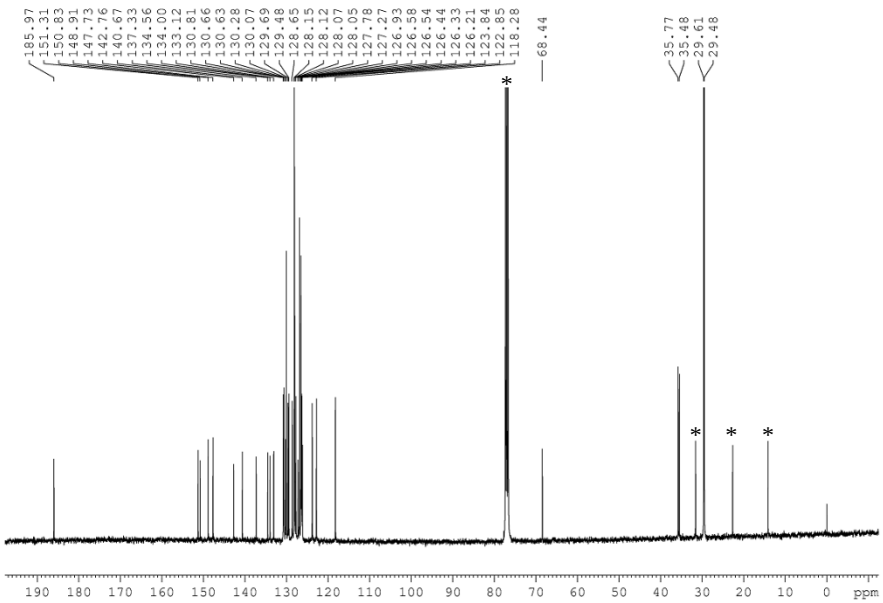

Figure 4.2.10. ^{13}C NMR spectrum of the colored isomer of **BN-PIC1** in $CDCl_3$ (* solvent peaks).

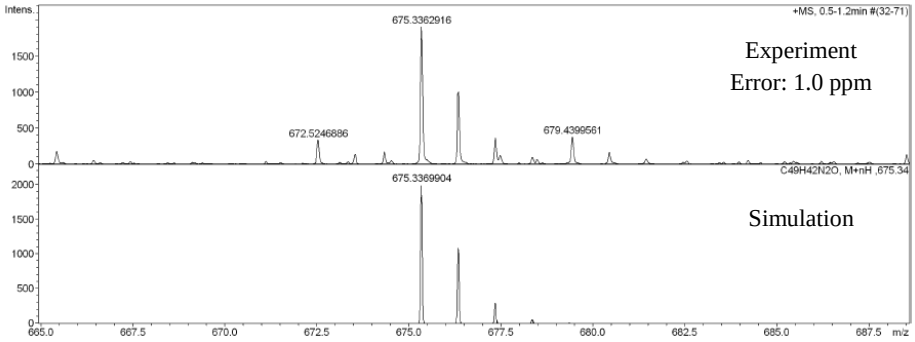

Figure 4.2.11. HR-ESI-TOF MS spectra of the colored isomer of **BN-PIC1**.

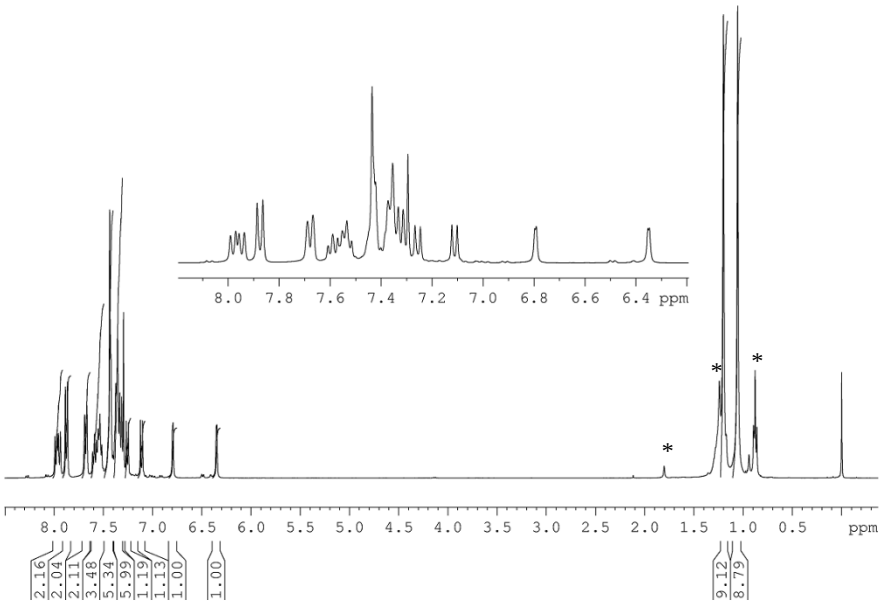

Figure 4.2.12. ^{1}H NMR spectrum of the colorless isomer of **BN-PIC1** in $CDCl_3$ (* solvent peaks).

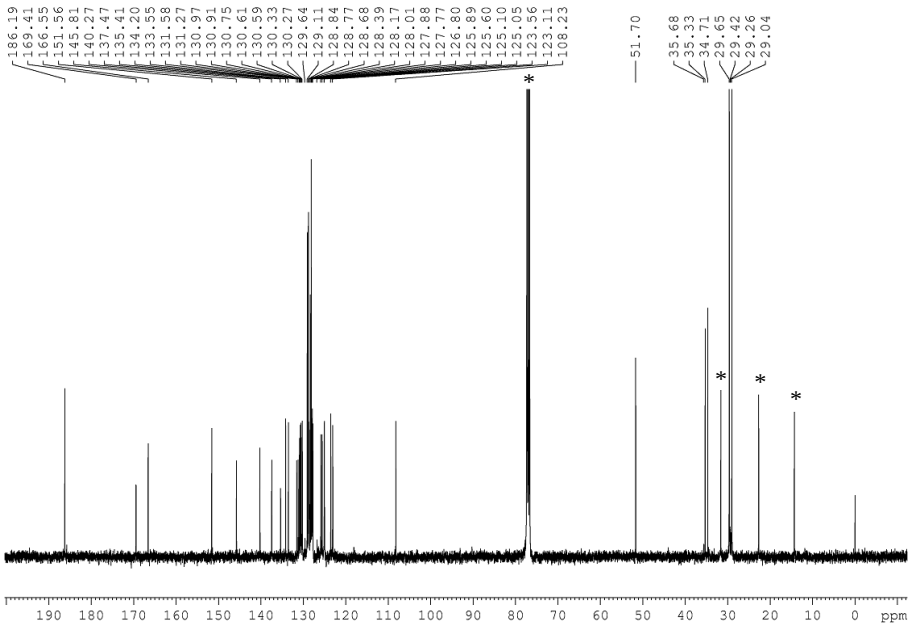

Figure 4.2.13. ^{13}C NMR spectrum of the colorless isomer of **BN-PIC1** in $CDCl_3$ (* solvent peaks).

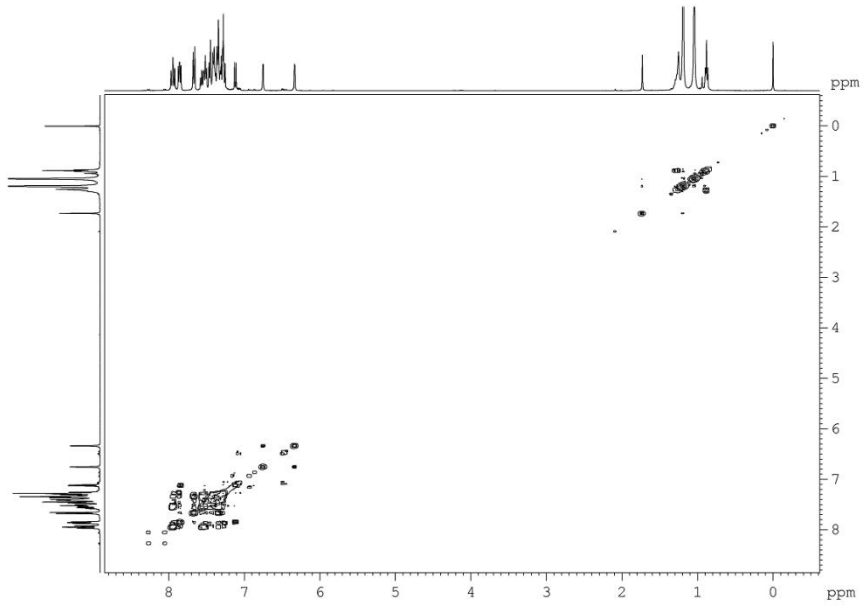

Figure 4.2.14. ^{1}H-^{1}H COSY spectrum of the colorless isomer of **BN-PIC1** in $CDCl_3$.

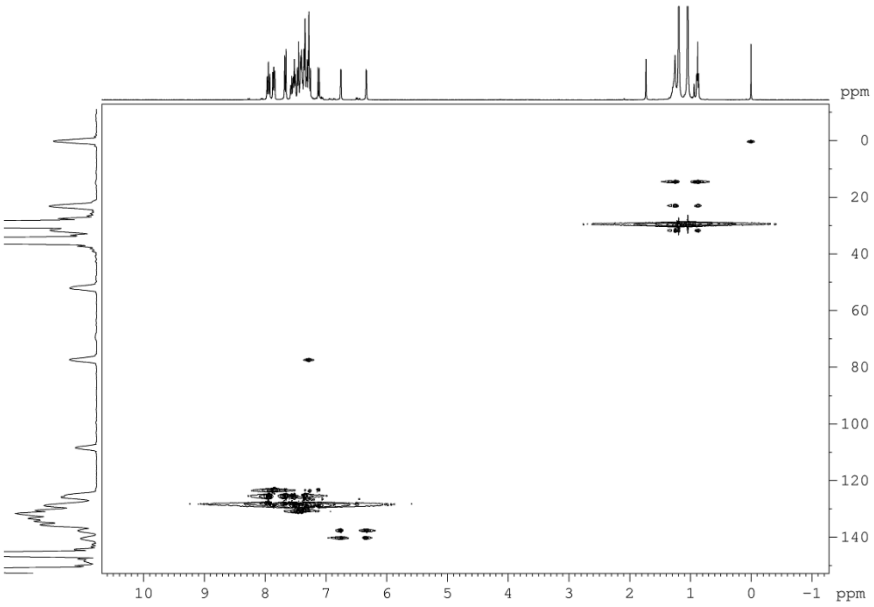

Figure 4.2.15. ^{1}H-^{13}C HSQC spectrum of the colorless isomer of **BN-PIC1** in $CDCl_3$.

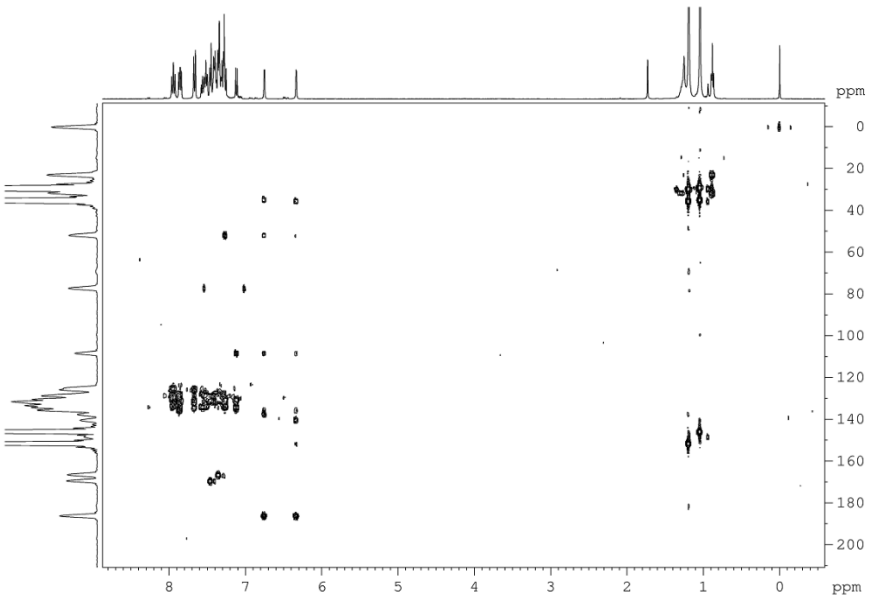

Figure 4.2.16. ^{1}H-^{13}C HMBC spectrum of the colorless isomer of **BN-PIC1** in $CDCl_3$.

4-(2´-(1H-phenanthro[9,10-d]imidazol-2-yl)-[1,1´-binaphthalen]-2-yl)-2,6-di-tert-butylphenol (16)

4-(2´-(1,3-Dioxolan-2-yl)-[1,1´-binaphthalen]-2-yl)-2,6-di-*tert*-butylphenol (**14**) (51 mg, 0.096 mmol), 9,10-phenanthrenequinone (24 mg, 0.12 mmol), ammonium acetate (270 mg, 3.5 mmol) and acetic acid (1.3 mL) were added to a sealed tube and refluxed for 1 day. The resulting mixture was cooled to room temperature and neutralization with NH_3 aq. The residue was filtrated and dried in vacuo. The crude product was purified using column chromatography on silica gel (CH_2Cl_2/hexane = 2/1) to yield **16** as a pale yellow solid (25 mg, 39 %). ^{1}H NMR (400 MHz, DMSO-d_6), δ: 12.80 (s, 1H), 8.76 (d, J= 7.8 Hz, 1H), 8.70 (d, J= 8.5 Hz, 1H), 8.40 (d, J= 8.2 Hz, 1H), 8.20–8.04 (m, 5H), 7.68–7.42 (m, 10H), 7.26 (t, J= 7.9 Hz, 1H), 7.17 (d, J= 8.7 Hz, 1H), 6.47 (s, 3H), 0.76 (s, 18H); m/Z (HR-ESI-TOF-MS): calculated for $C_{49}H_{43}N_2O$ $[M+H]^+$: 675.3370, found: 675.3380.

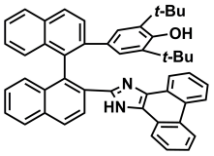

16

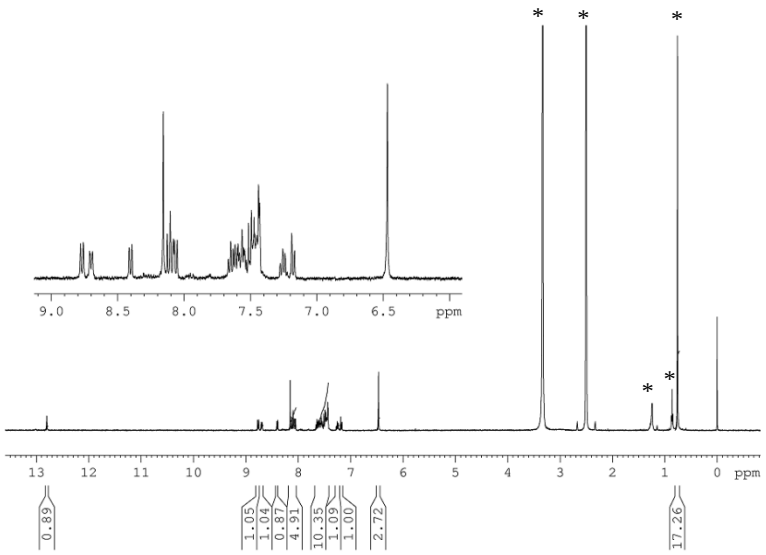

Figure 4.2.17. ^{1}H NMR spectrum of compound **16** in DMSO-d_6 (* solvent peaks).

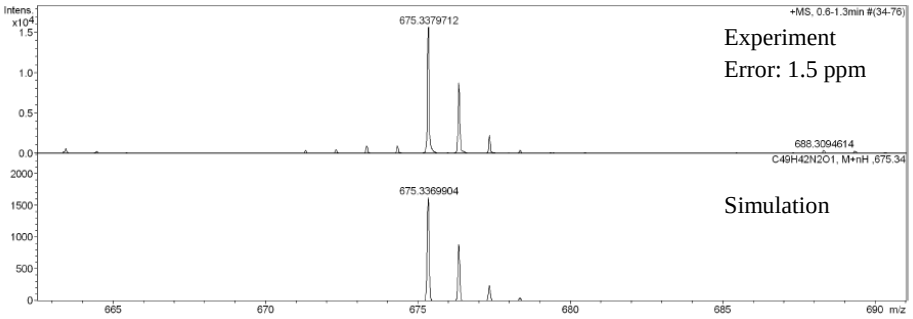

Figure 4.2.18. HR-ESI-TOF MS spectra of compound **16**.

BN-PIC2

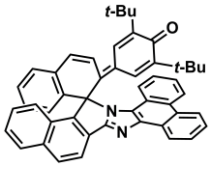

BN-PIC2

A water solution (1.7 mL) contained potassium ferricyanide (179 mg, 0.54 mmol) and KOH (76 mg, 1.4 mmol) was added to a benzene solution (1.7 mL) of 4-(2´-(1*H*-phenanthro[9,10-d]imidazol-2-yl)-[1,1´-binaphthalen]-2-yl)-2,6-di-*tert*-butylphenol (**16**) (10 mg, 0.015 mmol). After stirring for 1 h at room temperature, the resultant mixture was then extracted with benzene and the organic extract was washed with water. After removal of the solvents, **BN-PIC2** was given without further purification as an orange solid (10 mg, 96 %). ^{1}H NMR (400 MHz, $CDCl_3$), δ: 8.82 (t, J= 8.6 Hz, 2H), 8.75 (d, J= 7.8 Hz, 1H), 8.38 (d, J= 8.4 Hz, 1H), 8.29 (d, J= 7.9 Hz, 1H), 8.27 (d, J= 9.9 Hz, 1H), 8.14 (dd, J_1= 2.6, J_2= 7.5 Hz, 1H), 7.87–7.76 (m, 4H), 7.73–7.65 (m, 3H), 7.60–7.51 (m, 3H), 7.43 (t, J= 7.6 Hz, 1H), 7.21 (t, J= 7.7 Hz, 1H), 6.91 (t, J= 7.9 Hz, 1H), 6.62 (s, 1H), 6.34 (d, J= 8.3

Hz, 1H), 1.11 (s, 9H), 0.67 (s, 9H); ^{13}C NMR (100 MHz, $CDCl_3$) δ: 186.00, 156.25, 152.82, 149.05, 148.50, 143.15, 138.89, 135.67, 134.73, 133.99, 131.47, 131.38, 130.97, 130.22, 129.71, 128.76, 128.63, 128.41, 128.34, 128.18, 128.13, 128.02, 127.88, 127.25, 126.75, 126.41, 126.30, 126.07, 125.67, 125.56, 125.16, 124.97, 124.57, 123.71, 123.24, 123.09, 122.74, 122.49, 122.25, 118.49, 35.64, 35.60, 29.55, 29.39; m/Z (HR-ESI-TOF-MS): calculated for $C_{49}H_{41}N_2O$ $[M+H]^+$: 673.3213, found: 673.3171.

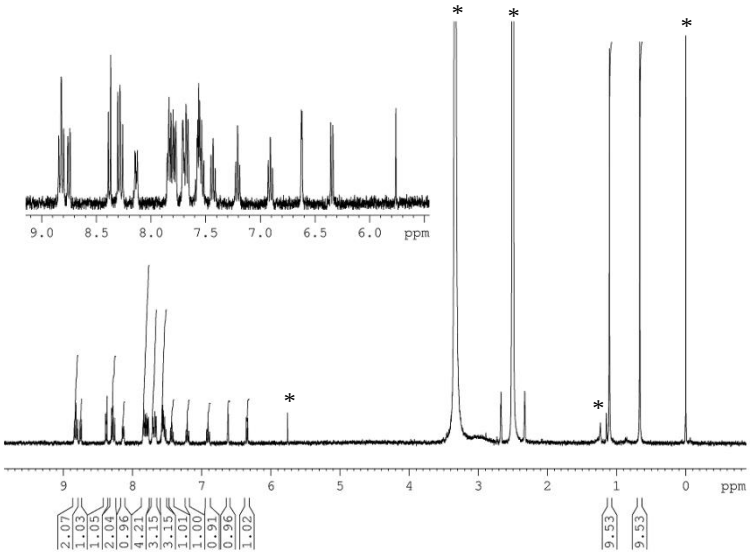

Figure 4.2.19. ^{1}H NMR spectrum of the colored isomer of **BN-PIC2** in DMSO-d_6 (* solvent peaks).

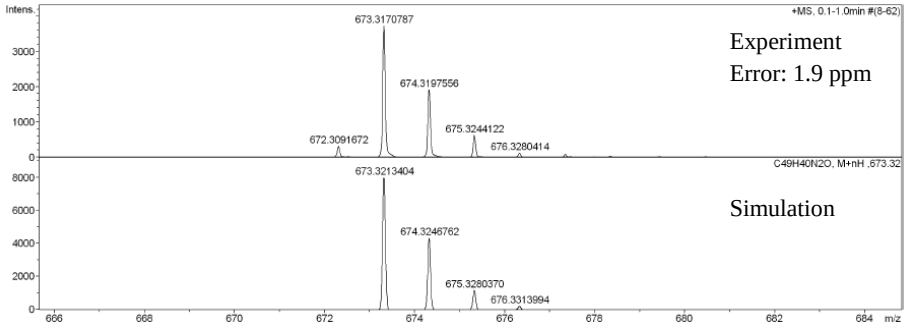

Figure 4.2.20. HR-ESI-TOF MS spectra of the colored isomer of **BN-PIC2**.

4.2.2 Experimental detail for laser flash photolysis

The laser flash photolysis experiments were carried out with a time-resolved spectrophotometer (TSP-2000, Unisoku Co., Ltd.). The samples were excited by a Q-switched Nd:YAG laser (Continuum Minilite II; 355 nm, pulse duration: 5 ns). The probe beam from a halogen lamp (OSRAM HLX64623) was focused into the sample to be arranged in an orientation perpendicular to the exciting laser beam. The probe beam was monitored with a photomultiplier tube (Hamamatsu R2949) through a spectrometer (Unisoku MD2000). To obtain the transient absorption spectra of the biradical species, the author measured the transient absorption spectra of the colorless forms at low temperature (−50 and −80 °C for **BN-PIC1** and **BN-PIC2**, respectively). Before the transient absorption measurements, a halogen lamp was irradiated for several minutes to convert the initial colored forms to the colorless forms at low temperature. A Xe flash lamp (Hamamatsu L2437, pulse duration: ~2 μs) and ICCD-spectrometer combination (Andor iStar DH320T-18U-03 and Shamrock 163) were used for a probe light and detector, respectively. The gate duration of the ICCD was set to 20 ns and a spectrum was obtained by the average of 150 scans (the average of the 50 scans, then the halogen light was irradiated to the sample, and repeat these procedures for three times to exclude the effect of the thermal back reaction from the colorless to colored forms). The author confirmed that the thermal back reaction of from the colorless to colored forms is negligible during the experiments under those temperatures.

4.3 HPLC chromatograms

HPLC analyses were carried out on a ODS reversed phase column (Mightysil RP-18 GP, Kanto Chemical Co., Inc.). The HPLC system consists of a pump unit (PU-2080 plus, JASCO), a UV detector (UV-2075, JASCO), and a control unit (LC-NetII/ADC,JASCO).

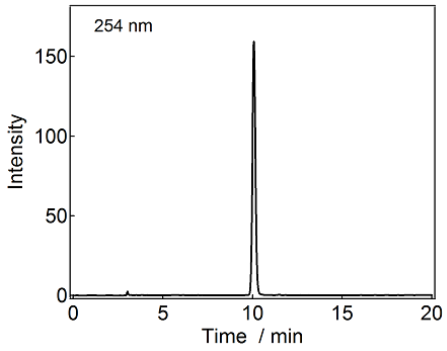

Figure 4.3.1. HPLC chromatogram of the colored form of **BN-PIC1**; 97 % purity. HPLC analysis was performed by using a reverse phase analytical column (Mightysil RP18, 25 cm × 4.6 mm, 5 μm particle) from Kanto Chemical Industries, equipped with a UV detector; the mobile phase was CH_3CN with a flow rate of 1.0 mL/min, detection wavelength; 254 nm.

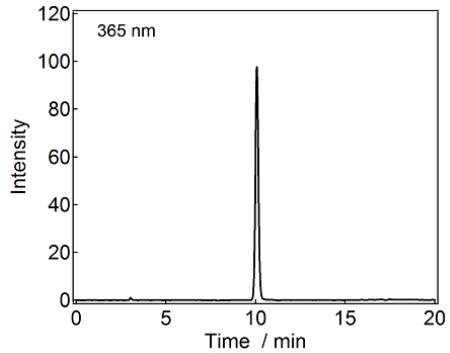

Figure 4.3.2. HPLC chromatogram of the colored form of **BN-PIC1**; 97 % purity. HPLC analysis was performed by using a reverse phase analytical column (Mightysil RP18, 25 cm × 4.6 mm, 5 μm particle) from Kanto Chemical Industries, equipped with a UV detector; the mobile phase was CH_3CN with a flow rate of 1.0 mL/min, detection wavelength; 365 nm.

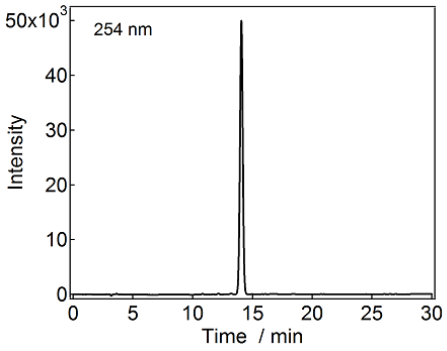

Figure 4.3.3. HPLC chromatogram of the colored form of **BN-PIC2**; 99 % purity. HPLC analysis was performed by using a reverse phase analytical column (Mightysil RP18, 25 cm × 4.6 mm, 5 μm particle) from Kanto Chemical Industries, equipped with a UV detector; the mobile phase was CH_3CN with a flow rate of 1.0 mL/min, detection wavelength; 254 nm.

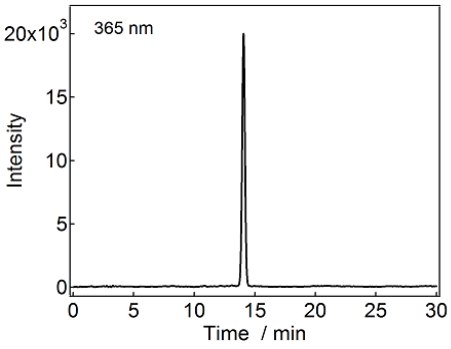

Figure 4.3.4. HPLC chromatogram of the colored form of **BN-PIC2**; 99 % purity. HPLC analysis was performed by using a reverse phase analytical column (Mightysil RP18, 25 cm × 4.6 mm, 5 μm particle) from Kanto Chemical Industries, equipped with a UV detector; the mobile phase was CH_3CN with a flow rate of 1.0 mL/min, detection wavelength; 365 nm.

4.4 Molecular structures of the colored form

The diffraction data of the single crystals were collected on the Bruker APEX II CCD area detector (Mo*K*α, λ = 0.71073 nm). During the data collection, the lead glass doors of the diffractometer were covered to exclude the room light. The data refinement was carried out by the Bruker APEXII software package with SHELXT program.[42,43] All non-hydrogen atoms were anisotropically refined. In the analysis of the colored form of **BN-PIC1**, one of the solvent molecules included the crystal was squeezed due to the critical disorder.

The molecular structures of the stable colored forms of **BN-PIC1** and **BN-PIC2** were revealed by X-ray crystallographic analysis as shown in Figures 4.4.1a and 4.4.1b. They are similar to those of the previously reported 1,1´-binaphthyl-bridged imidazole dimers in a point that the C–N bond is formed between the nitrogen atom of the imidazole ring and the carbon atom of the 1-position of naphthalene moiety.[16,25]

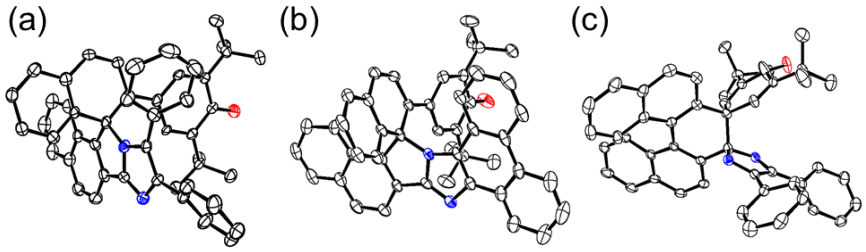

Figure 4.4.1. The ORTEP representations of (a) the colored form of **BN-PIC1**, (b) the colored form of **BN-PIC2** and (c) the colorless form of **BN-PIC1** with thermal ellipsoids (50 % probability), where nitrogen and oxygen atoms are highlighted in blue and red, respectively. The hydrogen atoms, the solvent molecules and the disorders of *tert*-butyl and carbonyl groups of the colorless form of **BN-PIC1** are omitted for clarity.

Table 4.4.1. X-ray crystallographic data of the colored form of **BN-PIC1**.

Identification code	Colored isomer of **BN-PIC1**	
Empirical formula	$C_{51}H_{45}N_3O$	
Formula weight	715.90	
Temperature	90 K	
Wavelength	0.71073 Å	
Crystal system	triclinic	
Space group	P −1	
Unit cell dimensions	a = 11.619(2) Å	α = 77.068°
	b = 18.416(3) Å	β = 81.666(2)°.
	c = 19.597(4) Å	γ = 89.163(2)°
Volume	4043.1(13) $Å^3$	
Z	4	
Density (calculated)	1.176 g/cm^3	
Absorption coefficient	0.070 mm^{-1}	
F(000)	1520	
Theta range for data collection	1.38 to 24.53°	
Index ranges	-13<=h<=13, -21<=k<=16, -22<=l<=20	
Reflections collected	18592	
Independent reflections	13266 [R(int) = 0.0176]	
Absorption correction	empirical	
Refinement method	Full-matrix least-squares on F^2	
Data / restraints / parameters	13266 / 0 / 1005	
Goodness-of-fit on F^2	0.984	
Final R indices [I>sigma (I)]	R1 = 0.0425, wR2 = 0.1018	
R indices (all data)	R1 = 0.0622, wR2 = 0.1104	
Largest diff. peak and hole	0.244 and -0.218e.$Å^{-3}$	

Table 4.4.2. X-ray crystallographic data of the colored form of **BN-PIC2**.

Identification code	Colored isomer of **BN-PIC2**	
Empirical formula	$C_{53}H_{48}N_2O_3$	
Formula weight	760.93	
Temperature	90 K	
Wavelength	0.71073 Å	
Crystal system	monoclinic	
Space group	P 1 21/n 1	
Unit cell dimensions	a = 10.089(9) Å	α= 90°
	b = 18.210(15) Å	β= 99.557(14)°.
	c = 22.72(2) Å	γ = 90°
Volume	4116(6) $Å^3$	
Z	4	
Density (calculated)	1.228 g/cm^3	
Absorption coefficient	0.075 mm^{-1}	
F(000)	1616	
Theta range for data collection	1.44 to 25.3°	
Index ranges	-9<=h<=12, -21<=k<=21, -27<=l<=19	
Reflections collected	19591	
Independent reflections	7469 [R(int) = 0.0701]	
Absorption correction	empirical	
Refinement method	Full-matrix least-squares on F^2	
Data / restraints / parameters	7469 / 0 / 532	
Goodness-of-fit on F^2	0.986	
Final R indices [I>sigma (I)]	R1 = 0.0658, wR2 = 0.1585	
R indices (all data)	R1 = 0.1400, wR2 = 0.1937	
Largest diff. peak and hole	0.371 and -0.492 e.$Å^{-3}$	

Table 4.4.3. X-ray crystallographic data of the colorless form of **BN-PIC1**.

Identification code	Colorless isomer of **BN-PIC1**	
Empirical formula	$C_{49}H_{42}N_2O$	
Formula weight	674.84	
Temperature	90 K	
Wavelength	0.71073 Å	
Crystal system	monoclinic	
Space group	P 1 21/c 1	
Unit cell dimensions	a = 19.913(6) Å	α= 90°
	b = 10.816(3) Å	β= 96.843(4)°.
	c = 17.349(5) Å	γ = 90°
Volume	3710.0(19) $Å^3$	
Z	4	
Density (calculated)	1.208 g/cm^3	
Absorption coefficient	0.071 mm^{-1}	
F(000)	1432	
Theta range for data collection	2.06 to 24.76°	
Index ranges	-23<=h<=22, -8<=k<=12, -20<=l<=20	
Reflections collected	16906	
Independent reflections	6320 [R(int) = 0.0981]	
Absorption correction	empirical	
Refinement method	Full-matrix least-squares on F^2	
Data / restraints / parameters	6320 / 72 / 545	
Goodness-of-fit on F^2	0.934	
Final R indices [I>sigma (I)]	R1 = 0.0584, wR2 = 0.1058	
R indices (all data)	R1 = 0.1458, wR2 = 0.1370	
Largest diff. peak and hole	0.200 and -0.260 $e.Å^{-3}$	

4.5 UV-vis absorption spectra

The UV-vis absorption spectra of the colored forms of **BN-PIC1** and **BN-PIC2** are similar to each other as shown in Figure 4.5.1. The calculated absorption spectra obtained by the density functional theory (DFT) are well consistent with the experimental spectra. The colored forms of **BN-PIC1** and **BN-PIC2** have a broad absorption band from UV region to 500 nm. The DFT calculations suggest that these absorption bands are attributed to the π–π* transition around the cyclohexadienone moiety (Figures 4.5.2 and 4.5.3).

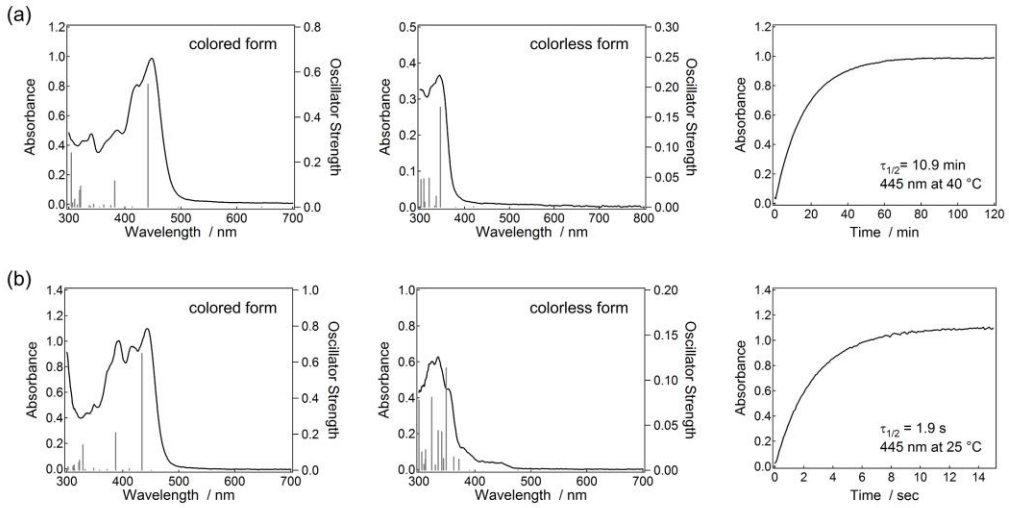

Figure 4.5.1. (a) UV-visible absorption spectra of the colored form (left), the colorless form (center), and the time profile of the absorbance changes at 445 nm of the solution of the colorless form obtained by visible light irradiation (right) of **BN-PIC1** in degassed benzene (3.2×10^{-5} M), and (b) those of **BN-PIC2** in degassed benzene (3.0×10^{-5} M). The measurement of the time profiles were carried out at 40 °C for **BN-PIC1** and at 25 °C for **BN-PIC2**. The calculated absorption spectra (DFT MPW1PW91/6-31+G(d,p)//M052X/6-31G(d,p)) are shown by the perpendicular lines.

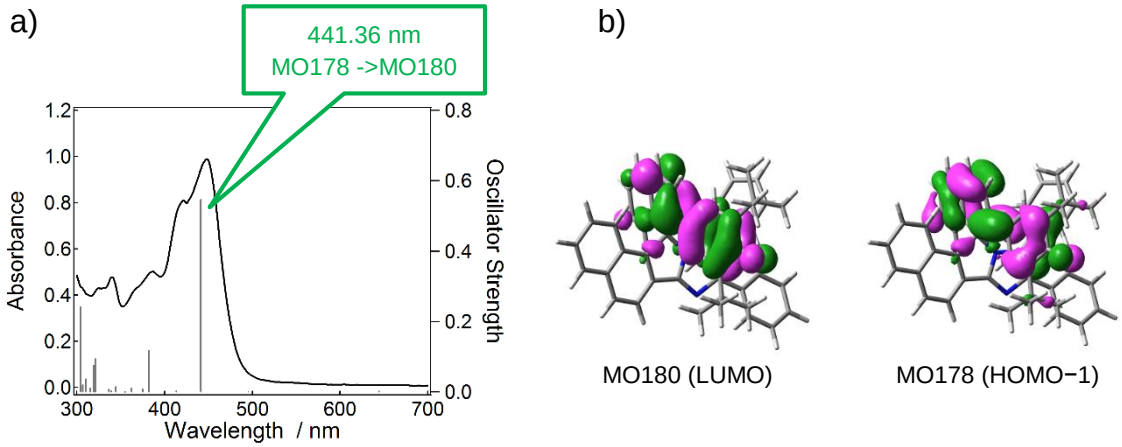

Figure4.5.2. a) UV–vis absorption spectrum and oscillator strength and b) the frontier molecular orbitals of the colored form of **BN-PIC1** at the MPW1PW91/6-31+G(d,p)//M052X/6-31G(d) level of the theory.

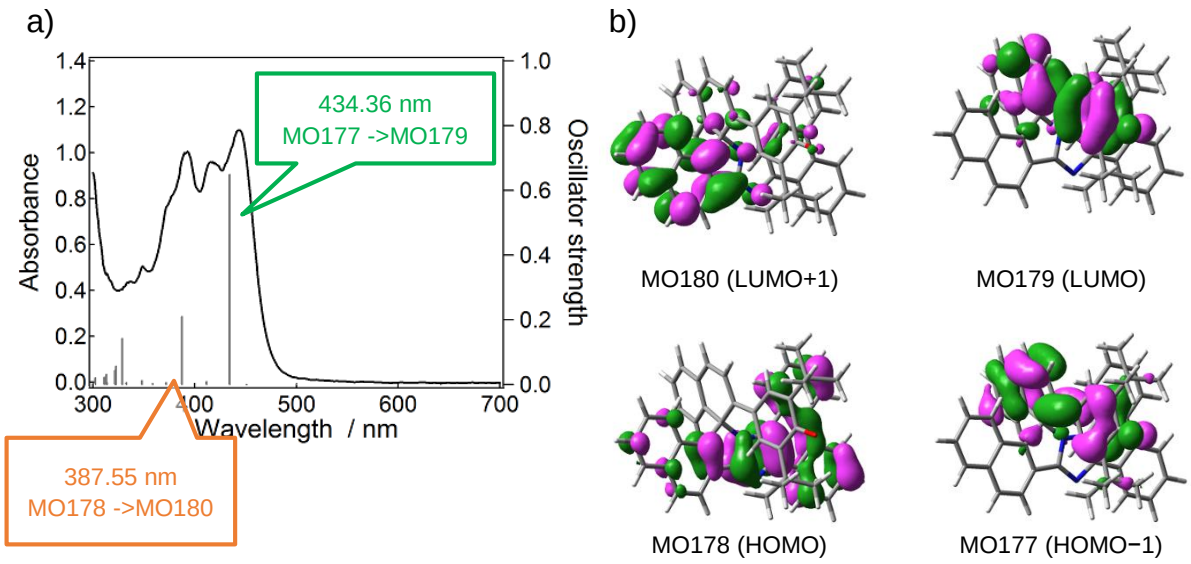

Figure 4.5.3. a) UV–vis absorption spectrum and oscillator strength and b) the frontier molecular orbitals of the colored form of **BN-PIC2** at the MPW1PW91/6-31+G(d,p)//M052X/6-31G(d,p) level of the theory.

4.6 Molecular structure of the colorless form

The photochromic response was not observed in crystalline states of the colored forms of **BN-PIC1** and **BN-PIC2**. On the other hand, they show the reversible color changes in solution upon visible light irradiation ascribed to negative photochromism, that is, BN-PICs show the decoloration reaction upon visible light irradiation and the photogenerated colorless species thermally revert to the initial colored forms. Though the crystals of the colorless form of **BN-PIC2** could not be obtained due to the fast thermal back reaction leading to the formation of the stable colored form, visible light irradiation at −40 °C on the saturated solution (dichloromethane/acetonitrile = 1/6) of the colored form of **BN-PIC1** gave crystals of the colorless form. Moreover, the single crystal of the colorless form of **BN-PIC1** colorizes to yellow upon continued heating overnight at 60 °C, indicating the occurrence of the thermal back reaction in crystal. The molecular structure of the colorless form of **BN-PIC1** was revealed by X-ray crystallographic analysis as shown in Figure 4.4.1c. The similarity in the molecular framework and the negative photochromic behavior of **BN-PIC2** indicates that the colorless form of **BN-PIC2** is considered to have the similar molecular structure as that of **BN-PIC1**.

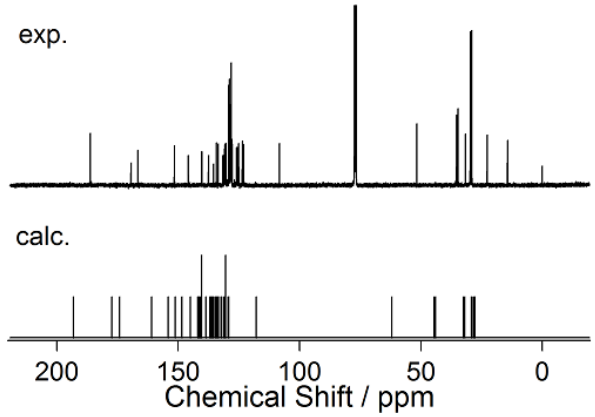

Figure 4.6.1. Experimental (top) and calculated (bottom) ^{13}C NMR spectra of the colorless form of **BN-PIC1** at B3LYP/6-31+G(d,p) level of theory.

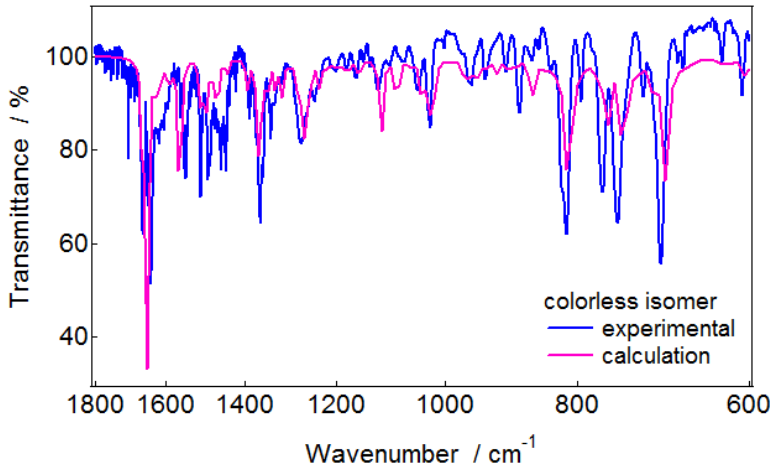

Figure 4.6.2. Experimental and calculated IR spectra of the colorless form of **BN-PIC1** at B3LYP/6-31+G(d,p) level of theory.

4.7 Photochromic properties

The absorption spectra of **BN-PIC1** and **BN-PIC2** in benzene just after visible light irradiation are shown in the center of Figure 4.5.1a and 4.5.1b, respectively. The spectra were measured by using multichannel photodiode array ultraviolet-visible detector to reduce the effect of the thermal back reaction on the spectral measurements. The absorbance in the visible region of the colored form of **BN-PIC1** completely disappeared upon visible light irradiation of 100 W Xe lamp at 25 °C, whereas that of **BN-PIC2** remained slightly at the same irradiation condition due to the faster recovery of the colored form. The calculated absorption spectra are in fair agreement with the experimental spectra. As shown in Figure 4.5.1, the time profiles of the recovery of the absorbance in visible region of the colorless solutions of **BN-PIC1** and **BN-PIC2** follow the first order kinetics (Figures 4.7.3 and 4.7.6). The half-lives of the colorless forms are estimated to be 10.9 min at 40 °C and 1.9 s at 25 °C for **BN-PIC1** and **BN-PIC2**, respectively. The decay kinetics of the colorless forms were not affected by the presence of molecular oxygen (Figure 4.7.8). It should be emphasized that the thermal back reaction of **BN-PIC2** is the fastest among the so far reported negative photochromic systems which take more than minutes or more.

Figure 4.7.2 and 4.7.5 shows the temperature dependence of the thermal back reaction measured over the temperature ranges from 25 to 50 °C for **BN-PIC1** and from 5 to 40 °C for **BN-PIC2**, respectively. As described below, the thermal back reaction proceeds via the thermally accessible biradical species. Therefore, the activation parameters ($\Delta H^{\ddagger}$, $\Delta S^{\ddagger}$, and $\Delta G^{\ddagger}$) for the thermal back reaction derived from the Eyring equation (Figures 4.7.4 and 4.7.7) are only apparent values. The $\Delta H^{\ddagger}$, $\Delta S^{\ddagger}$ and $\Delta G^{\ddagger}$ at 25 °C for the thermal back reaction of **BN-PIC1** are 99.8 kJ mol^{-1}, 16.4 J K^{-1} mol^{-1}, and 94.9 kJ mol^{-1}, respectively. The corresponding values for **BN-PIC2** are 77.2 kJ mol^{-1}, 6.16 J K^{-1} mol^{-1}, and 75.4 kJ mol^{-1}, respectively.

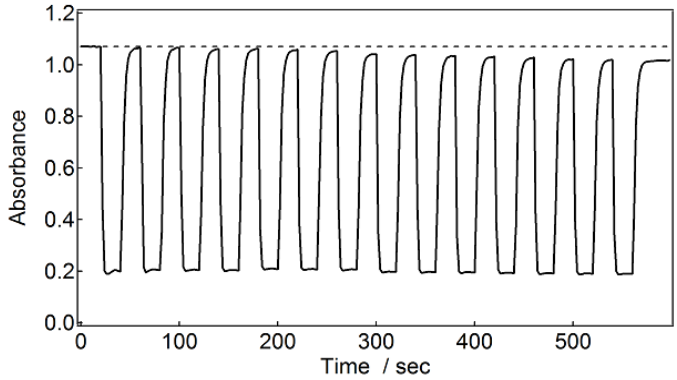

Figure 4.7.1. Cycles of decoloration by light irradiation and subsequent thermal coloration when the irradiation was ceased of **BN-PIC2** in benzene at 298 K. Absorbance was monitored at 445 nm. A Xe light source with Xe 100 W lamp (400–700 nm) was employed for the light irradiation.

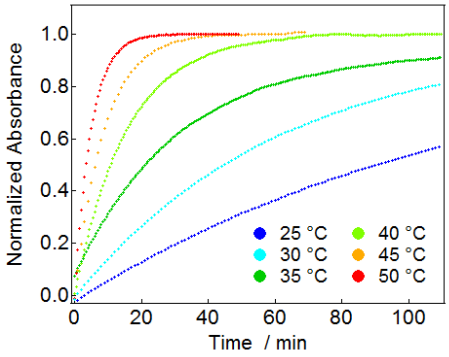

Figure 4.7.2. Time profiles of the thermal back reactions of **BN-PIC1** in benzene at several temperatures.

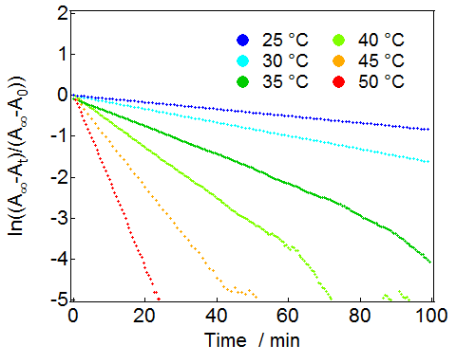

Figure 4.7.3. First order kinetics of the thermal back reactions of **BN-PIC1** in benzene at several temperatures.

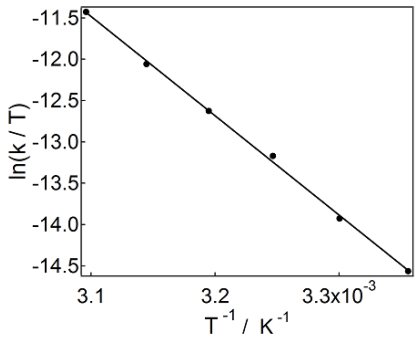

Figure 4.7.4. Eyring plot of the thermal back reaction of **BN-PIC1** in benzene.

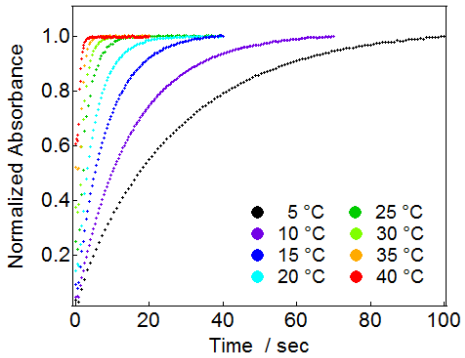

Figure 4.7.5. Time profiles of the thermal back reactions of **BN-PIC2** in benzene at several temperatures.

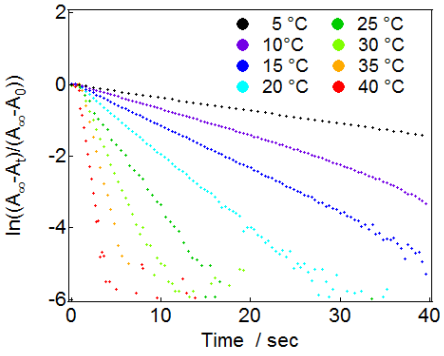

Figure 4.7.6. First order kinetics of the thermal back reactions of **BN-PIC2** in benzene at several temperatures.

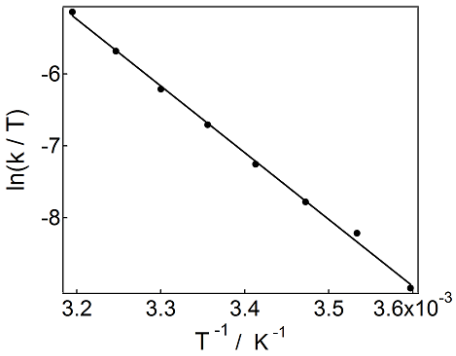

Figure 4.7.7. Eyring plot of the thermal back reaction of **BN-PIC2** in benzene.

Table 4.7.1. Rate constants and half-lives of the colorless forms and the activation parameters for the thermal back reactions of **BN-PIC1** and **BN-PIC2** in benzene at 25 °C.

Compound	k s^{-1}	$\tau_{1/2}$	$\Delta H^{\ddagger}$ kJ mol^{-1}	$\Delta S^{\ddagger}$ J K^{-1} mol^{-1}	$\Delta G^{\ddagger}$ kJ mol^{-1}
BN-PIC1	1.41×10^{-4}	81.9 min	99.8	16.4	94.9
BN-PIC2	3.73×10^{-1}	1.86 s	77.2	6.16	75.4

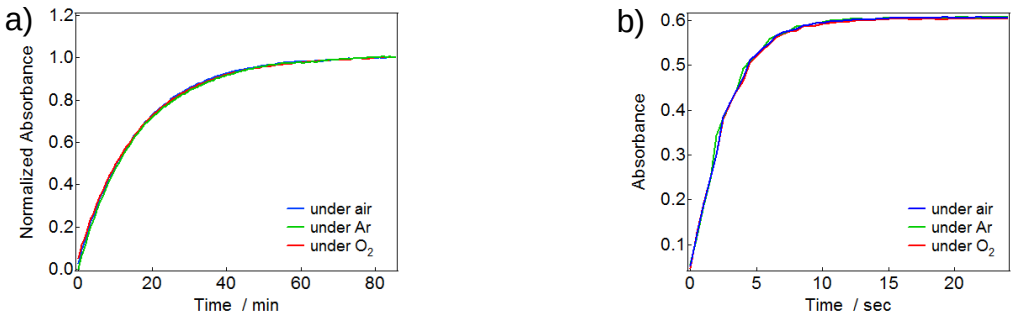

Figure 4.7.8. Thermal back reactions of a) **BN-PIC1** and b) **BN-PIC2** under air, Ar and O_2 atmosphere in benzene. The measurements of **BN-PIC1** (2.7×10^{-5} M) and **BN-PIC2** (1.6×10^{-5} M) were performed at 40 and 25 °C, respectively, and detected at 445 nm.

4.8 Transient absorption spectra

Previous studies have revealed that the photoisomerization from the colored to colorless forms of 1,1´-binaphthyl-bridged imidazole dimers occurs via a short-lived biradical species.[16] To investigate whether the biradical species is involved in the negative photochromism of BN-PICs, transient absorption spectra were measured by using a 355 nm of nanosecond laser pulse as an excitation light source. As shown in Figure 4.9.1, the transient absorption spectra of the stable colored forms of BN-PICs show a large bleach signal from 400 nm to 500 nm due to the depletion of the ground state population and a broad absorption band longer than 500 nm in both compounds. The absorption minimum of each bleach signal corresponds to the peak top of the absorption spectra of the colored forms. Although the transient absorption spectra at the shorter wavelength are overlapped with the negative bleach signal, the broad positive transient absorption signal at the longer wavelength looks similar to that of the biradical species reported previously. By considering the similarity of the photochromic property of BN-PICs and those of the bridged imidazole dimers,[16,29,30] The author assigned the positive transient signal to the absorption signal of the biradical species.

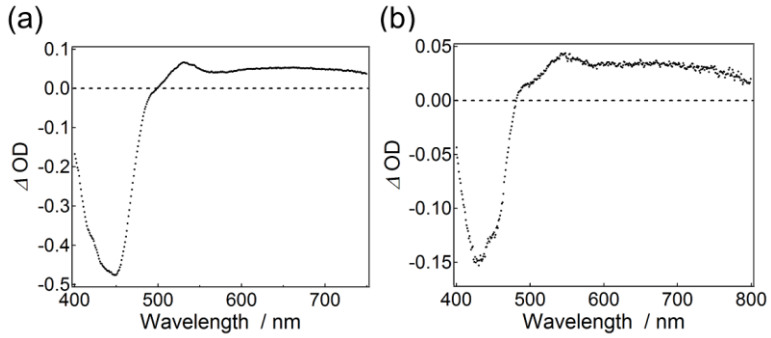

Figure 4.9.1. Transient vis–NIR absorption spectra of the colored forms of (a) **BN-PIC1** in degassed benzene solution (2.4×10^{-5} M) and (b) **BN-PIC2** in degassed benzene solution (2.3×10^{-5} M) at 25 °C. The spectra were recorded at 10 ns after excitation with a nanosecond laser pulse (excitation wavelength; 355 nm, pulse duration; 5 ns, power; 7 mJ/pulse).

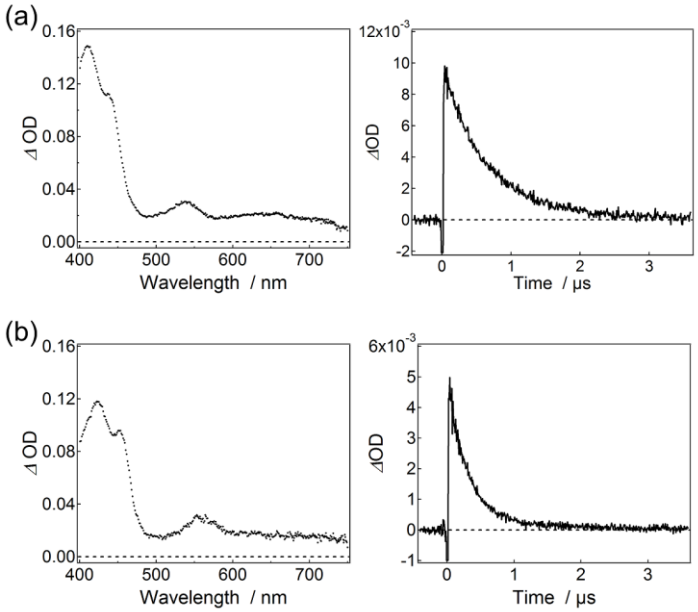

Figure 4.9.2. (a) Vis–NIR transient absorption spectrum recorded at 1 μs after the excitation with a nanosecond 355-nm laser pulse (4 mJ/pulse) at −50 °C for the colorless degassed toluene solution (1.3×10^{-4} M) of **BN-PIC1** (left). Transient absorption profile of **BN-PIC1** in degassed benzene (2.4×10^{-5} M) at 25 °C excited with nanosecond 355-nm laser pulses (7.5 mJ/pulse) and probed at 650 nm (right). (b) Vis-NIR transient absorption spectrum recorded at 1 μs after the excitation with a nanosecond 355-nm laser pulse (4 mJ/pulse) at −80 °C for the colorless degassed toluene solution (9.1×10^{-5} M) of **BN-PIC2** (left). Transient absorption profile of **BN-PIC2** in degassed benzene (2.3×10^{-5} M) at 25 °C excited with nanosecond 355-nm laser pulses (7.5 mJ/pulse) and probed at 650 nm (right). The calculated absorption spectra (DFT UMPW1PW91/6-31+G(d,p)//UM052X/6-31G(d,p)) of the singlet spin state of the biradical species are shown by the perpendicular lines.

To reveal the whole spectral shapes of the biradical species, the author performed the measurements of the transient absorption spectra of the colorless forms of both compounds at low temperature, where the thermal back reaction of the colorless forms populated by visible light irradiation can be suppressed. Under the low temperature condition, it is not necessary to take into account the bleach signal due to the depletion of the ground state population of the colorless form because the colorless form has no absorption bands longer than 400 nm as shown in Figure 4.5.1. The transient absorption spectra of the colorless forms were measured at −50 °C for **BN-PIC1** and at −80 °C for **BN-PIC2**. Figures 4.9.2a and 4.9.2b show the transient absorption spectra attributable to the biradical species of **BN-PIC1** and **BN-PIC2**, respectively. The spectral shapes longer than 500 nm are same as

those obtained for the colored form. Moreover, the author confirmed that the decay kinetics of the radical species do not show significant difference regardless the composition between the colored and the colorless forms. These experimental results strongly support that the colored and colorless forms of BN-PICs give the same biradical species upon light irradiation. The half-lives of the biradical species generated from **BN-PIC1** and **BN-PIC2** were estimated to be 380 ns and 240 ns, respectively (Figure 4.9.2). The effect of molecular oxygen on the half-life of the biradical species was negligibly small (Figures 4.9.3 and 4.9.4).

As described above, the colorless forms can be obtained upon visible light irradiation to the solution of the colored form of BN-PICs. On the other hand, UV light irradiation to the colorless forms of BN-PICs give only a trace of the colored form. Thus the major reaction path for the deactivation of the biradical species is the formation of the colorless form, suggesting the difference in the activation energy barriers for the formation of each isomer. Thus the negative photochromic behavior of BN-PICs includes three isomers and can be explained as Scheme 4.1. The thermally stable colored forms isomerize to the

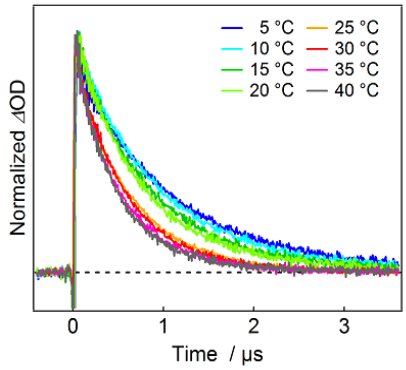

Figure 4.9.3. Decay profiles of the transient species generated from **BN-PIC1** in Ar-bubbled benzene monitored at 650 nm (2.4×10^{-5} M, λ_{ex}= 355 nm, pulse duration: 5 ns, power: 7.5 mJ/pulse).

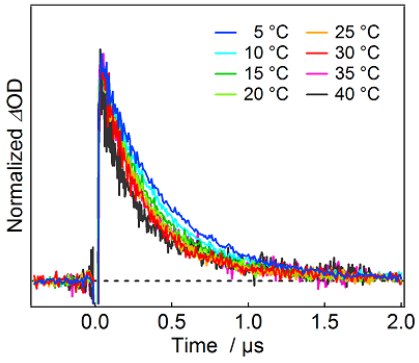

Figure 4.9.4. Decay profiles of the transient species generated from **BN-PIC2** in Ar-bubbled benzene monitored at 650 nm (2.3×10^{-5} M, λ_{ex}= 355 nm, pulse duration: 5 ns, power: 7.5 mJ/pulse).

colorless forms via the short-lived biradical species by visible light irradiation. The colorless forms isomerize slightly to the colored forms via the radical species by UV light irradiation. The photogenerated colorless forms thermally return to the initial colored forms with time scales of minutes and seconds for **BN-PIC1** and **BN-PIC2**, respectively.

4.9 Conversion efficiency

The photochemical conversion efficiencies from the colored forms to the colorless forms of **BN-PIC1** and **BN-PIC2** were estimated by nanosecond laser flash photolysis by using 1,2-bis(2-methylbenzo[*b*]thiophen-3-yl)perfluorocyclopentene[31] (DAE) as a standard. The colorless open-ring isomer of DAE can undergo cyclization in a conrotatory fashion to the colored closed-ring isomer upon UV light irradiation. The thermal back reaction is symmetry-forbidden, giving excellent thermal stability to the closed-ring isomer. Thus the cycloreversion reaction from the closed-ring isomer to the open-ring isomer occurs only by irradiating with a visible light. The laser power was measured by an energy detector (OE12LP-S-MB-D0, Gentec). The number of incident photons was calculated to be 5.57×10^{15} (photons/pulse) at the laser power of 5.48 mJ by using the reported method.[44] The quantum yield of the ring opening reaction of DAE was estimated by using eq. 4.1:

$$\varphi_{DAE} = \frac{\Delta OD_{436\mathrm{nm}} \times V \times LP_0}{\varepsilon_{436\,nm} \times l \times L \times LP} \qquad \text{(eq. 4.1)}$$

where ΔOD_{436nm} is the change of the absorbance of DAE at 436 nm (6.86×10^{-3}), V is the volume of the DAE solution irradiated the laser pulse (2 mL), LP_0 is the 5.48 mJ laser power, ε_{DAE} is the molar absorption coefficient of DAE at 436 nm (3.50×10^3 $M^{-1}cm^{-1}$), l is the optical length of the cuvette (1.0 cm), I is the number of photon estimated from the chemical actinometer (5.57×10^{15} photons) and LP is the laser power irradiated to the DAE solution (5.23×10^{15} photons), respectively. The quantum yield of the ring opening reaction of DAE at 436 nm was estimated to be 0.45 by using potassium trisoxalatoferrate (III) trihydrate as a chemical actinometer. Solutions of the colored forms of BN-PICs in benzene and the closed-ring isomer of DAE in hexane with matched absorbances at the excitation wavelength of 436 nm were irradiated at various laser energies. The absorbance changes for the colored form of BN-PIC, ΔOD(BN-PIC), were plotted against those before and after a laser pulse irradiation at 436 nm for the closed-ring isomer of DAE, ΔOD(DAE). The conversion efficiency was estimated from the slope of the fit of the data to the following equation[32,33]

$$\Delta\mathrm{OD(BN - PIC)} = \frac{\varphi_{\mathrm{BN\text{-}PIC}} \times \varepsilon_{\mathrm{BN\text{-}PIC}}}{\varphi_{\mathrm{DAE}} \times \varepsilon_{\mathrm{DAE}}} \Delta\mathrm{OD(DAE)} \qquad \text{(eq. 4.2)}$$

where, φ_{DAE} (0.45) is the quantum yield of cycloreversion reaction of DAE excited at 436 nm, $\varphi_{BN\text{-}PIC}$ is the conversion efficiency from the colored form to the colorless form of BN-PIC, ε_{DAE} (3.50×10^3 $M^{-1}cm^{-1}$) and $\varepsilon_{BN\text{-}PIC}$ (2.73×10^4 M^{-1} cm^{-1} for **BN-PIC1**, 3.39×10^4 M^{-1} cm^{-1} for **BN-PIC2**) are the absorptivity coefficients of DAE and the colored forms of BN-PICs at 436 nm, respectively. As shown in Figures 4.10.6 and 4.10.7, $\varphi_{BN\text{-}PIC1}$ and $\varphi_{BN\text{-}PIC2}$ were obtained from the slopes of the fits of the data to eq. 4.2 and were determined to be 0.09 and 0.08, respectively. The full experimental data are shown in the Supporting Information. These values were nearly three times higher than that of the previously reported negative photochromic 1,1´-binaphthyl-bridged imidazole dimer.[16]

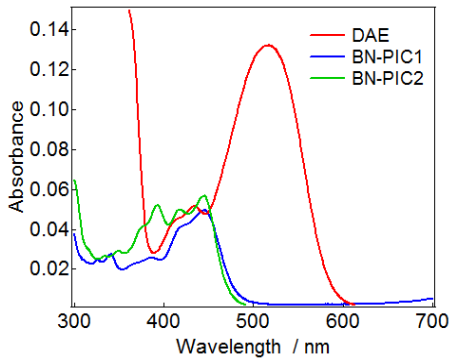

Figure 4.10.1. UV−vis absorption spectra of the benzene solution of **BN-PIC1** and **BN-PIC2** and hexane solution of DAE.

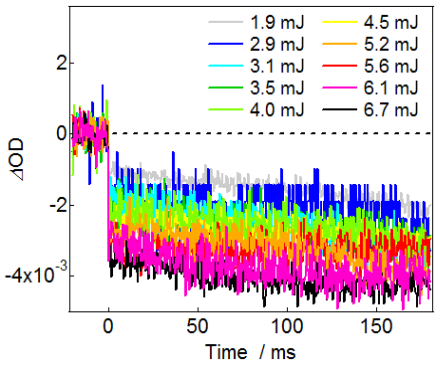

Figure 4.10.2. Laser power dependence of the *Δ*OD of DAE in hexane at 298 K monitored at 436 nm (excitation wavelength: 436 nm, laser duration: 5 ns).

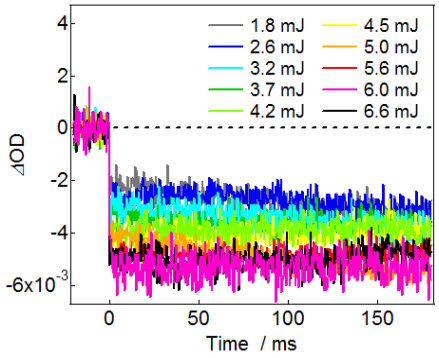

Figure 4.10.3. Laser power dependence of the *Δ*OD of **BN-PIC1** in benzene at 298 K monitored at 436 nm (excitation wavelength: 436 nm, laser duration: 5 ns).

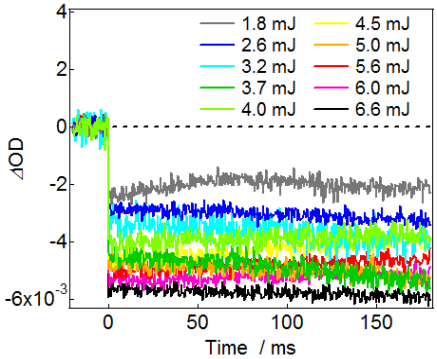

Figure 4.10.4. Laser power dependence of the *Δ*OD of **BN-PIC2** in benzene at 298 K monitored at 436 nm (excitation wavelength: 436 nm, laser duration: 5 ns).

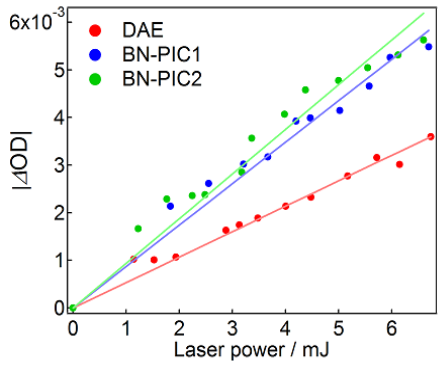

Figure 4.10.5. Linear relationship between the laser power and *Δ*OD values monitored at 436 nm.

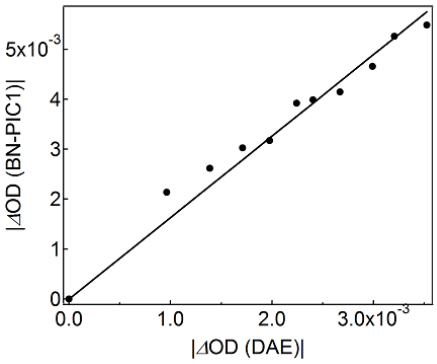

Figure 4.10.6. |⊿OD (**BN-PIC1**)| vs. |⊿OD (DAE)|. The photochemical conversion efficiency from the colored form to the colorless form of **BN-PIC1** was obtained from the slope of the fit of the data to eq. 4.2.

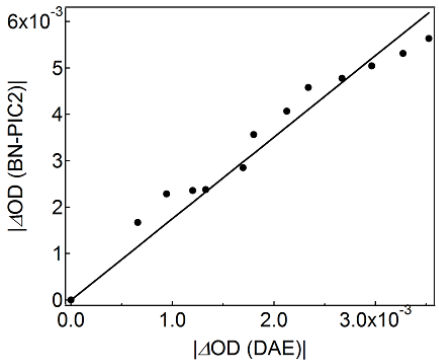

Figure 4.10.7. |⊿OD (**BN-PIC2**)| vs. |⊿OD (DAE)|. The photochemical conversion efficiency from the colored form to the colorless form of **BN-PIC2** was obtained from the slope of the fit of the data to eq. 4.2.

4.10 DFT calculations for the isomers

All calculations were carried out using the Gaussian09 program (Revision D.01).[45] The molecular structures of **BN-PIC1** and **BN-PIC2** were fully optimized at the (U)M052X/6-31G(d,p) level of the theory and analytical second derivatives were computed using vibrational analysis to confirm each stationary point to be a minimum. TDDFT calculations were performed at the MPW1PW91/6-31+G(d,p) level of theory for the optimized structures.

The author carried out the DFT calculations to understand the photochemical and thermochemical isomerization behavior of BN-PICs. The molecular geometries of the colored form, the colorless form, and the biradical species were fully optimized at the M05-2X/6-31G(d,p) level of the theory. The TDDFT calculations were performed at the MPW1PW91/6-31+G(d,p) level of the theory for the optimized geometries obtained by the

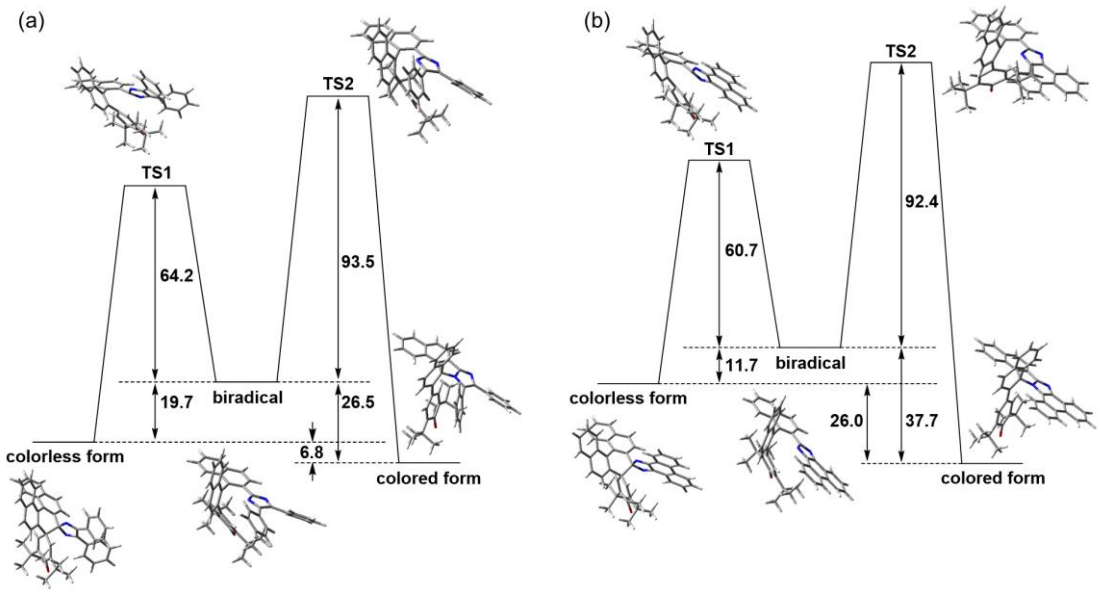

Figure 4.11.1. Energy diagrams for the thermal back reactions and the optimized molecular structures of (a) **BN-PIC1** and (b) **BN-PIC2** calculated by the DFT M05-2X/6-31G(d,p). The Gibbs free energies at 298.15 K are given in the unit of kJ mol^{-1}.

M05-2X/6-31G(d,p) method. Moreover, the transition states for the radical coupling reaction were investigated to understand the difference in the activation energy barriers for the formation of each isomer. The stationary nature of the structures was confirmed by harmonic vibrational frequency calculations, i.e., equilibrium species possess all real frequencies, whereas transition states possess only one imaginary frequency. The M05-2X function is known to give improved performance for energies of reactions involving radicals, for barrier heights of radical reactions.[34] The Gibbs free energy barriers, $\Delta G^{\ddagger}$, of

the radical coupling reaction of [2.2]paracyclophane-bridged imidazole dimers were well in fair agreement with the experimental values.[18] The calculated energy diagrams for **BN-PIC1** and **BN-PIC2** are shown in Figures 4.11.1a and 4.11.6b, respectively. The experimental observations can be well accounted for by the DFT calculations.

Firstly, the colored forms are more stable than the colorless forms. Secondly, the activation energy barriers for the formation of the colorless forms are smaller than those for the formation of the colored forms. That's why, the major reaction path for the deactivation of the biradical species is the formation of the colorless form, and the colorless forms isomerize slightly to the colored forms via the radical species by UV light irradiation. The colorless form gradually isomerizes to the colored form because the colored form is produced from the biradical species by the thermodynamic controlled reaction, whereas the formation of the colorless form is the kinetic controlled reaction. Thirdly, both of the activation energy barriers for the formation of the biradical species and the colored form of **BN-PIC2** are smaller than those of **BN-PIC1**, leading to the faster thermal back reaction of **BN-PIC2** compared with that of **BN-PIC1**. Thus the photochemical and thermochemical isomerization behavior of BN-PICs can be well described by the energy diagrams obtained by the DFT calculations.

4.11 Chiroptical property

As described in the introduction, negative photochromic compounds are promising not only because of their unique photochromic property but also because of the potential to induce the photochromism at the inside of the material. Therefore, the combination of negative photochromic property with other properties would open up the possibility for developments of novel highly functional materials. BN-PICs have an axial chirality originated from the 1,1´-binaphthyl structure. Here, as a demonstration, the author investigated the effect of the chiral environment on the thermal back reaction of the optically resolved **BN-PIC1**. The author choses **BN-PIC1** as an example because **BN-PIC1** and **BN-PIC2** have similar molecular structures and **BN-PIC1** is easy to analyze because of its slow thermal back reaction from the photogenerated colorless form to the thermally stable colored form. Both enantiomers of **BN-PIC1** were optically resolved by using chiral HPLC and the optical purities were up to 97 %ee and 99 %ee for (R)- and (S)-enantiomers, respectively (Figure 4.12.1). Circular dichroism (CD) spectra of the colored forms of **BN-PIC1** are shown in Figure 7a. The colored form of **BN-PIC1** in acetonitrile shows CD signals from UV to visible region. This spectrum indicates that the chiroptical property originated from the 1,1´-binaphthyl unit expands over the cyclohexadienone moiety. Upon visible light irradiation, the CD signal in visible region disappeared and the strong CD signal due to the colorless form was observed at the UV region (Figure 4.12.2b). Since it is known that the 1,1´-binaphthyl moiety exhibits a positive Cotton effect around 300 nm,[35] the author assigned the enantiomer of the colorless form which gives a positive Cotton effect around 300 nm to the (R)-form. (Figures 4.12.2b). The colored enantiomer returned from (R)-colorless form is also regarded as (R)-colored form in this study. The CD spectrum of the photogenerated colorless form gradually reverts to the initial CD spectrum assigned to the colored form in the dark (Figure 4.12.3). Furthermore, the (S)-colored form was not racemized by continuous irradiation of 365 nm UV light for 1 min (100 mW) as was revealed by the chiral HPLC analyses (Figure 4.12.4). These results show that the negative photochromism of **BN-PIC1** also induces the drastic change of the chiroptical property and the enantiomers are not photoracemized by continuous light irradiation.

Moreover, the thermal back reaction from the colorless to colored forms is found to be affected by the solvent chirality. Figure 4.12.5 shows the time evolution of the absorbance of **BN-PIC1** during the thermal back reaction from the colorless to the colored forms in different chirality of 1-phenylethanol. The kinetics of the (R)-form in the (R)-solvent is obviously different from that of the (R)-form in the (S)-solvent. The kinetics of the (S)-form in the (S)-solvent follows the kinetics of the (R)-form in the (R)-solvent. Alternatively, the kinetics of the (R)-form in the (S)-solvent follows the kinetics of the (S)-form in the (R)-solvent. Although the difference is small, these results clearly show that the thermal

back reaction of **BN-PIC1** is affected by the chiral environment of the solvent. While there are many examples that the chiral environment affects the reaction products of the enantiomer excess,[36–39] this is an unusual behavior of the thermal back reaction of negative photochromism affected by the chiral environment.[40,41] The activation parameters of the (S)- and (R)-forms in each enantiomer of 1-phenylethanol were analyzed by the Eyring equation (Figures 4.12.5 and 4.12.6). The $\Delta G^{\ddagger}$ value of thermal back reaction for the (S)-form in (S)-1-phenylethanol at 25 °C (89.2 kJ mol^{-1}) was slightly smaller than that for the (S)-form in (R)-1-phenylethanol (89.5 kJ mol^{-1}). This is also the case for the kinetics of the (R)-form in (R)-1-phenylethanol (89.1 kJ mol^{-1}) and the (R)-form in (S)-1-phenylethanol (89.5 kJ mol^{-1}).

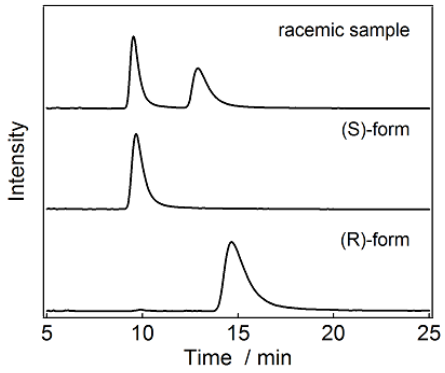

Figure 4.12.1. HPLC chromatograms of **BN-PIC1** before and after the optical resolution (enantiomer 1: 99 %ee and enantiomer 2: 97 %ee, elu: THF: hexane= 1: 20, flow rate: 1 mL/min, λ_{obs}= 254 nm).

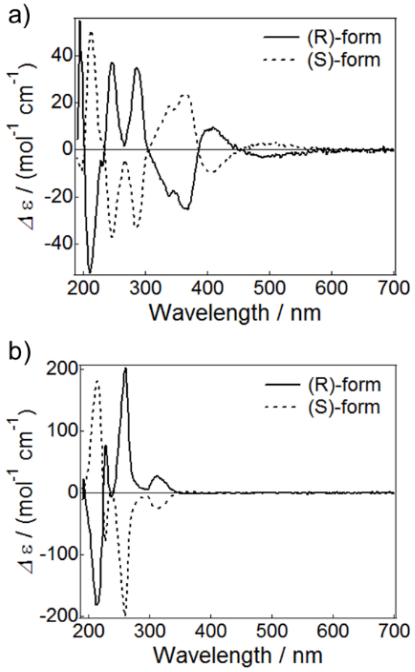

Figure 4.12.2. CD spectra of a) the colored isomers and b) the colorless isomers of **BN-PIC1** in acetonitrile at room temperature. The CD spectra of the colorless forms were measured after visible light (400–700 nm) irradiation for 30 s.

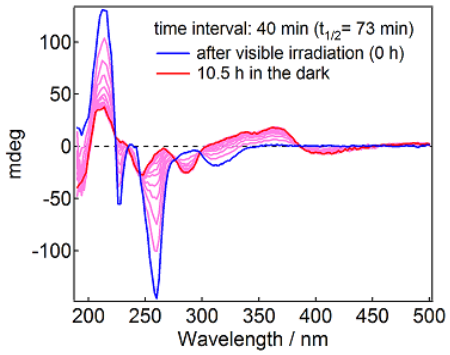

Figure 4.12.3. CD spectral change of the CH_3CN solution of **BN-PIC1**. The measurement was started after visible light irradiation for 30 s at room temperature.

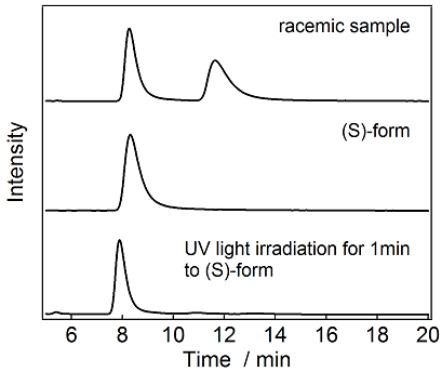

Figure 4.12.4. HPLC chromatograms of **BN-PIC1** before UV light irradiation and after UV light irradiation for 1 min and isomerized for 30 min at 70 °C in the dark (elu: THF: hexane= 1: 20, flow rate: 1 mL/min, λ_{obs}= 254 nm, λ_{ex}= 365 nm).

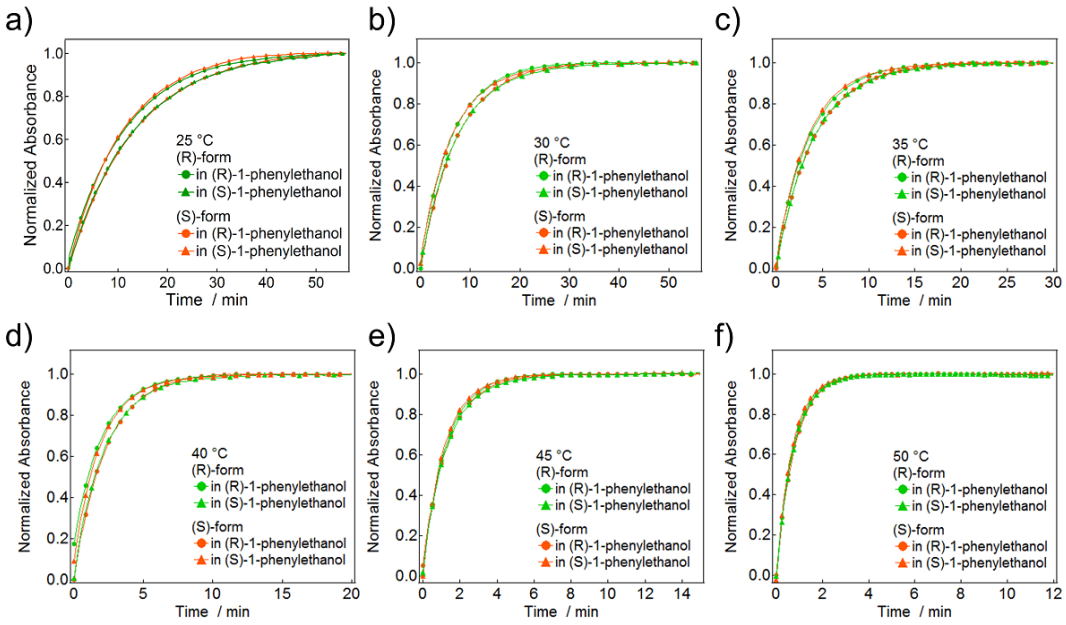

Figure 4.12.5. Time profiles of the thermal back reaction (R)-form and (S)-form in (R)-1-phenylethanol (circle plots) and (R)-form and (S)-form in (S)-1-phenylethanol (triangle plots) of **BN-PIC1** at several temperature.

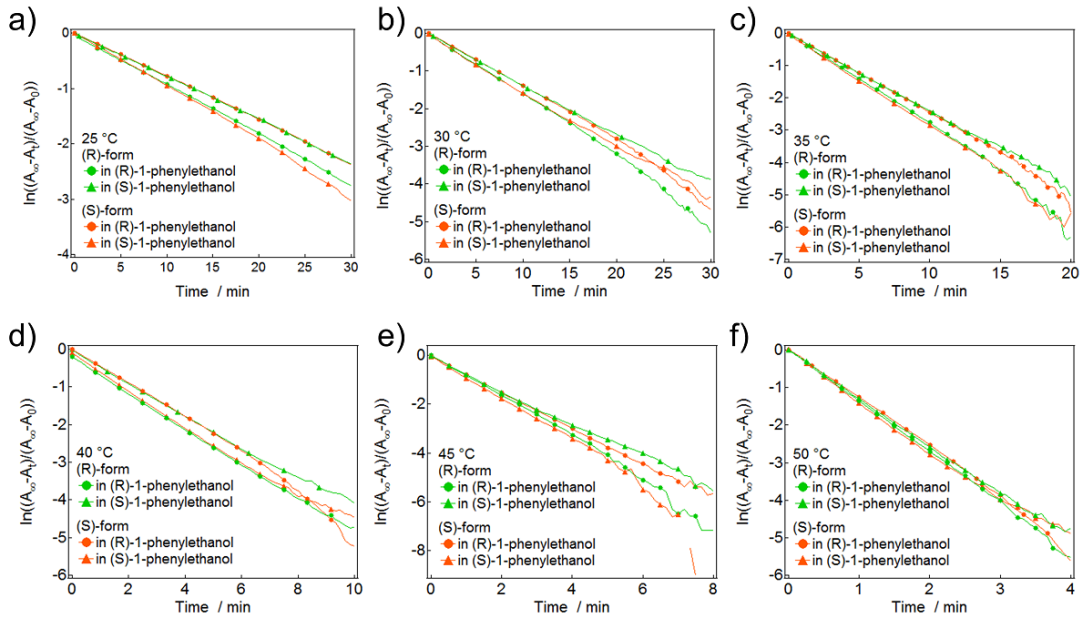

Figure 4.12.6. Log plots of the thermal back reaction of (R)-form and (S)-form in (R)-1-phenylethanol (circle plots) and (R)-form and (S)-form in (S)-1-phenylethanol (triangle plots) of **BN-PIC1** at several temperature.

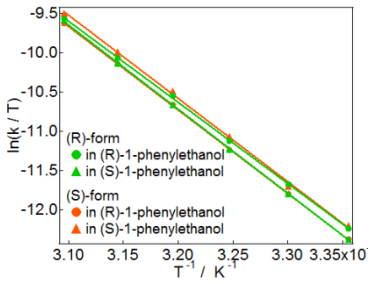

Figure 4.12.7. Eyring plot of the thermal back reaction of (R)- and (S)-form in (R)-1-phenylethanol (circle plots) and in (S)-1-phenylethanol (triangle plots) of **BN-PIC1**.

Table 4.12.1. Rate constants, activation parameters for the thermal back reaction and half-lives for the colorless isomers of **BN-PIC1** in (S)- and (R)-1-phenylethanol at 25 °C.

solvent	**BN-PIC1**	$\tau_{1/2}$ (s)	$\Delta H^{\ddagger}$ [kJ/mol]	$\Delta S^{\ddagger}$ [J/K·mol]	$\Delta G^{\ddagger}$ [kJ/mol]
(S)-1-phenylethanol	(S)-isomer	465.2	88.0	−3.9	89.2
	(R)-isomer	550.1	89.0	−1.7	89.5
(R)-1-phenylethanol	(S)-isomer	554.8	88.3	−4.0	89.5
	(R)-isomer	482.0	85.7	−11.5	89.1

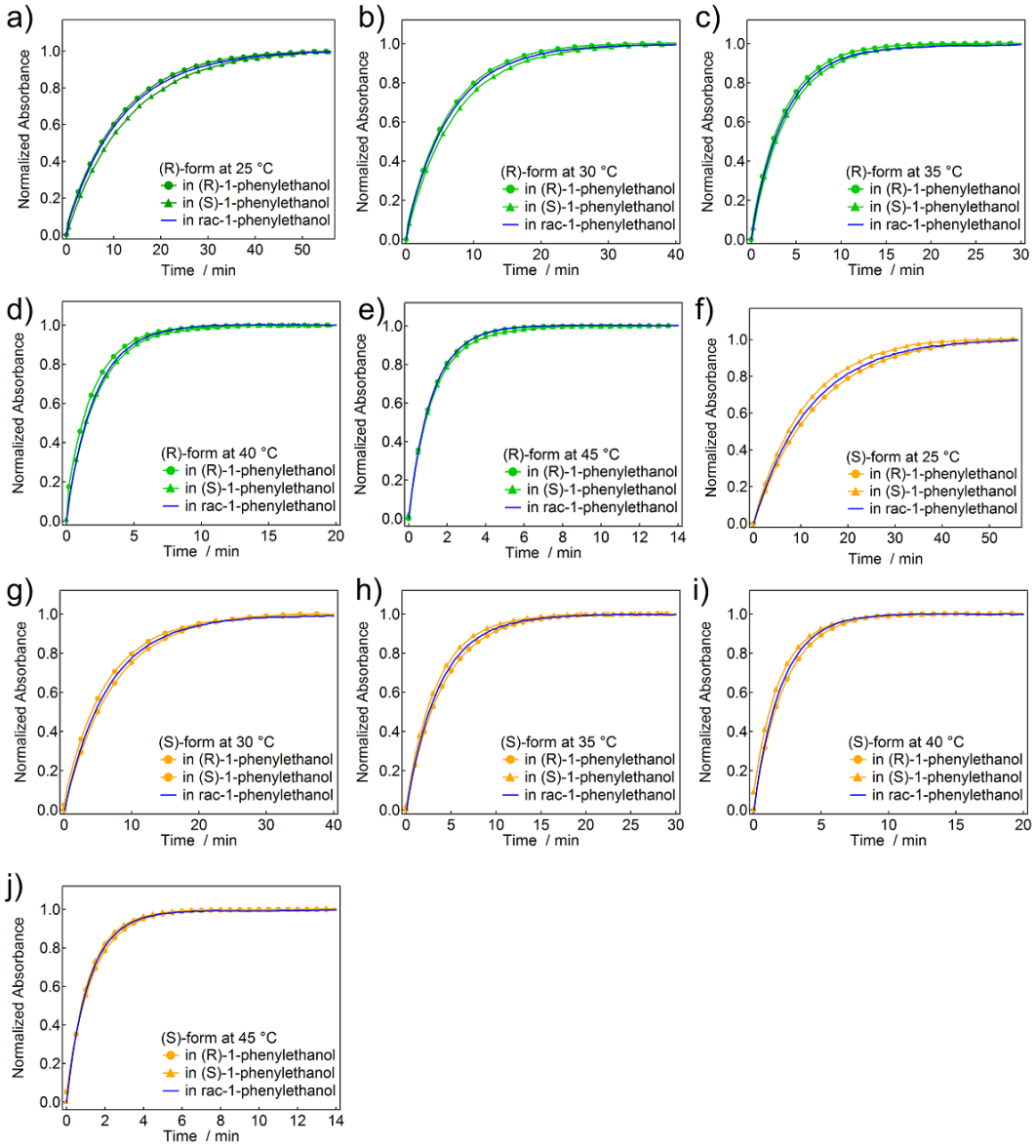

Figure 4.12.8. Time profiles of the thermal back reactions of (R)-form and (S)-form in (R)-1-phenylethanol (circle plots), in (S)-1-phenylethanol (triangle plots) and racemic 1-phenylethanol (blue line) of **BN-PIC1** at several temperatures in the atmosphere.

4.12 Conclusion

The author has developed the novel negative photochromic molecules, **BN-PIC1** and **BN-PIC2**. The negative photochromic behavior of BN-PICs includes three isomers, that is, the colored form, the colorless form and the biradical species. The colored and colorless forms of BN-PICs give the same biradical species upon light irradiation. The major reaction path for the deactivation of the biradical species is the formation of the colorless form. The thermally stable colored forms isomerize to the colorless forms via the biradical species by visible light irradiation, whereas the colorless forms isomerize slightly to the colored forms via the radical species by UV light irradiation. The thermal back reaction from the photogenerated colorless form to the colored form takes 10.9 min at 40 °C and 1.9 s at 25 °C for **BN-PIC1** and **BN-PIC2**, respectively.

Furthermore, the CD spectroscopy revealed that the negative photochromism of BN-PICs induces the large change in the chiroptical property. Since negative photochromism can induce the photochromic reaction at the deep inside of the material, which cannot be achieved in conventional photochromism, the fast negative photochromic systems with large changes in their chiroptical properties associated with the photochromic reaction are useful for photomechanical materials, real-time holographic materials, and photoresponsive chiral dopants for liquid crystals.

4.13 References

(1) Irie, M.; Yokoyama, Y.; Seki, T. *New Frontiers in Photochromism*; Springer: Japan, 2013.

(2) Feringa, B. L.; Browne, W. R. *Molecular Switches*; Wiley-VCH Verlag: Weinheim, 2011.

(3) Düerr, H.; Bouas-Laurent, H. *Photochromism: Molecules and Systems*; Elsevier: Amsterdam, 2003.

(4) Crano, J. C.; Guglielmetti, R. J. *Organic Photochromic and Thermochromic Compounds*; Plenum Press: New York, 1999.

(5) Ubukata, T.; Takahashi, K.; Yokoyama, Y. *J. Phys. Org. Chem.* **2007**, *20*, 981–984.

(6) Ciardelli, F.; Fabbri, D.; Pieroni, O.; Fissi, A. *J. Am. Chem. Soc.* **1989**, *111*, 3470–3472.

(7) Fissi, A.; Pieroni, O.; Ruggeri, G.; Ciardelli, F. *Macromolecules* **1995**, *28*, 302–309.

(8) Roldan, D.; Cobo, S.; Lafolet, F.; Vilà, N.; Bochot, C.; Bucher, C.; Saint-Aman, E.; Boggio-Pasqua, M.; Garavelli, M.; Royal, G. *Chem. –Eur. J.* **2015**, *21*, 455–467.

(9) Tanaka, M.; Ikeda, T.; Xu, Q.; Ando, H.; Shibutani, Y.; Nakamura, M.; Sakamoto, H.; Yajima, S.; Kimura, K. *J. Org. Chem.* **2002**, *67*, 2223–2227.

(10) Minami, M.; Taguchi, N. *Chem. Lett.* **1996**, 25, 429–430.

(11) Tomasulo, M.; Yildiz, I.; Raymo, F. M. *Inorg. Chim. Acta* **2007**, *360*, 938–944.

(12) Mitchell, R. H.; Ward, T. R.; Chen, Y.; Wang, Y.; Weerawarna, S. A.; Dibble, P. W.; Marsella, M. J.; Almutairi, A.; Wang, Z. Q. *J. Am. Chem. Soc.* **2003**, *125*, 2974–2988.
(13) Bohne, C.; Mitchell, R. H. *J. Photochem. Photobiol., C Photochem. Rev.* **2011**, *12*, 126–137.
(14) Honda, K.; Komizu, H.; Kawasaki, M. *J. Chem. Soc., Chem. Commun.* **1982**, 253–254.
(15) Helmy, S.; Leibfarth, F. A; Oh, S.; Poelma, J. E.; Hawker, C. J.; de Alaniz, J. R. *J. Am. Chem. Soc.* **2014**, *136*, 8169–8172.
(16) Hatano, S.; Horino, T.; Tokita, A.; Oshima, T.; Abe, J. *J. Am. Chem. Soc.* **2013**, *135*, 3164–3172.
(17) Kishimoto, Y.; Abe, J. *J. Am. Chem. Soc.* **2009**, *131*, 4227–4229.
(18) Harada, Y.; Hatano, S.; Kimoto, A.; Abe, J. *J. Phys. Chem. Lett.* **2010**, *1*, 1112–1115.
(19) Iwasaki, T.; Kato, T.; Kobayashi, Y.; Abe, J. *Chem. Commun.* **2014**, *50*, 7481–7484.
(20) Yamashita, H.; Abe, J. *Chem. Commun.* **2014**, *50*, 8468–8471.
(21) Yamashita, H.; Ikezawa, T.; Kobayashi, Y.; Abe, J. *J. Am. Chem. Soc.* **2015**, *137*, 4952–4955.
(22) Arai, K.; Kobayashi, Y.; Abe, J. *Chem. Commun.* **2015**, *51*, 3057–3060.
(23) Tomasulo, M.; Sortino, S.; Raymo, F. M. *Org. Lett.* **2005**, *7*, 1109–1112.
(24) Garcia-Amorós, J.; Bučinskas, A.; Reig, M.; Nonell, S.; Velasco, D. *J. Mater. Chem. C* **2014**, *2*, 474–480.
(25) Ishii, N.; Kato, T.; Abe, J. *Sci. Rep.* **2012**, *2*, 819.
(26) Ishii, N.; Abe, J. *Appl. Phys. Lett.* **2013**, *102*, 163301.
(27) Deniz, E.; Tomasulo, M.; Cusido, J.; Sortino, S.; Raymo, F. M. *Langmuir* **2011**, *27*, 11773–11783.
(28) Deniz, E.; Tomasulo, M.; Cusido, J.; Yildiz, I.; Petriella, M.; Bossi, M. L.; Sortino, S.; Raymo, F. M. *J. Phys. Chem. C* **2012**, *116*, 6058–6068.
(29) Yamaguchi, T.; Hatano, S.; Abe, J. *J. Phys. Chem. A* **2014**, *118*, 134–143.
(30) Yamaguchi, T.; Hilbers, M. F.; Reinders, P. P.; Kobayashi, Y.; Brouwer, A. M.; Abe, J. *Chem. Commun.* **2015**, *51*, 1375–1378.
(31) Hanazawa, M.; Sumiya, R.; Horikawa, Y.; Irie, M. *J. Chem. Soc., Chem. Commun.* **1992**, 206–207.
(32) Wintgens, V.; Johnston, L. J.; Scaiano, J. C. *J. Am. Chem. Soc.* **1988**, *110*, 511–517.
(33) Sheepwash, M. A. L.; Ward, T. R.; Wang, Y.; Bandyopadhyay, S.; Mitchell, R. H.; Bohne, C. *Photochem. Photobiol. Sci.* **2003**, *2*, 104–112.
(34) Zhao, Y.; Truhlar, D. G. *J. Phys. Chem. A* **2008**, *112*, 1095–1099.
(35) Mislow, K.; Bunnenberg, E.; Records, R.; Wellman, K.; Djerassi, C. *J. Am. Chem. Soc.* **1963**, *85*, 1342–1349.
(36) Inoue, Y. *Chem. Rev.* **1992**, *92*, 741–770.

(37) North, M.; Villuendas, P. *Org. Lett.* **2010**, *12*, 2378–2381.
(38) Ding, J.; Desikan, V.; Han, X.; Xiao, T. L.; Ding, R.; Jenks, W. S.; Armstrong, D. W. *Org. Lett.* **2005**, *7*, 335–337.
(39) Baudequin, C.; Brégeon, D.; Levillain, J.; Guillen, F.; Plaquevent, J. C.; Gaumont, A. C. *Tetrahedron: Asymmetry* **2005**, *16*, 3921–3945.
(40) Yamamoto, S.; Matsuda, K.; Irie, M. *Org. Lett.* **2003**, *5*, 1769–1772.
(41) Fukagawa, M.; Kawamura, I.; Ubukata, T.; Yokoyama, Y. *Chem. –Eur. J.* **2013**, *19*, 9434–9437.
(42) Sheldrick GM. SHELXS-97 and SHELXL-97; University of Gottingen, Germany, 1997.
(43) Sheldrick GM. SADABS; University of Gottingen, Germany, 1996.
(44) Hatchard, C. G.; Parker, C. A. *Proc. R. Soc. A Math. Phys. Eng. Sci.* **1956**, *235*, 518–536.
(45) Frisch, M. J.; Trucks, G. W.; Schlegel, H. B.; Scuseria, G. E.; Robb, M. A.; Cheeseman, J. R.; Scalmani, G.; Barone, V.; Mennucci, B.; Petersson, G. A.; Nakatsuji, H.; Caricato, M.; Li, X.; Hratchian, H. P.; Izmaylov, A. F.; Bloino, J.; Zheng, G.; Sonnenberg, J. L.; Hada, M.; Ehara, M.; Toyota, K.; Fukuda, R.; Hasegawa, J.; Ishida, M.; Nakajima, T.; Honda, Y.; Kitao, O.; Nakai, H.; Vreven, T.; Montgomery, J. A., Jr.; Peralta, J. E.; Ogliaro, F.; Bearpark, M.; Heyd, J. J.; Brothers, E.; Kudin, K. N.; Staroverov, V. N.; Kobayashi, R.; Normand, J.; Raghavachari, K.; Rendell, A.; Burant, J. C.; Iyengar, S. S.; Tomasi, J.; Cossi, M.; Rega, N.; Millam, N. J.; Klene, M.; Knox, J. E.; Cross, J. B.; Bakken, V.; Adamo, C.; Jaramillo, J.; Gomperts, R.; Stratmann, R. E.; Yazyev, O.; Austin, A. J.; Cammi, R.; Pomelli, C.; Ochterski, J. W.; Martin, R. L.; Morokuma, K.; Zakrzewski, V. G.; Voth, G. A.; Salvador, P.; Dannenberg, J. J.; S. 50 Dapprich, S.; Daniels, A. D.; Farkas, Ö.; Foresman, J. B.; Ortiz, J. V.; Cioslowski, J.; Fox, D. J. Gaussian 09, Revision D.01; Gaussian, Inc.: Wallingford CT, 2009.

Chapter 5
Conclusions

In this thesis, several biaryl (BA)-bridged radical complexes were synthesized and their photochromic properties were investigated. As a result, a new negative photochromic system that includes kinetically and thermodynamically controlled reactions was developed. Moreover, the binaphthyl-bridged phenoxyl–imidazolyl radical complex exhibited rapid negative photochromism with a half-life of the colorless isomer of 2 s at room temperature. These results therefore demonstrate a new approach for the molecular design of negative photochromic compounds.

In Chapter 1, negative photochromism and the photochromism of imidazole dimers were described as background information for this study. Photochromism is a reversible transformation of chemical species induced in one or both directions by light irradiation between the two forms having different absorption spectra. In conventional T-type photochromic compounds, the molecular structures are converted from colorless to colored following UV light irradiation. Recently, real-time holography and photomechanical materials have been reported using T-type photochromic compounds as photoresponsive units. However, in conventional photochromic systems, the photogenerated colored isomer also absorbs the excitation UV light. Thus, the excitation light does not reach the inside the material, and photoconversion is limited. Conversely, some photochromic compounds exhibit negative photochromism, in which the stable colored isomer is converted to the colorless isomer upon visible light irradiation; the colorless isomer then returns to the initial colored isomer upon heating. In these materials, the photogenerated colorless isomer does not absorb the excitation visible light. Therefore, the excitation light reaches deeper inside the materials. Although a few examples of negative photochromism have been reported, the reasonable molecular design and systematic investigation of negative photochromic molecules have not been reported. Moreover, the fast switching properties required for photofunctional materials based on T-type photochromic molecules have not been achieved in negative photochromic systems.

Several photochromic materials were designed and synthesized based on a binaphthyl (BN)-bridged imidazole dimer in this thesis. BN-bridged imidazole dimer has diphenylimidazole substituents at the 2- and 2′-positions of the binaphthyl moiety. There are several structural isomers of BN-bridged imidazole dimer; the most stable isomer is

the colored isomer with diazafulvene structure. The solution of the colored isomer is red and undergo decoloration following visible light irradiation. The photogenerated colorless isomer is the 2,2′-isomer, which has C–C bonds between two imidazole rings. The colorless isomer reverts to the initial colored isomer upon heating. Thus, BN-bridged imidazole dimer exhibits negative photochromism.

In Chapter 2, the photochromism of a biphenyl (BP)-bridged imidazole dimer was investigated, and the photoinduced bond cleavage process was revealed. The BP-bridged imidazole dimer was obtained as the colorless 2,2′-isomer. Analysis of nanosecond transient absorption spectra revealed that BP-bridged imidazole dimer formed a biradical following UV light irradiation, and the life-time of the biradical was 103 ns at room temperature. Furthermore, femtosecond transient absorption measurements were performed in order to reveal the photoinduced bond cleavage process. It was found that vibrational relaxation from the Franck-Condon state to the S_1 state is followed by transition from the S_1 state to the hot state of the biradical and then vibrational cooling to the ground state of the biradical. These results suggest that the BP-bridged imidazole dimer exhibits ultrafast switching induced by UV irradiation.

In Chapter 3, the multi-state photochromism of a 1-phenylnaphthalene (PN)-bridged imidazole dimer was investigated. The PN-bridged imidazole dimer has four stable isomers whose molecular structures were revealed by X-ray crystallographic analysis. Oxidation of the precursor of PN-bridged imidazole dimer afforded the colorless 2,2′-isomer, which is the most thermodynamically unstable of the four stable isomers. A cyclohexane solution of the 2,2′-isomer exhibited a color change from colorless to red upon heating at 70 °C. This red solution contained the colored isomer, which has the diazafulvene structure. The colored isomer upon further heating converted to two different 1,2′-isomers, i.e., the most thermodynamically stable isomers. These four stable isomers generated the same biradical upon light irradiation, and the major product of radical recombination of the biradical was the 2,2′-isomer. Furthermore, the investigation of reported imidazole dimers and PN-bridge imidazole dimer indicated that the activation energy is greatest for isomerization from the biradical to the 1,2′-isomer and least for the isomerization of the biradical to the 2,2′-isomer. Based on this information, a mechanism for the isomerization of PN-bridged imidazole dimer was proposed. The biradical generated via light irradiation affords the most kinetically stable 2,2′-isomer. Since the 2,2′-isomer is in thermal equilibrium with the biradical, the 2,2′-isomer generates the biradical. In addition, a small quantity of the biradical is thermally converted to the second most kinetically stable colored isomer. Thus, the concentration of the colored isomer increases. Furthermore, Since the colored isomer is also in thermal equilibrium with the biradical, it generates the most thermodynamically stable 1,2′-isomers via the

biradical. It is believed that the concentration of the 2,2′-isomer does not increase after the thermal equilibrium moves from the 2,2′-isomer to the colored isomer because of the large rate constant for thermal generation of the biradical from the 2,2′-isomer. Thus, the PN-bridged imidazole dimer exhibits complicated photochromism including both kinetically and thermodynamically controlled reactions. It is the balance of the activation energies for conversion of the isomers between each other that causes the concentration change from the kinetically stable 2,2′-isomer to the thermodynamically stable 1,2′-isomers via the metastable colored isomer. Moreover, this concentration change can be reset to the initial state (only the 2,2′-isomer) via visible light irradiation.

In Chapter 4, the negative photochromism of binaphthyl-bridged phenoxyl–imidazolyl radical complexes (BN-PICs) was investigated, and rapid negative photochromism was achieved. In BN-PICs, one of the two imidazolyl radicals in BN-bridged imidazole dimers is replaced with a phenoxyl radical. BN-PIC solutions exhibit negative photochromism from yellow to colorless upon visible light irradiation. Although the chromophore in the colored isomer of the BN-bridged imidazole dimer is the diazafluorene structure, the chromophores in BN-PICs are quinoid groups. In addition, the colorless isomers of BN-PICs are 2,4-isomers with C–C bonds between the imidazolyl and cyclohexadienone moieties. The phenoxyl and imidazolyl radicals thus play the same role in BN-PICs. Nanosecond transient absorption spectra of the BN-PICs revealed that the colored and colorless isomers generated the same biradical upon light irradiation. There are therefore three isomers of BN-PICs: the colored isomer, colorless isomer, and biradical. The colored isomer and the biradical are the most thermodynamically stable and unstable isomers, respectively. The photogenerated biradical gives the kinetically stable colorless isomer, and the colorless isomer returns to the initial colored isomer via the biradical. Furthermore, BN-PICs have chirality originating from the BN-bridging unit. The colored isomer exhibited a circular dichroism (CD) signal in the UV to visible region and a drastic change in its CD spectrum following light irradiation. The colorless isomer had large CD signals in the UV region but none in the visible region. Thus, the BN-PICs exhibited large CD spectral changes upon light irradiation. The BN-PIC derivative with a phenanthroimidazole moiety also exhibited negative photochromism, and the half-life of the colorless isomer was 2 s at room temperature. This thermal back reaction is the fastest yet reported for negative photochromic molecules.

Considering all of the above results, it can be concluded that the photochromism of BA-bridged imidazole dimers depends on the structure of the bridging unit, and the mechanism of isomerization is determined by the thermodynamically stabilities of each isomer and the activation energies for conversion of the isomers from one to the other. As described in Chapter 3, the photochromism of PN-bridged imidazole dimers can be

explained by considering the thermal equilibrium of the 2,2′-isomer, the colored isomer and the biradical. On the other hand, in BP-bridged imidazole dimer system, the colored isomer is thermodynamically unstable compared to the 2,2′-isomer, and therefore, the activation energy for isomerization from the biradical to the colored isomer is greater. Moreover, the half-life of the biradical of BP-bridged imidazole dimer are shorter than those of other BA-bridged imidazole dimers. This result indicates that the activation energy from the biradical to the 2,2′-isomer of BP-bridged imidazole dimer is smaller than that for other BA-bridged imidazole dimers. Therefore, BP-bridged imidazole dimer exhibits ultrafast T-type photochromism. In BN-bridged imidazole dimer systems, the 2,2′-isomer is in thermal equilibrium with the biradical. Thus, a small amount of the biradical generated from the 2,2′-isomer affords the colored isomer. However, the colored isomer does not thermally form the biradical owing to its high thermodynamic stability. Consequently, BN-bridged imidazole dimers exhibit negative photochromism including the 2,2′-isomer, the colored isomer and the biradical. The isomerization process for BA-bridged imidazole dimers includes both kinetically and thermodynamically controlled processes and is determined by the balance of the activation energies for the conversion processes of the possible isomers. Previously reported negative photochromic systems have been considered to be two-state systems, and negative photochromism have been achieved by stabilizing the colored isomer with the molecular environment, including the solvent and coexisting ions. However, BA-bridged imidazole dimers have several isomers, and their photochromic behavior is determined by the activation energies for interconversion of the different isomers. Therefore the negative photochromism of BA-bridged imidazole dimers can be defined by new isomerization mechanism included the kinetically and thermodynamically controlled processes.

Furthermore, the transient species generated during a photochromic reaction has a different molecular and electronic structure compared to the initial isomer. Photochromic reactions can therefore change the molecular environment, and fast negative photochromic molecules enable fast environmental switching even inside the materials. Such behavior may be effective for the photoswitching of liquid crystals, which requires an environmental change in the interior of the liquid crystalline phase, or the photocontrol of enzymes and catalyses *in vivo*. In addition, organic photochromic compounds are employed for the photochromic lenses and expected to find applications as photoswitching materials and photoswitching units for real-time holography. The results reported in this thesis will therefore contribute to advancement of organic photochromic technology.

List of Publications

Publications Described in This Thesis

Original Paper

1) Multistate Photochromism of 1-Phenylnaphthalene-Bridged Imidazole Dimer That Has Three Colorless Isomers and Two Colored Isomers
Tetsuo Yamaguchi, Sayaka Hatano and Jiro Abe
J. Phys. Chem. A **2014**, *118*, 134-143.

2) Nanosecond Photochromic Molecular Switching of a Biphenyl-Bridged Imidazole Dimer Revealed by Wide Transient Absorption Spectroscopy
Tetsuo Yamaguchi, Michiel F. Hilbers, Paul P. Reinders, Yoichi Kobayashi and Jiro Abe
Chem. Commun. **2015**, *51*, 1375-1378.

3) Fast Negative Photochromism of 1,1′-Binaphthyl-Bridged Phenoxyl-Imidazolyl Radical Complex
Tetsuo Yamaguchi, Yoichi Kobayashi and Jiro Abe
J. Am. Chem. Soc. In press.

Other Publications Not Described in This Thesis

Original Papers

1) Entropy-Controlled Thermal Back-Reaction of Photochromic [2.2]Paracyclophane-Bridged Imidazole Dimer
Shigekazu Kawai, Tetsuo Yamaguchi, Tetsuya Kato, Sayaka Hatano and Jiro Abe
Dyes and Pigm. **2012**, *92*, 872-876.

2) Photochromism of a Naphthalene-Bridged Imidazole Diemr Constrained to the "*Anti*" Conformation
Katsuya Mutoh, Kentaro Shima, Tetsuo Yamaguchi, Masayuki Kobayashi and Jiro Abe
Org. Lett. **2013**, *15*, 2938-2941.

Acknowledgment

This work was carried out at ***Organic Functional Material Laboratory*** (***Abe Lab.***, Chemistry course, Graduate School of Science and Engineering, Aoyama Gakuin University) from April 2011 to March 2016.

I wish to express my sincere gratitude to Prof. Jiro Abe for his constant guidance, helpful suggestion, exciting discussion and hearty encouragement throughout this work.

I would like to express deepest appreciation to Prof. Akira Sakamoto and Prof. Tadashi Suzuki at Aoyama Gakuin University for the careful review and insightful suggestion to this doctoral thesis.

I really appreciate to Prof. Fred Brouwer at the University of Amsterdam for the wonderful experience visiting your group and working with him and his lab member and for the opportunity to collaboration to ultrafast spectroscopy (Chapter 2).

I wish thanks to Prof. Tomiki Ikeda at Chuo University for his kind treatment and gentle comments.

I gratefully acknowledge to Dr. Yoichi Kobayashi at Aoyama Gakuin University for his helpful discussion, comments and experimental support in my Ph.D. course.

I am truly grateful to Dr. Sayaka Hatano at Hiroshima University for her lots of advices and kind suggestion in my academic life.

I would like to express my thanks to Dr. Shigekazu Kawai for his kindness in the master's course.

I also wish to express my special thanks to all stuffs, colleagues and graduates in Abe Laboratory of Aoyama Gakuin University for the kind discussions, collaborations, help and heartful friendships.

I would like to appreciate Research Fellowship for Young Scientists, Japan Society for the Promotion of Science.

Finally, I sincerely express my appreciation to my family for their assistance and encouragement during my study.

March 2016